POLITECNICO
MILANO 1863

School of Civil, Environmental and Land Management Engineering

M.Sc. in Civil Engineering for Risk Mitigation

Numerical Modeling of the Mechanical Behavior of A SFRC beam Reinforced with FRCM Composites

Supervisor: Prof. Matteo Colombo

Co-supervisor: Eng. Marco Carlo Rampini

Thesis By:

Youssef Miaari

Academic year: 2019-2020

Page intentionally left blank

Table of Contents

List of Figures

List of Tables

Acknowledgments

Firstly, I would like to start by expressing my gratitude to my thesis supervisor, Prof. Matteo Colombo for his support and constructive feedback throughout the research period. Due to his continuous input, and proper guiding I managed to conclude my research confidently.

I am also appreciative and thankful to Eng. Marco Carlo Rampini, for his availability, patience, motivation, and immense knowledge. He has helped improve my knowledge and technical skills, which assisted in directing me throughout this research.

Finally, I would like to express my gratitude to the love and support of my family and friends. Especially, my mom Mrs. Doha Marroun, and dad Mr. Nabil Miaari, they have always kept me going and without them this opportunity would not have been possible.

Abstract

Glass fabrics and micro-steel fibers have proved their high efficiency in structural reinforcement and retrofitting. Many intense experimental campaigns were studying diverse kinds of specimens with composite materials reinforcement and under different testing methods. Non-linear numerical modeling is highly required to replicate their behaviors and response. Thus, this research aims, at a final point, to model a Steel Fibers Reinforced Concrete (SFRC) beam reinforced from the bottom side with a Fabric Reinforced Cementitious Matrix (FRCM) composite layer, using a non-linear finite element commercial software, ABAQUS. The main goal was to simulate the mechanical behavior of the composite members and better understand all the involved phenomena.

The modeling was divided into three main tasks. The first one was to model the uniaxial test of AR-glass fabric based FRCM, with two different mortars, a high-strength mortar (M1), and a commercial medium-strength (M2). Two different approaches were used: a simplified model "A" defined as a homogenous material, with a tensile behavior provided from the revised ACK, and model "B" with one-layer reinforced mortar. The later model's challenge is the GF calibration with the different meshes, as it was found that the MC2010 proposed formula did not directly result in a good outcome.

The second task was the modeling of SFRC notched beams behavior, in order to understand the best approach in the definition of the constitutive material law. These material laws were defined both in according with the MC2010 provisions and by means of inverse plane-section analysis.

Finally, the third task was the modeling of a four-point bending test on SFRC beam, taking advantages from the previous constitutive law calibration. Moreover, the effect of the addition of a FRCM composite reinforcing layer were numerically investigated on both damaged and undamaged SFRC beams.

Keywords: Fabric Reinforced Cementitious Matrix (FRCM), Steel Fibers Reinforced Concrete (SFRC), ABAQUS, Concrete Damage Plasticity (CDP), MC2010, Four-point bending test.

Sommario

I tessuti di vetro e le micro-fibre di acciaio hanno dimostrato la loro elevata efficienza nel rinforzo strutturale e nel retrofitting. Molte campagne sperimentali hanno studiato diversi tipi di campioni con rinforzi in materiali compositi e con diversi metodi di prova. La modellazione numerica non lineare è altamente richiesta per replicare i loro comportamenti e le loro risposte. Pertanto, questa ricerca mira modellare una trave in cemento armato con fibre di acciaio (SFRC) rinforzata dal lato inferiore con uno strato composito a matrice cementizia rinforzata in tessuto (FRCM), utilizzando un software commerciale non lineare a elementi finiti, ABAQUS. L'obiettivo principale è quello di simulare il comportamento meccanico degli elementi compositi e comprenderne meglio tutti i fenomeni coinvolti.

La modellazione è stata suddivisa in tre parte principali. La prima è stata quella di modellare il test di trazione uniassiale di FRCM basato su tessuto di vetro AR, con due diverse malte, una malta ad alta resistenza (M1) e una media resistenza commerciale (M2). Sono stati utilizzati due diversi approcci: un modello semplificato "A" definito come materiale omogeneo, con un comportamento a trazione fornito dalla revisione del modello di letteratura ACK, e il modello "B" con malta rinforzata monostrato. L'obiettivo è la calibrazione dell'energia di frattura GF con le diverse maglie, poiché è stato riscontrato che la formula proposta da MC2010 non ha prodotto direttamente un buon risultato.

La seconda parte riguarda la modellazione del comportamento delle travi intagliate SFRC, al fine di comprendere l'approccio migliore nella definizione della legge materiale costitutiva. Queste leggi sono state definite sia in accordo con le disposizioni dell'MC2010 sia mediante analisi inverse.

Infine, il terzo compito è stato la modellazione di un test di flessione a quattro punti su trave SFRC, sfruttando la precedente calibrazione della legge costitutiva. Inoltre, l'effetto dell'aggiunta di uno strato di rinforzo composito FRCM è stato studiato numericamente su travi SFRC danneggiate e non danneggiate.

Parole chiave: Matrice Cementizia Rinforzata con Tessuto (FRCM), Calcestruzzo Armato con Fibre d'Acciaio (SFRC), ABAQUS, Plasticità del Danno al Calcestruzzo (CDP), MC2010, Esperimento di Flessione a Quattro Punti.

1 INTRODUCTION

The Retrofitting of structural elements is a challenge that always requires progress and the invention of new solutions, in order to improve the resilience to all the natural and human-made hazards occurring every day. The use of new retrofitting methods requires many investigations, checks, and approvals. For example, the introduction of composite materials, fibers and fabrics based concrete discussed in this manuscript, needs a deep study and both experimental and numerical investigation.

Many ways to prevent a wide range of hazards from occurring or to reduce their impacts on the structures are continuously delivered, for example, firefighting methods and artificial dampers for earthquakes. However, with the high growth of cities and civilizations, increasing the hazard exposure, resilience was the key to adapt to their effects. This cannot be accomplished without an outstanding structural retrofitting methods, instead of demolishing and newly constructing, that weaken the cultural heritage.

Beams being one of the main structural elements, consequently subjected to severe damage, requires effective reinforcement to retain their capacity. The problem is that having more than half of the beam cross-section directly connected to the slab leads to significant difficulties with the retrofitting. In this paper, reinforcing the beams will be at the bottom part, in the tension zone between the two supports, allowing easy access to apply the reinforcement.

FRCM, Fabric Reinforced Cementitious Matrix, is one effective way to reinforce the beams under out-of-plane actions. These materials have a very high-tension capacity, they are easy to be attached on the bottom surfaces, applying mortar and fabric directly, without increasing the weight of the structure because of the typical used thickness of 20 mm. Experiments were made on FRCM specimens to understand its tensile behavior and appreciate the transition of the loads between the mortar and the fabric mesh. Two different mortars were used in these experiments, with different capacities and five different AR-glass fabric meshes, with different capacities, mesh distribution, and area of fabrics.

Reinforced concrete is the material most used to realize structures and it has proved its effectiveness concerning its price and implantation. Innovative reinforcing methods uses micro-fibers in the concrete mixture to increase the tensile capacity and to give a better behavior of the full beam. Fibers, made of steel or glass, have proved their efficiency with the

transition of loads between them and the concrete mixture. In this research, the beams that were tested and reinforced were made by SFRC, Steel Fiber Reinforced Concrete, and the investigation of the fibers effect on the constitutive material law was one of the goals of the study.

The main scope of the research was to simulate the previously mentioned element behavior with and without the attachment of the FRCM bottom layer. In order to do this, a preliminary calibration of both the notched SFRC beams and FRCM tensile coupons were necessary.

The FRCM was modeled in ABAQUS with two different approaches used. The first was a simplified approach implying a homogenous material that was defined by the revised ACK. While the second more complex defining a one-layer reinforced mortar, with the fracture energy describing the mortar's cracking. Two different meshes were defined, rough and fine, allowing results comparison and effects from the defined parameters according to the mesh element size.

This research aims to expand the numerical simulations of FRCM composites applied as a beam reinforcement, highlighting some un-common or new issues in the modeling that can affect the results dramatically in some cases. Varying the distribution and number of cracks in the composite by increasing the fabrics' stiffness with different defined characteristic length, lcs, is one example of the ability to model and obtain good results of such complex mechanical behavior by adjusting the tools of commercial software.

1.1 Thesis Outline

In chapter 2 an overview of the principal characteristics of the FRCM composite acknowledged by different experiments is described. In addition to a different numerical modeling approaches presented, along with the ABAQUS utilized tool Concrete Damage Plasticity (CDP) that simulates of the composite's nonlinear behavior.

In Chapter 3 the experimental results obtained from another research are presented. First the uniaxial tensile test of the FRCM, and then two different experiments of SFRC, the notched beams, and the pre-damaged and reinforced four points bending beams. In which these results will be used for numerical evaluation and comparison.

In chapter 4 the numerical modeling and simulations with the two approaches of FRCM uniaxial tensile test are explained. The homogenous model "A", and the one-layer reinforced

model “B”, with a composite of (M1) or (M2) mortars reinforced with the F4 fabrics, with a challenge of the fracture energy and mesh calibration of the second model method.

In chapter 5 the MC2010 constitutive laws and the modification of the two provided inverse laws are evaluated. The notched beam experimental results are used in the process and validation of the laws response. Then by defining the notched beam model material with the obtained laws, the results are compared with the experimental ones.

In Chapter 6 the four-points bending beam test simulation is presented. The beams are defined with the laws chosen in the previous chapter. Then the FRCM reinforcement is applied, with F4 fabrics and (M2) mortar, to compare the response capacity improvements. Finally, with a simplified approach, the reinforcement is applied to a beam that is partially defined with a residual capacity to simulate the pre-damaged reinforced beam experiments.

Chapter 7 the results and observations of this research are summarized. Some essential guidance to better simulate such complex composites are highlighted. Then some expanding topics using this research conclusion are suggested.

2 STATE OF THE ART

In this state of the art the attention was focused on the description of the mechanical behavior of the composite materials involved in the experiments subjected to the numerical modeling in the following chapters.

2.1 FRCM PROPERTIES

FRCM is a composite made by mortar and two direction fabric mesh (weft and warp). The interaction between the mortar and the fabrics gives an excellent behavior, developing the strain hardening response of the composite. This type of reinforcement is a promising solution for the use in structural retrofitting and, in this special case, for beams.

In the paper [1] different combinations of mortar and AR-glass fabrics were studied, checking their characteristics effect on the behavior. The difference between the mortars was caused by their capacity. While fabrics differ in wires spacing and area, single or double wires shape, and in the nature (i.e. epoxy or styrene-butadiene rubber). The coating nature is the most affecting factor of the fabric behavior.

The bond between the FRCM specimen and the substrate has a key role on the reinforcement's strength [2]. The bond-slip behavior describes the slippage of the reinforcement from the beam, as in Figure 2.1. This phenomenon can critically decrease the strength of the whole system, preventing the delivery of its full capacity.

Figure 2.1 Reinforcement-Substrate Delamination[3]

2.1.1 AR-Glass Fabrics Samples

The behavior of the FRCM under tension is trilinear. The first part describing the mortar's elastic behavior, the second part is the loads transition between the mortar and fabrics, and the third shows the pure fabrics response after the failure of the mortar. It ensures the full trilinear behavior of the composite is essential.

In the paper [1] Alkali-Resistant glass fabrics was studied , delivering different trilinear responses, due to the textile's geometry and tensile capacity.

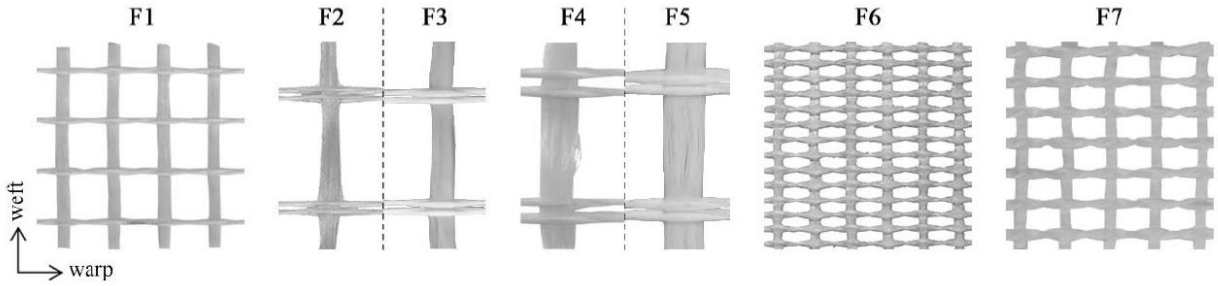

Figure 2.2 Alkali-resistant fabrics samples (70x70m²) [1]

This set of different textiles, shown in Figure 2.2, share some characteristics, illustrating each property's different effect on the plain sample's behavior, and when used with the FRCM composite.

As shown in Table 2.1, the fabrics couples F2 and F3, F4 and F5 have the same geometrical characteristics, with a different coating nature; where the first one is epoxy, and the second is SBR coated.

		F1	F2	F3	F4	F5	F6	F7
Fabrication technique		Leano weave	Double leano weave	Double leano weave	Double leano weave	Double leano weave	Leano weave	Leano weave
Coating nature		SBR	Epoxy	SBR	Epoxy	SBR	SBR	SBR
Warp	Wire spacing (mm)	18	38	38	38	38	5	10
	Roving fineness (Tex)	2 × 1200	2 × 1200	2 × 1200	2 × 2400	2 × 2400	2 × 1200	2 × 2400
	Filament diameter (μm)	19	19	19	27	27	19	27
	Equivalent reinforcement thickness* t_{eq} (mm)	0.050	0.046	0.046	0.093	0.093	0.179	0.179
Weft	Wire spacing (mm)	18	38	38	38	38	12	14.3
	Roving fineness (Tex)	2400	2 × 2400	2 × 2400	4 × 2400	4 × 2400	2400	2 × 1200
	Filament diameter (μm)	27	27	27	27	27	27	19
	Equivalent reinforcement thickness* t_{eq} (mm)	0.050	0.046	0.046	0.093	0.093	0.071	0.062

* calculated over a width of 1 m.

Table 2.1 Alkali-resistant Fabrics characteristics [1]

The warp and weft directions have the same reinforcements, except F6 and F7. This is demonstrated by the equivalent thickness, which is a geometrical parameter defined in [1].

2.1.2 Tensile Behavior of the AR-Glass Fabrics

Experiments were done in [1] under displacement control, to get a full behavior even after the peak strength of the fabrics. The fabrics exhibited a linear elastic response up to failure, then a softening branch. This response can be observed if the fabrics do not slip from the resin tabs, that are applied at both ends to ensure a uniform loading on the specimens without creating a stress localization [1], as shown in Figure 2.3.

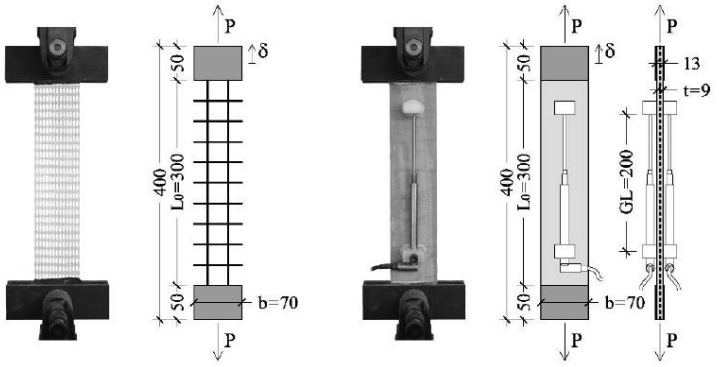

Figure 2.3 Setup of uniaxial tensile tests, Fabrics(left) and FRCM (right)[1]

It was proven after the experiments that not all the fabrics are effective, meaning that, even with a high area of fabrics in some textiles, the peak capacity was close to ones having a lower area. The reason behind this was mainly the coating, since the epoxy resin coat proved to be more effective and allow a higher capacity by impregnating the glass filaments[1]. Due to this, an efficiency factor for each textile was calculated, equation (1). The evaluation of this factor can be considered as a correction of the strength provided by the manufacturer.

$$EF_f = \frac{P_{f,max,avg}}{A_f * \sigma_{fu}} \tag{1}$$

Where P_f is the peak load carried by the fabrics, A_f is the area of the fabrics, Table 2.2, and σ_{fu} is provided by the manufacturer as 2000 MPa. Therefore, the reinforcing material utilization rate can be provided by this EF_f factor, which can be referred to when considering the cost-efficiency ratio [1].

		F1	F2	F3	F4	F5	F6	F7
Warp	A_f (mm^2)	3.582	3.582	3.582	7.164	7.164	12.537	12.537
	$P_{f,max,avg}$ (kN)	5.72	6.41	6.21	12.50*	11.44*	15.98	12.20*
	(std)	(0.27)	(0.29)	(0.31)	(0.67)	(0.63)	(0.15)	(0.20)
	(std%)	(4.80%)	(4.53%)	(4.92%)	(5.34%)	(5.48%)	(0.93%)	(1.63%)
	EF_f	0.80	0.89	0.87	0.87	0.80	0.64	0.49
Weft	A_f (mm^2)	3.582	3.582	3.582	7.164	7.164	5.373	4.478
	$P_{f,max,avg}$ (kN)	5.36	4.81	5.51	11.70	10.09*	8.69	6.34
	(std)	(0.27)	(0.33)	(0.76)	(0.75)	(0.82)	(0.71)	(0.41)
	(std%)	(5.13%)	(6.86%)	(13.78%)	(6.42%)	(8.09%)	(8.15%)	(6.40%)
	EF_f	0.75	0.67	0.77	0.82	0.70	0.81	0.71

Table 2.2 The averaged tensile peak load and other mechanical properties (Averaged over four samples)[1]

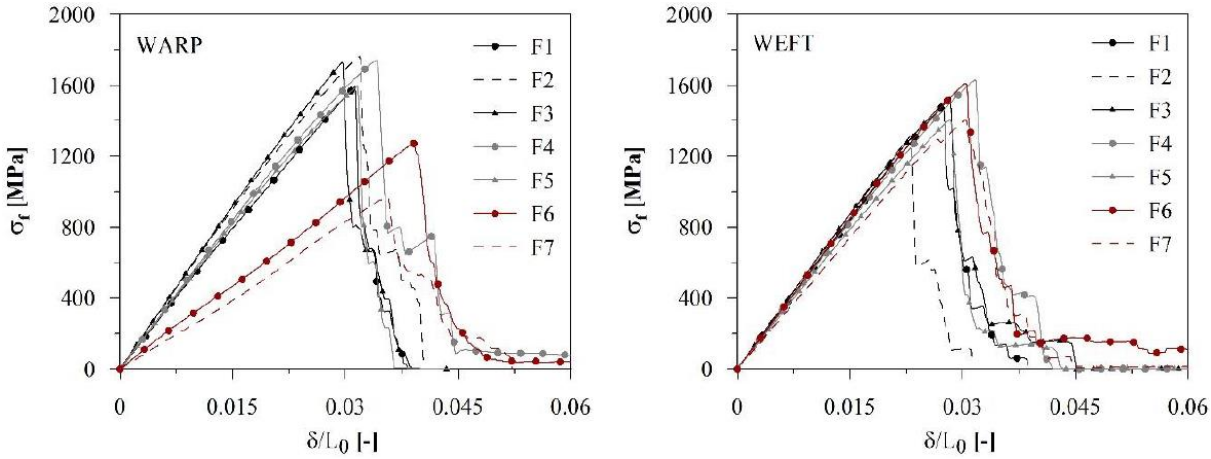

Figure 2.4 Fabric Stress against normalized displacement (Averaged over four samples), in warp direction (left) and weft direction (right) [1]

Figure 2.4 shows that none of the glass fabrics was able to reach maximum strength capacity, 2000 MPa, proving the need for the efficiency factor EF_f.

2.1.3 Bond-Slip Behavior of FRCM Composite

The bond-slip is referred to as the bond between the substrate and its reinforcement composite, that could be weak to cause the delamination of the reinforcement, preventing the FRCM from giving its full capacity due to the early failure. A significant role of the FRCM reinforcement was the behavior of the interaction with the substrate, the bond-slip, where early failures of delamination are usually prevented [2].

An example of the methods to check the bond-slip behavior, was in an experimental study done in [4]. It performed a single-lap shear test on a FRCM composite attached to a concrete substrate with the scheme in Figure 2.5. Three different displacements were measured, the FRCM, the stroke coming from the fabrics, and the slip one showing any movement of the composite from the substrate. The test was done with three composites of different materials,

explained in the paper. The results in shown Figure 2.6, prove that the failure was only due to the fabrics rupture, with its typical response in Figure 2.6(a). All the displacements measured were zero, except the stroke representing the fabrics movement, Figure 2.6 (b), proving again that no delamination occurred.

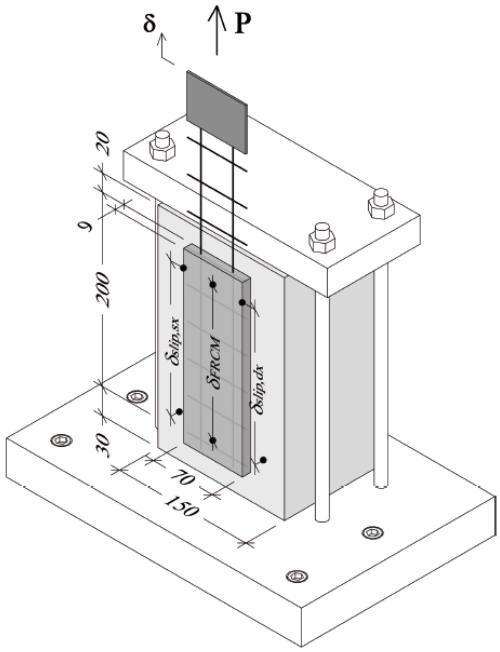

Figure 2.5 The single-lap shear test performed in [4]

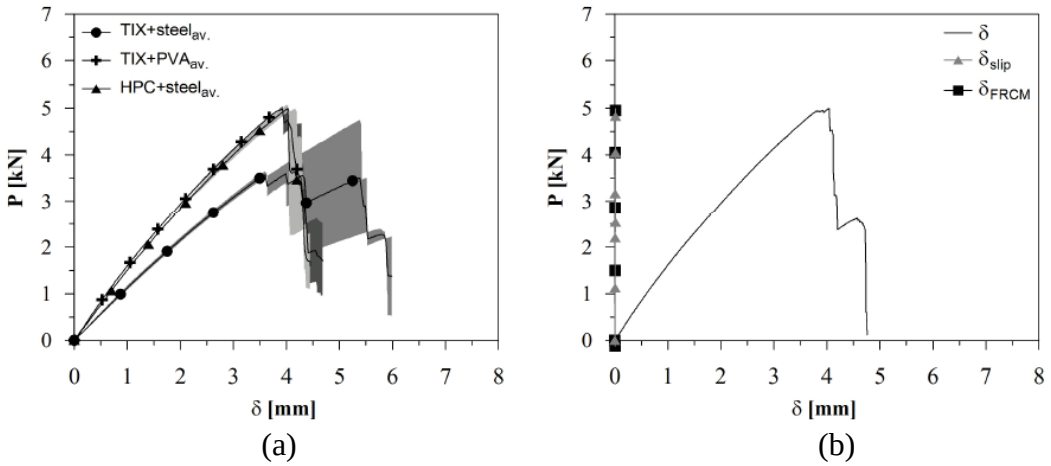

Figure 2.6 Single lap shear test results, load vs. stroke for all specimens (a) for TIX+PVA with all displacements (b) [4]

Furthermore, this section refers to two types of research, highlighting the factors affecting the bond and some methods to increase its strength. Two main methods can improve the

interaction with the concrete substrates: sandblasting and hydro-scarification using water pressure.

An experimental campaign studied in [3] performed a single lap shear, with the same setup in Figure 2.5, in order to better understand factors affecting the bond of the composite and the substrate. Concrete substrates were treated with sandblasting, while with the masonry ones were done in different matters, a smooth B1 a rough B2 substrates. This setup done was to show the different behaviors due to the bond strength, with a FRCM of fabrics F1, F2, and F4.

In the concrete sandblasted substrate, the F2 FRCM failed due to rupture, while the F4 FRCM failed due to delamination. Proving that the sandblasting was not enough in the F4 case since the bond capacity was less than the fabrics capacity, unlike the F2 case.

While in the case of masonry substrate, the specimens of F1-B2, F2-B1, F2-B2 failed in rupture, unlike F1-B1 that failed in delamination, which is the combination of the weakest fabrics with the smoothest substrate.

Another experiments in the same paper [3] were done using sandblasting with a double edge wedge splitting (DEWS) test. Eight sets for experiments, with a reinforcement of F2, an average strength commercial mortar (M2), and PVA micro-fibers. An advantage of this test was the direct stress transferring from the substrate to the FRCM composite, through the mechanical and chemical adhesion [3].

Only one of the eight sets, as shown in Figure 2.7, reached the almost full capacity of the FRCM, as the others failed with the delamination of the reinforcements.

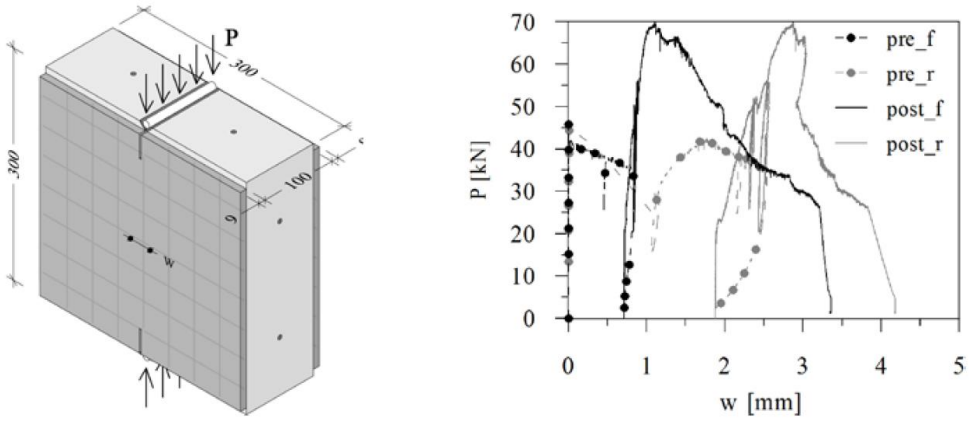

Figure 2.7 DEWS test setup (left) and the one successful set results (right) [3]

As a result, it can be appreciated in Figure 2.7 and Figure 2.8 an improvement of the bond-slip behavior by increasing the roughness. Nevertheless, a more effective method to increase the interaction with the substrate, such as hydro-scarification.

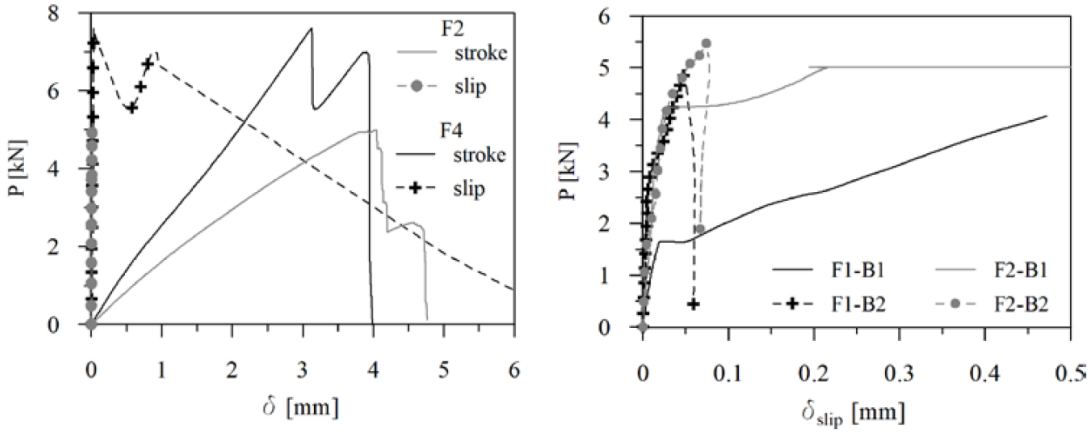

Figure 2.8 Single lap shear of sandblasted concrete (left) and masonry with different roughness (right) [3]

With a pressurized waterjet, hydro-scarification removes a small part of the concrete substrate's external layer, resulting in the best machining method to get the suitable roughness [2]. For this reason, the concrete chosen was with a high compressive strength to handle this pressure without damaging the inner layers.

This method is usually suggested for large areas and with adequate water pressure, thus these experiments aimed to find the best water pressure that provides a good roughness.

A Laser Optical Displacement Sensor was used to measure the substrate's roughness, as shown in Figure 2.9, and then three roughness indices were evaluated in [2] to compare the peak load or displacement against the roughness.

Figure 2.9 Hydro-scarification test (left) roughness measurements (center and right) [2]

The single lap shear tests were carried with a small anchorage of 100mm, while, as suggested, it should be around 300mm [5], illustrating better the effect of the roughness on the bond-slip behavior [2].

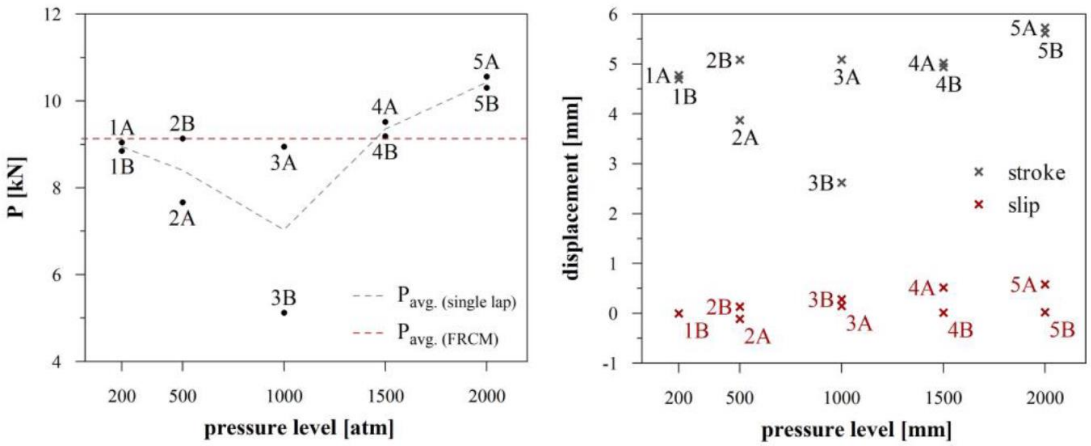

Figure 2.10 Peak loads (left) and stroke and slip displacements (right) against the water pressure level [2]

As shown in both graphs of Figure 2.10, the higher water pressure in most cases gave better results. But it should be known that the increase of the pressure, even with better mechanical results, was more expensive. The higher the pressure was, a more thick part of concrete was removed, thus a larger thickness of the mortar was required to restore the substrate before the application of the FRCM [2].

2.2 Numerical Simulation of FRCM Composite Behavior

The FRCM composite's behavior was simulated with a non-linear analysis since the fabrics effects begin in the inelastic zone. Using the nonlinear FE software, ABAQUS, the FRCM was modeled with the Concrete Damage Plasticity CDP, defining the concrete or the mortar's post-elastic behavior.

2.2.1 Concrete Damage Plasticity

Employing scalar damage variables of the concrete behavior, its tensile and compressive constitutive law can be defined by the CDP model, which combines the elastic-plastic laws and the elastic damage models, as in Figure 2.11 [6].

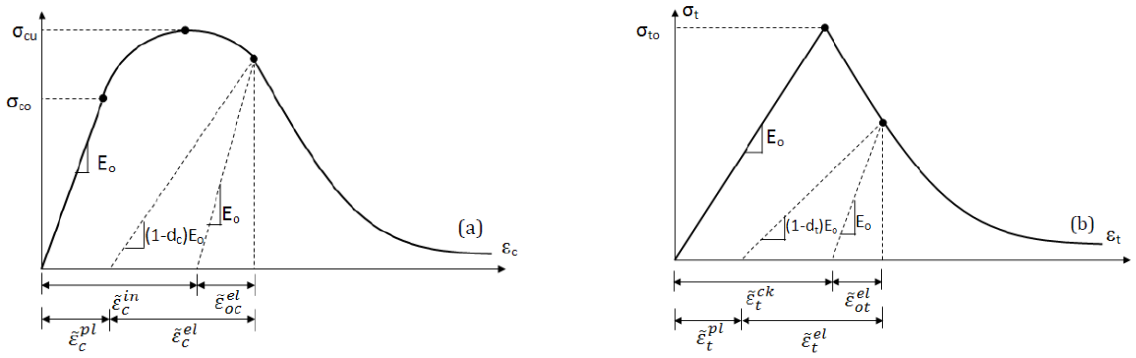

(a) (b)

Figure 2.11 Concrete axial compressive strength (a) and concrete axial tensile strength (b) [6]

The input for the tensile behavior of concrete in CDP is usually by a (fictitious yield) stress- cracking strain, as in the second part of the behavior in Figure 2.11 (b). A problem arises with no dense reinforcement in some regions, or rough mesh elements, and the cracking failure is not distributed evenly, as this is the case of the FRCM, making the model mesh sensitive. To avoid this issue, CDP can directly allow the definition of yield stress with the corresponding cracking displacement using Hillerborg's (1976) fracture energy GF, as shown in Figure 2.12. It describes in the material the amount of energy required to open a crack unit area, and as a more simplified method, GF can be directly implemented with the yield stress [7].

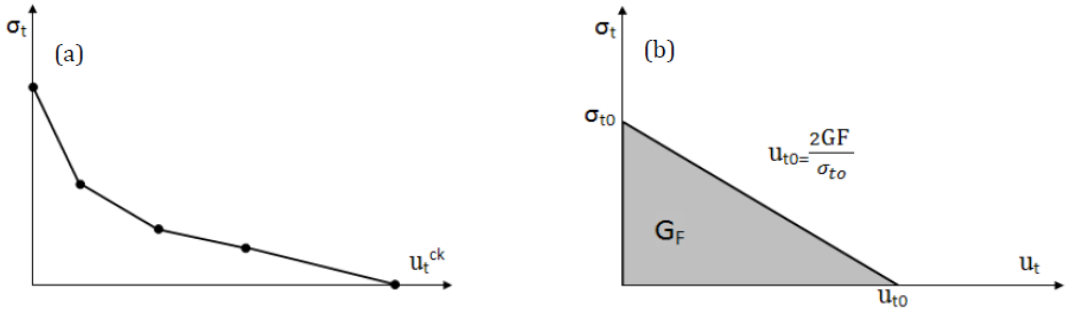

(a) (b)

Figure 2.12 Hillberbors's yield stress vs. displacement (a) and Yield stress with fracture energy area (1976) [7]

With three experiments described in [6], it was proved that CDP was able to almost fully describe the loading trends for an RC beam. It was concluded the importance of the calibration of the fracture energy, dilation angle, and the mesh density, which in this research will be very highlighted.

2.2.2 Different FRCM Models Examples

There are three approaches to model the FRCM in the nonlinear commercial software ABAQUS, as suggested in detail in [8], defining the composite with a 3D continuum shell

elements. Both the ends of the FRCM were modeled as elastic for the reduction of numerical stress concentration in the uniaxial tensile test [8].

The first and most simplified method, referred as model “A”, was using the analytical curves from the revised ACK model, stress-strain, as the CDP was defining the mortar as a homogenous material. This model's results were good, describing the multi-cracking as a simplified smooth branch with a curve of the same slope, shown in Figure 2.13. This method's main drawback was the lack of simulating the FRCM in both directions, warp, and weft, since the analytical curve defining the tensile properties was evaluated in one direction of the composite.

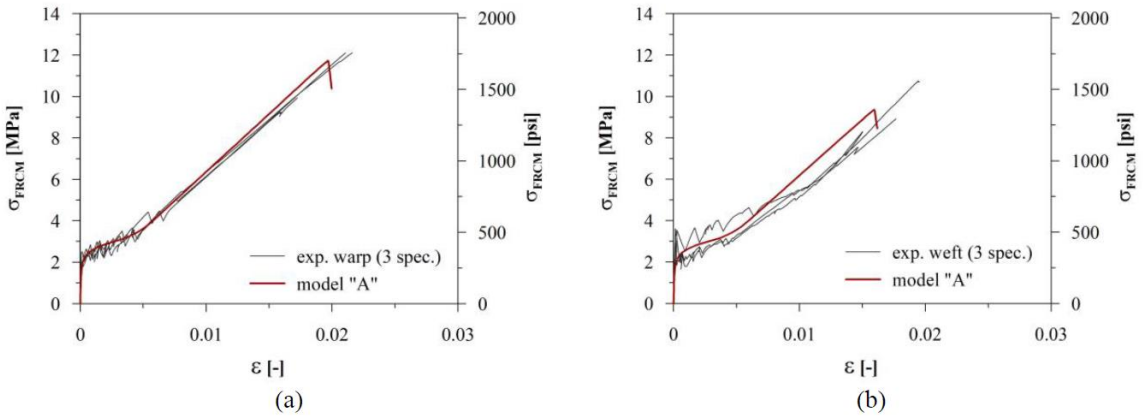

Figure 2.13 Model "A" simulation with the experimental results in the warp (a) and weft (b) directions [8]

The second approach was a continuum shell with an embedded rebar, referred as model “B”. The fracture energy was used to describe the mortar's tensile post-peak behavior, and the fabrics was defined as two rebar layers into the shell, allowing the model to be able to describe the behavior in both directions. This method's issue was the high need for calibrating the GF, as it was suggested to start with 20% of the one defined in the Model Code 2010. This model was able to catch the typical stress jumps in the 2nd branch of the behavior, with a horizontal slope related to the uniform f_{ct} value used, as shown in Figure 2.14.

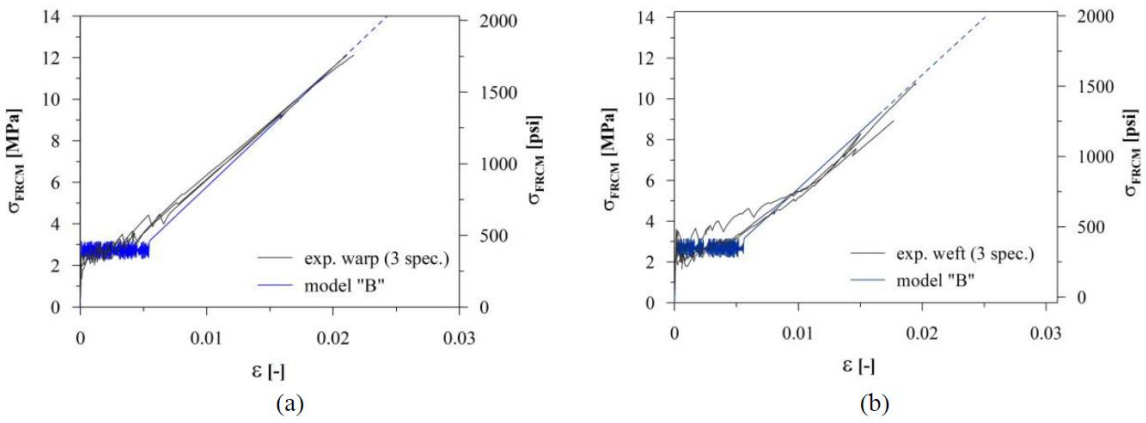

Figure 2.14 Model "B" simulation with the experimental results in the warp (a) and weft (b) directions [8]

The third approach referred to as "C", which is similar to the model "B", but with two differences. First, is that the mesh in this case was defined as strips, not 5 mm square elements, and the strips were randomly assigned with diverse tensile strengths. Second, is the distribution of the tensile mortar strength in the different strips. These values were based on the two-parameter Weibull function, computed using the experimental results performed in the same research [8]. This model was able to perfectly catch the full behavior of the FRCM, with the second branch's slope that was described by the increasing values of the mortar's f_{ct}, as shown in Figure 2.15.

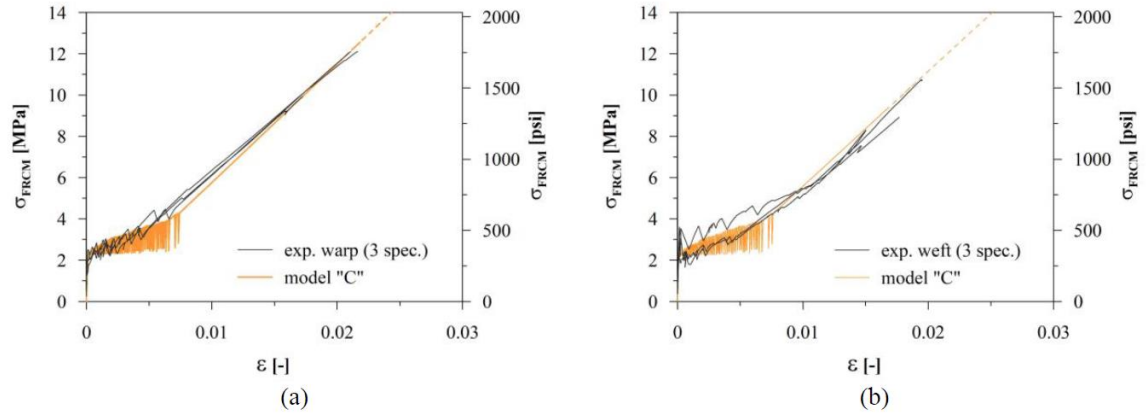

Figure 2.15 Model "C" simulation with the experimental results in the warp (a) and weft (b) directions [8]

2.3 SFRC Mechanical Behavior

The brittle behavior of concrete lacks the delivery of an energy absorbing capacity beyond the peak. Introducing the fibers reinforcement in the mixture with a random distribution, leads to the increasing of the resistance to loadings and providing a higher energy after the peak, caused by the debonding and pulling out of the fibers[9].

The portions of these fibers may differ, but even with the small portions a noticeable improvement of the behavior could be seen, compared to the one of plain concrete. In Figure 2.16, the behavior of the fibers reinforced concrete provided a higher energy in the post-peak phase, compared to the plain concrete that even with similar peak load values could not give such response. The SFRC was able to resist until displacements higher than 10 mm, proving the high increase of its ductility, delivered by the fiber's ability to absorb energy.

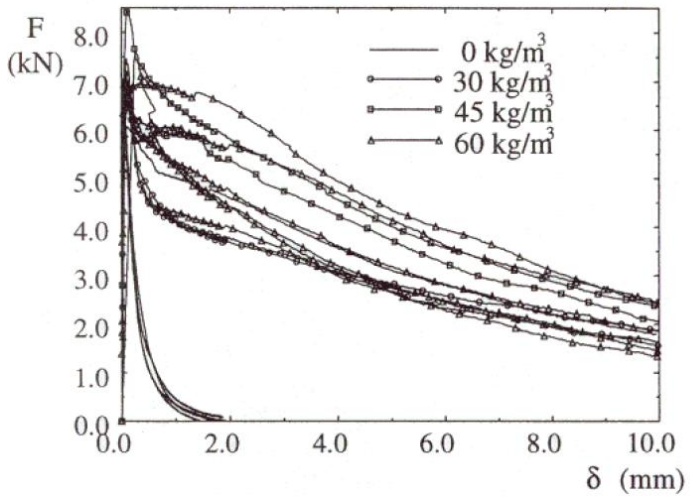

Figure 2.16 Load - displacement of a three-point bending test of a notched beam, the response of different portions of fibers in the concrete mixture[9]

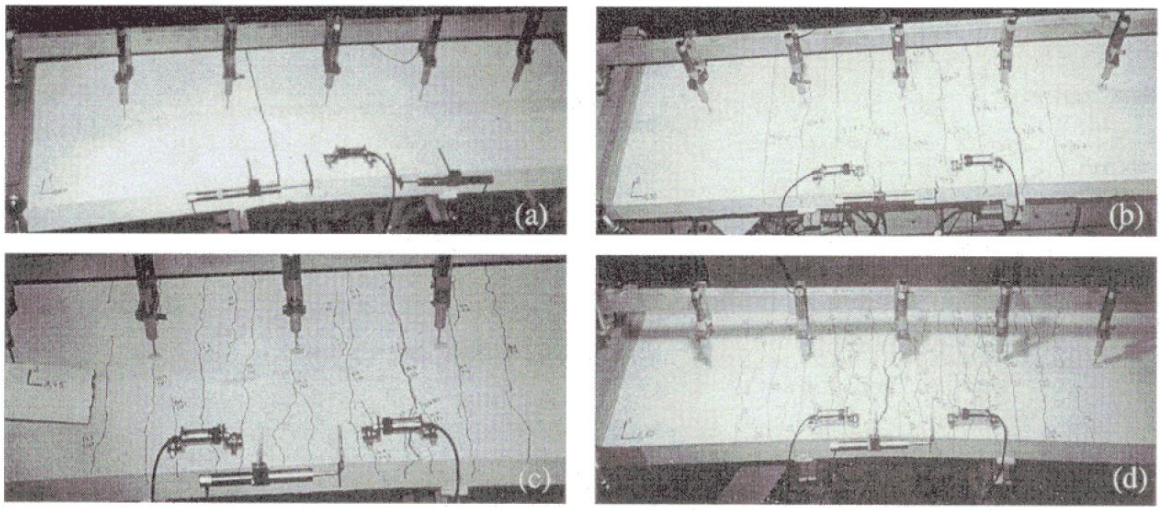

Figure 2.17 Cracking patterns of slab strips reinforced with a steel wire mesh under bending, with different portions of steel fibers, 0 kg/m^3(a); 30 kg/m^3(b); 45 kg/m^3(c); and 60 kg/m^3(d) [9]

The effect of the steel fibers of the cracking patterns can be appreciated in Figure 2.17, of slab strips tested under bending and ordinarily reinforced with a steel mesh. Figure 2.17(a) without any steel fibers added to the mixture, shows one crack with a large opening diameter. While for the following figures with the increasing of the fibers portion, the number of cracks

was increasing along with their diameters shrinking. Therefore, these added fibers can be considered as crack capturing, blocking any crack localization from occurring, hence providing a better ductility and durability to the structural element.

3 EXPERIMENTAL DATABASE

Several experimental campaigns done by the Politecnico di Milano, are shown in this chapter. The results were used as a base data, simulating the performed tests, as this research did not include any experimental task. The experimental campaigns descripted in the following refer to the [1] and [10] papers, in which the tests used in the numerical modeling as a benchmark are contained.

3.1 FRCM MECHANICAL CHARACTERIZATION

3.1.1 Material's Properties

Two different mortars were used in these experiments. The first was a high-strength mortar (M1), with an average cubic compressive strength f_{cc} of 93.55 MPa, and 14.26 MPa flexural tensile strength f_{ctf}. While a commercial second mortar (M2) had a 58.94 MPa f_{cc} and 7.02 MPa f_{ctf}. Their elastic moduli were 42.9 GPa and 28 GPa, for (M1) and (M2), respectively.

These experiments of the FRCM composite and their later simulations were describing its tensile behavior, thus the mortar's tensile strength was required. The Model Code 2010[11] proposed the α formula to evaluate the yield tensile strength, using either the flexural or compressive strengths. The evaluated tensile strengths of (M1) and (M2) were 6.31 MPa and 3.1 MPa, respectively, from the flexural strength. While the formula with the compressive strengths calculated a tensile ones of 4.59 MPa for M1 and 3.46 MPa for M2.

The alkali-resistant (AR) glass fabric was placed as one layer in the middle thickness of the mortar. Seven different samples of fabrics were used, as shown in Figure 2.2, with the geometric details in Table 2.1.

3.1.2 Plain Fabric Tensile Tests

Direct tensile tests were performed on 70 x 400 mm^2 samples of fabrics, following the setup shown in Figure 2.3. The fabrics' mechanical properties stated in Table 3.1, and their monotonic behavior in Figure 3.1, show that the fabrics F4 had the highest efficiency in both warp and weft directions; hence for this reason it was chosen to be modeled in this research.

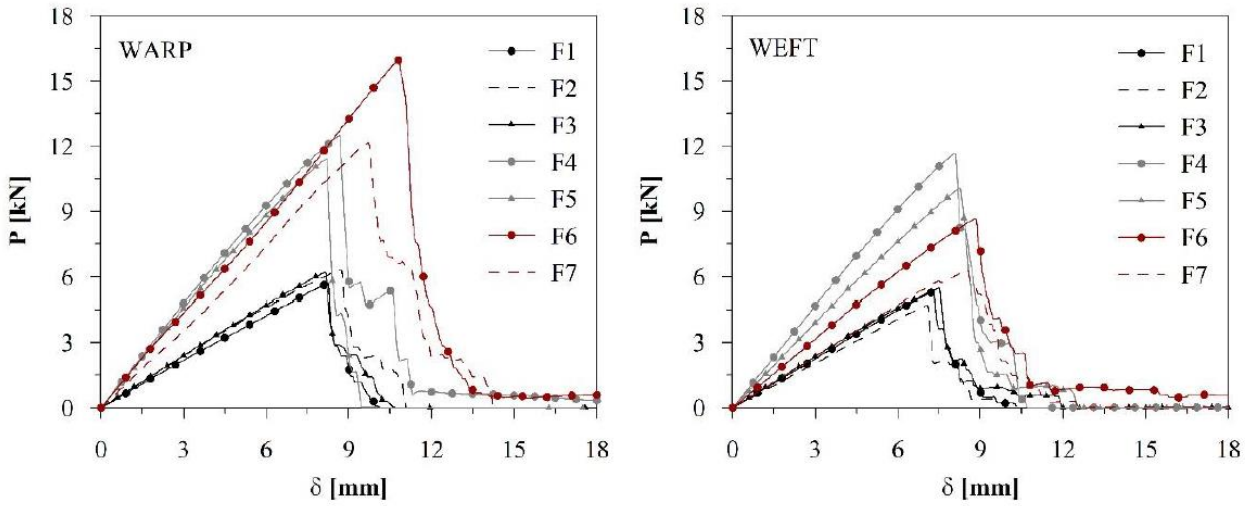

Figure 3.1 Load vs. displacement tensile response of fabrics in warp direction (left) and weft direction (right) [1]

		F1	F2	F3	F4	F5	F6	F7
Warp	A_f (mm^2)	3.582	3.582	3.582	7.164	7.164	12.537	12.537
	$P_{f,max,avg}$ (kN)	5.72	6.41	6.21	12.50*	11.44*	15.98	12.20*
	(std)	(0.27)	(0.29)	(0.31)	(0.67)	(0.63)	(0.15)	(0.20)
	(std%)	(4.80%)	(4.53%)	(4.92%)	(5.34%)	(5.48%)	(0.93%)	(1.63%)
	EF_f	0.80	0.89	0.87	0.87	0.80	0.64	0.49
Weft	A_f (mm^2)	3.582	3.582	3.582	7.164	7.164	5.373	4.478
	$P_{f,max,avg}$ (kN)	5.36	4.81	5.51	11.70	10.09*	8.69	6.34
	(std)	(0.27)	(0.33)	(0.76)	(0.75)	(0.82)	(0.71)	(0.41)
	(std%)	(5.13%)	(6.86%)	(13.78%)	(6.42%)	(8.09%)	(8.15%)	(6.40%)
	EF_f	0.75	0.67	0.77	0.82	0.70	0.81	0.71

Table 3.1 Mechanical properties of fabrics after the test's results, averaged on four samples [1]

3.1.3 FRCM Composite Tensile Tests

The same size of the fabrics samples was used for the composite, 70 x 400 mm^2, with the test setup shown in Figure 2.3. The composite gave a trilinear tensile response, Figure 3.2 and Figure 3.3, clearly showing the transition of the stress between the fabrics and the mortar in the second branch.

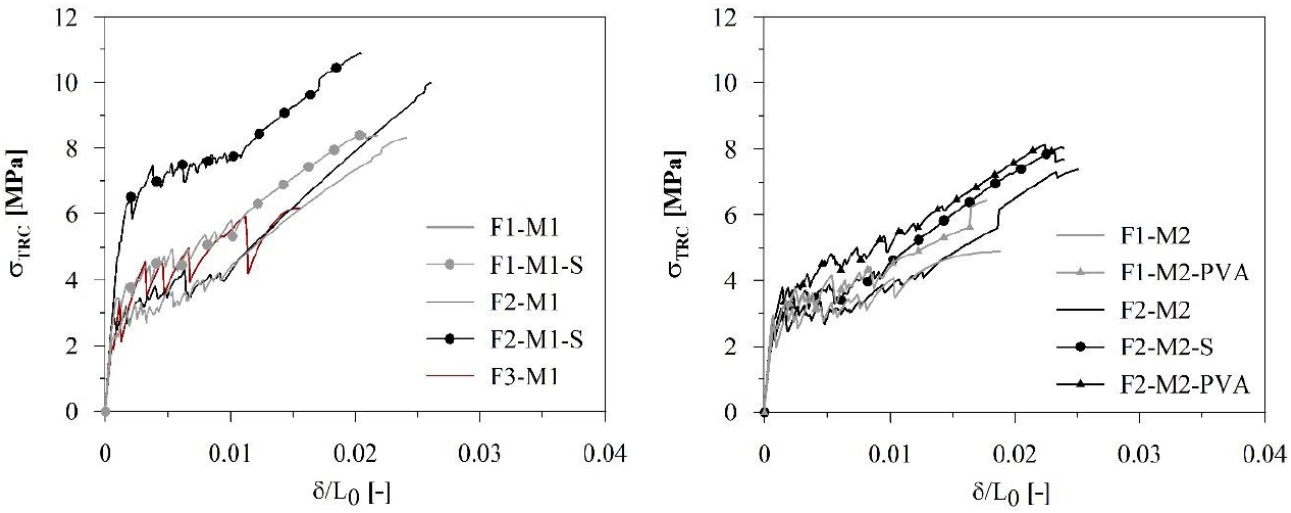

Figure 3.2 Stress vs. normalized displacement tensile response of the composites with M1 (left) and M2 (right) and fabrics from F1 to F3 [1]

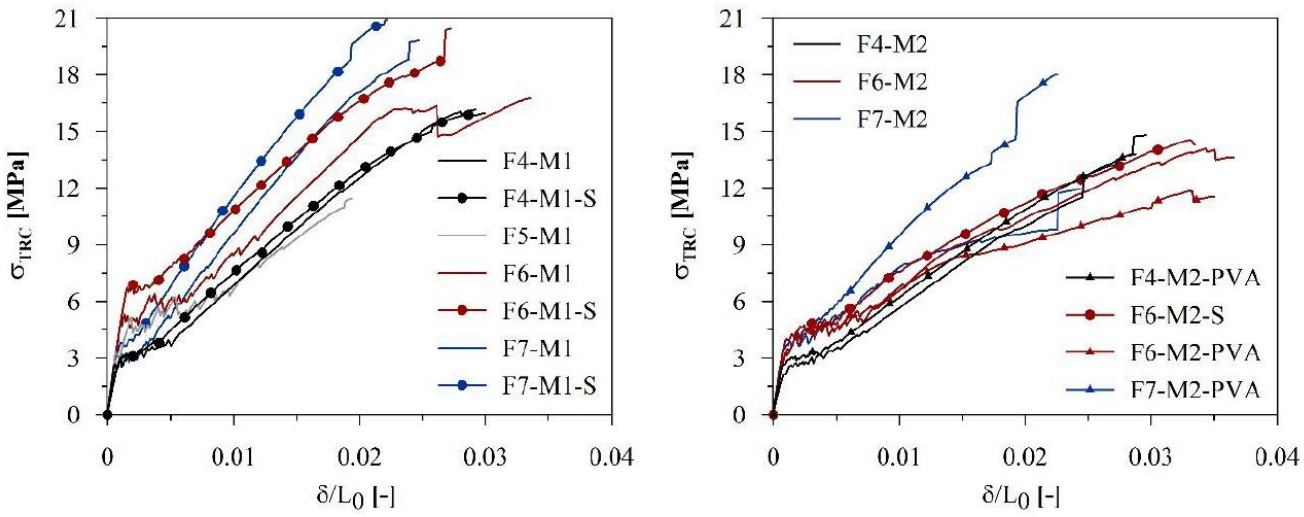

Figure 3.3 Stress vs. normalized displacement tensile response of the composites with M1 (left) and M2 (right) and fabrics from F4 to F7 [1]

Figure 3.4 of the composites reinforced with F4 and F5 fabrics, that had the same geometrical properties but different coating, gave a different cracking pattern, proving the effect of coating in this matter. The epoxy coated fabrics F4, allowed the composite to give a better behavior, exploiting a higher mortar capacity, also noticed in the tensile response's 2nd branch.

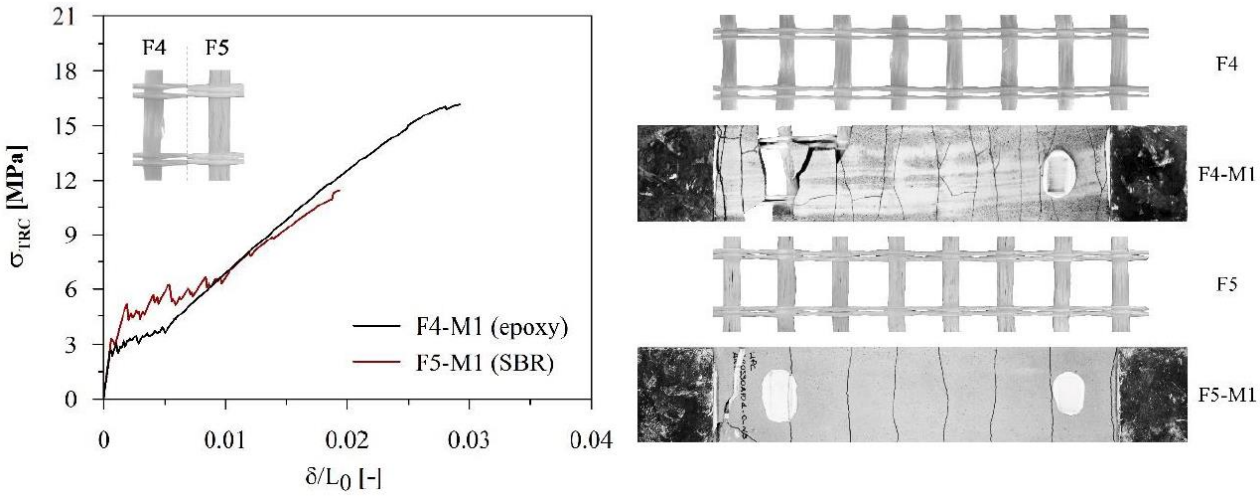

Figure 3.4 Different coating comparison of fabrics F4 and F5 in tensile response , with stress-strain results (left) and cracking pattern (right) [1]

3.2 SFRC MECHANICAL CHARACTERIZATION

3.2.1 Specimens Details

As a part of the experimental campaign reported in [10], fourteen 600 x 150 x 150 mm SFRC prismatic beams, with a mid-span 25 mm notch were tested in a three-point bending setup. The difference was with the curing age of the concrete, highlighting its effect on the strength, where five beams were tested after 34 days, other five at 167 days, and the last four at the end of the campaign at 220 days. The beams material's composite consisted of a 58 MPa average cubic compressive strength concrete, rebars of resulting 527 MPa yielding strength, and 35 kg/m^3 of double hooked, 60 mm long, short fibers with a 1500 MPa tensile strength. The short fibers provided the concrete with the capability of tension support with a higher number of cracks of narrower openings, achieved due to the short fibers' effect of higher ductility.

3.2.2 Experimental Setup and Results

The tests were performed with the Crack Mouth Opening Displacement (CMOD) control, measured at the notch's tip. The residual flexural strengths reported in Table 3.2 were reported, respectively, from 1 to 4, at CMOD equal to 0.5, 1.5, 2.5, and 3.5 mm, to characterize the post-peak residual strengths according to the Modal Code 2010 [11].

The results plotted in Figure 3.5 and reported in Table 3.2 highlight the evident increase of the post residual strength peaks, with the more extended curing period allowed.

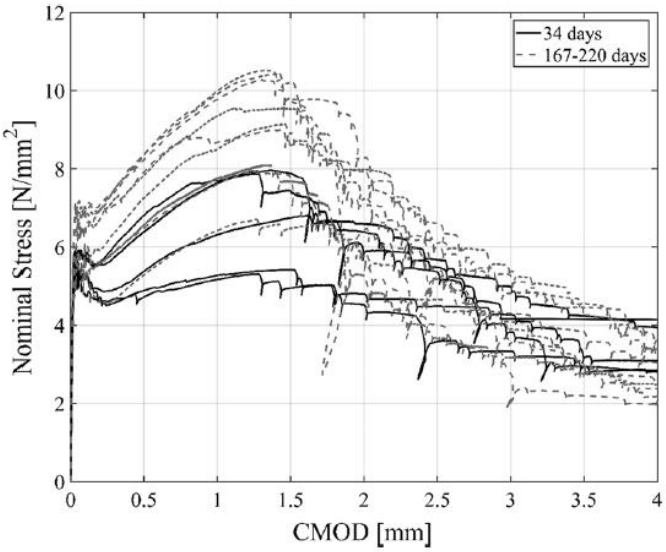

Figure 3.5 Test results with nominal stress vs. CMOD with different curing ages [10]

Group of specimens	f_{ct_fl}	$f_{R,1}$	$f_{R,2}$	$f_{R,3}$	$f_{R,4}$
34 (5 specimens)					
Mean	5.7	5.64	6.49	4.92	3.48
Std[a]	0.21	0.92	1.27	0.87	0.65
CV[b]	0.04	0.16	0.2	0.18	0.19
Charac-Normal[c]	5.21	3.48	3.54	2.88	1.96
Charac-LogN[d]	5.22	3.82	3.99	3.1	2.24
167 + 220 (9 specimens)					
Mean	6.32	7.36	8.73	5.2	3.39
Std	0.53	1.05	1.22	0.96	0.88
CV	0.08	0.14	0.14	0.18	0.26
Charac-Normal	5.28	5.3	6.34	3.32	1.67
Charac-LogN	5.34	5.39	6.48	3.5	1.97

[a]Standard deviation
[b]Coefficient of variation
[c]Characteristic value considering a normal distribution
[c]Characteristic value considering a log-normal distribution

Table 3.2 Stress values according to statistical parameters and curing age in MPa [10]

3.3 Reinforced SFRC Full Scale Experiments

3.3.1 Different Specimens Details

The FRCM composite, as described in the previous chapters, is used to retrofit damaged structural elements, with this research highlighting its usage with beams. Thus, the experiments in [12] aimed to show the effect of the addition of a FRCM reinforcing layer on SFRC beams, simulating a real reinforcement intervention. The first step is by testing two 350 x 1450 x 150 mm^3 SFRC beams, with the same materials specified in the previous section for the notched

beams. The beams were loaded with displacement control, on the top part with two knives, 450 mm apart, and a bottom measurement of the Crack Opening Displacement COD of 500 mm gauge length.

The pre-damaged beams were then reinforced from the bottom with a 20 mm thick and 350 mm wide FRCM. The reinforcing composite had the same details as the one described in 3.1.1, with (M2) mortar and a one layer of AR-glass F4 fabric. The composite was placed, with the warp parallel to the beam longitudinal direction. The beam was hydro-scarificated before the application of the FRCM, preventing a failure with delamination.

3.3.2 Pre-Damaged and Post-Reinforced Tests Results

The crack patterns shown in Figure 3.6 verify the ability of the FRCM to re-distribute the cracks with narrower ones around the previous beam cracks. Therefore, the reinforcement layer was able to better distribute and stabilize the beam's cracking mechanism.

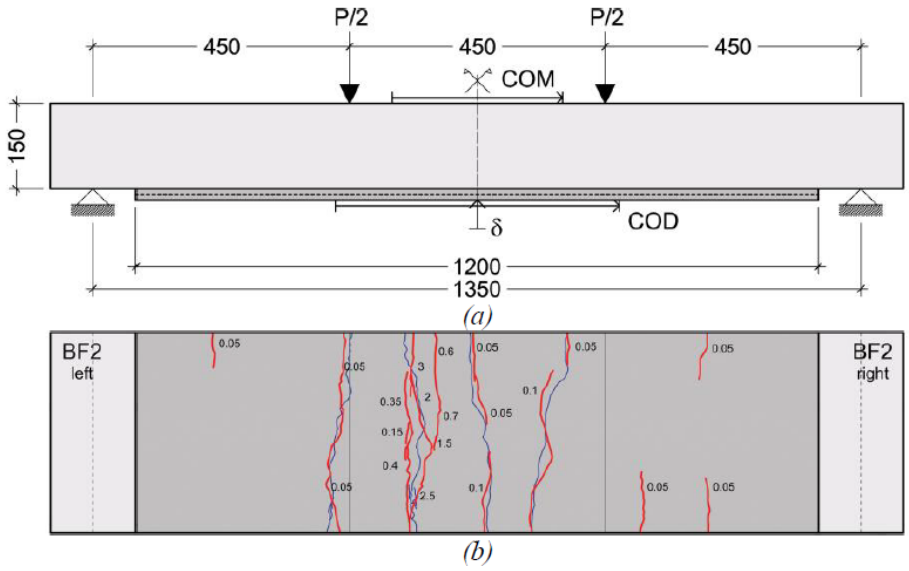

Figure 3.6 The bending test setup (a) and the cracking pattern on the bottom of the beam, blue for pre-damaged and red for post-reinforced beam, in mm [12]

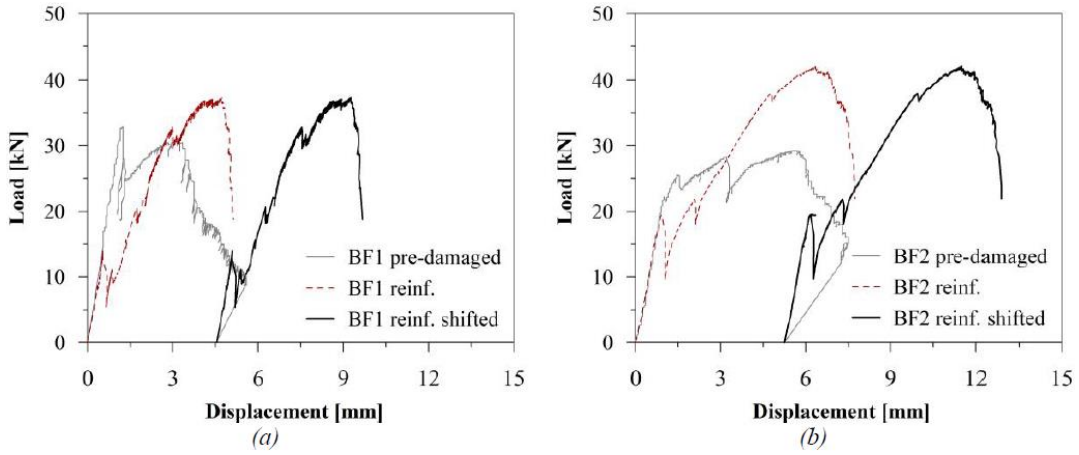

Figure 3.7 Load vs. mid-span displacement response of the pre-damaged and post-reinforced BF1 and BF2 beams [12]

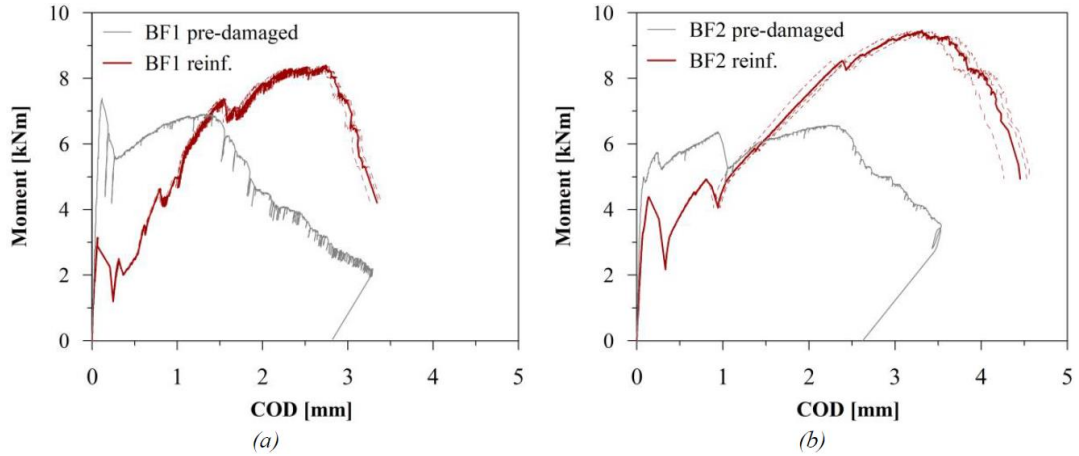

Figure 3.8 Moment vs. COD response of the pre-damaged and post-reinforced BF1 and BF2 beams [11]

As shown in Figure 3.7 and Figure 3.8, the FRCM reinforcement with only a 20 mm thick layer had great effects, by increasing the beams capacities with respect to not only the residual one, but also compared with the previous maximum. In addition to the recovery of the system's initial stiffness.

4 NUMERICAL MODELLING OF FRCM UNIAXIAL TENSILE TESTS

4.1 ABAQUS MODELLING

4.1.1 Modeling Approaches

Using the commercial nonlinear Finite Element FE software, ABAQUS, the FRCM model in the warp direction, 70 x 400 mm^2, was defined as a shell element, a 9 mm defined thickness. As suggested in [8], the two 50 mm edges of the model were modeled as a plain mortar with a perfectly elastic behavior, to reduce any stress concentration at the load application area. This was done in the experiments [1] by placing epoxy resin tabs on both sides of the edges, as shown in Figure 2.3. Thus, only the elastic modulus of the mortar and a passion ratio of 0.1 were used.

The 300 mm middle part of the model was modeled as fabrics reinforced mortar, with two different approaches, increasing their complexity and preciseness, A and B. These two models are explicitly explained in [8].

The simple approach, Model A, is defining the mortar and the reinforcement as one homogenous material. The elastic behavior was defined by a plain mortar, and a post behavior definition of the Concrete damage Plasticity CDP with a tensile behavior, evaluated from the revised ACK [1], as stress- cracking strain law, Figure 4.1. The model will simulate this behavior is in the warp direction, the strong direction only.

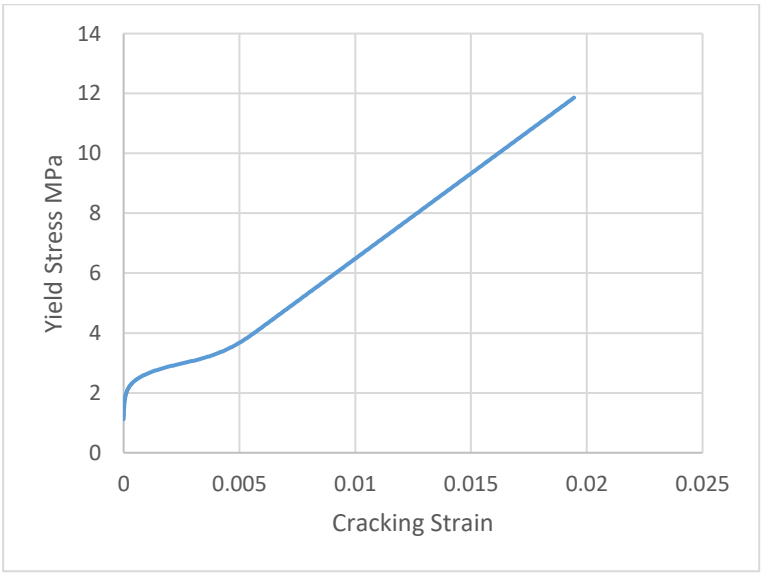

Figure 4.1 The revised ACK law of the M2 mortar and F4 fabrics tensile behavior

The more complicated and time-consuming approach of model B was done by defining the middle section with two different materials, as a continuum shell model with embedded rebars, which represent the wires of the fabric. The mortar with a post-peak behavior definition with CDP, where its tensile behavior parameters are only its fictitious yield stress and the facture energy, a parameter to be highlighted afterwards. The fabrics are defined as two different materials, in the weft and the warp directions, with an elastic and fragile behavior. Then shell section was then defined with the mortar as a base material and two reinforcement layers parallel and perpendicular to the longitudinal direction of the composite (warp and weft).

The reinforcement is defined with the glass fabrics area and their spacing, as shown in Table 2.1 and Table 2.2. The composite's number of lines in the width was two, with the area of a single bar equal to 3.889 mm^2, and a spacing of 38 mm.

The modeling is performed to simulate the F4 fabrics [1] FRCM composite with both mortars (M1) and (M2) with model B, and only (M2) with model A. Their mechanical properties are defined in 3.1.1 and summarized in Table 4.1. The fictitious cracking stress of (M2) used was the one evaluated from the bending test, 3.1 MPa. In the case of (M1), two values were used, starting with the cracking yield stress from the bending test, 6.31 MPa, which gave higher peaks, thus a second case was produced with the stress evaluated from the compression test, 4.59 MPa.

The viscosity parameter defined in ABAQUS CDP behavior is highly required in this model since it allows the test's full convergent performance. It is merely viscous-plasticity, allowing stresses, for a particular increment time, to be outside the yield surface [13], thus, not failing at the first critical point. This model's second branch is highly present with the cracking and stress transition between the mortar and the fabrics, coming along with a significant calculation time reduction with the increase of this parameter.

The compressive behavior defined in Table 4.1 with inserting a fictitious inelastic strain, from zero to five, at the same stress level. Hence not allowing any change of behavior in compression, which does not affect the model results since it is a uniaxial tensile one.

	M1	M2
Elastic		
Young Modulus E	42900	28000
Poisson's Ratio ν	0.2	0.2
CDP Plasticity		
Dilation Angle	38°	
Eccentricity	0.1	
fb0/fc0	1.16	
K	0.67	
Viscosity	1.00E-06	
CDP Compressive		
Yield Stress	93	50
CDP Tensile Model A		
Yield Stress – Cracking Strain	-	From ACK
CDP Tensile Model B		
Yield Stress	6.31 & 4.59	3.1
Fracture Energy	From the Model Code	

Table 4.1 Material defining parameters in ABAQUS of M1 & M2, stresses in MPa

As for the fabrics F4, their elastic modulus provided by the manufacturer was 70 MPa, but as it was proved, with the experiments in [1], they were not fully effective, according to the efficiency factor, equation (1). Hence this factor, 0.87 and 0.82 for warp and weft, respectively, was multiplied by the modulus of elasticity, giving input 60.9 GPa for warp and 57.4 MPa for weft, along with a Poisson's ratio of 0.1. The plastic behavior was defined as a fictitious linear one, by highly decreasing the stress with an almost zero value of plastic strain, after the yield stress of the transition to the plastic zone.

The model was supported from one side and loaded from the other, Figure 4.2, by applying a displacement load equal and increasing linearly with time increment.

Figure 4.2 FRCM ABAQUS model, loading scheme

4.1.2 Fracture Energy

One of the most critical parameters highlighted in the model B case was the fracture energy GF. It is defined as sufficient energy needed for a unit area tensile crack propagation [11]. In simpler words, it can be described as the area under strain – crack opening curve, Figure 4.3.

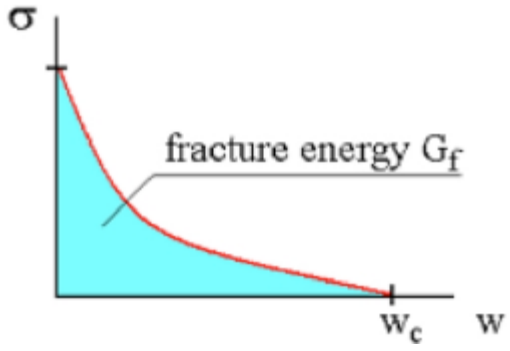

Figure 4.3 Strain - Crack Opening curve defining GF [11]

The Model Codes 1990 and 2010 gave different formulas to approach the correct GF. Since it depends on the crack of a unit area, and these models are FE with different meshes, leading to different element areas, a need is present to calibrate the GF values with the different meshes. Therefore, the MC values, Table 4.2, are not directly used in the proceeding chapters.

$$GF = 73 \,.\, f_{cm}{}^{0.18} \quad [N/m] \tag{2}$$

$$GF = GF_0 \,.\, \left(\frac{f_{cm}}{f_{cm0}}\right)^{0.7} \quad [N/m] \tag{3}$$

The f_{cm} used in both equations, (2) of the Model Code 2010 and (3) of the 1990 one, was the mean compressive yield strength of the mortar, 93.55 MPa, and 58.94 MPa for (M1) and (M2), respectively. Where f_{cm0} is 10 MPa as given by the code, and GF_0 is 0.025 N/m defined by the code for aggregate diameter size less than 8 mm. The final values for both mortars are summarized in Table 4.2.

	M1	**M2**
Model Code 2010 GF	0.165	0.152
Model Code 1990 GF	0.119	0.086

Table 4.2 GF of M1 and M2, evaluated from the Model Codes 2010 & 1990

To find the perfect GF that fits the model and give the most accurate results of the same mortar and mesh, a parametric analysis should be performed. The first attempts were usually

of 11 values of GF, the one of the Model Code 1990, and 10 values ranging from 10% to 100% of the Model Code 2010. Therefore, this analysis was done with the four combinations of a fine or a rough mesh of M1-based or M2-based FRCM model.

4.1.3 Different Meshes

The accuracy of the model results was an essential factor, yet the calculation time cost should be reduced to the least possible to grant sufficiently accurate results. This type of models, especially with the model B approach, required a massive amount of time to finish one model, where it was reaching 4 hours, mostly caused by the 2nd branch of the behavior. Since the stress transition and cracking of the mortar is a very detailed process.

Due to the previous reasons, it was essential to model each case with two different meshes, a rough and a fine one, then compare both the results with the experimental data. If the rough mesh gave sufficient accuracy, it could be used in the reinforced beam model, with a reduced calculation time. The two meshes shown in Figure 4.4 & Figure 4.5 were created as a square element's size around 15 mm and 5 mm, for the rough and fine mesh, respectively. These results were reached after a quick check and calibration of the meshes with a decreasing tendency from 30 mm to finally reach the used ones.

The mesh element type in both approaches, model A and B, was S4R with the linear reduced integration, and a quadrilateral shell shape.

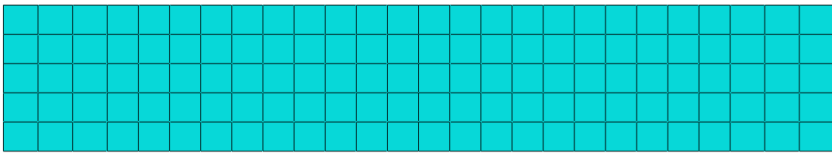

Figure 4.4 The "Rough" mesh of the FRCM ABAQUS model

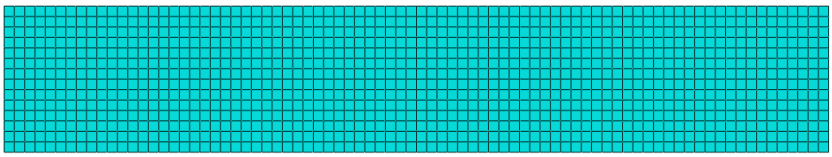

Figure 4.5 The " Fine" mesh of the FRCM ABAQUS model

4.2 Results of the Homogenous Model Approach of FRCM

The results are graphically plotted, along with the experimental results, which were of three specimens. They were plotted with stress vs. strain representation; hence some calculations were made to evaluate them.

The horizontal displacement (COD) of the two middle nodes of the edges of the 300 mm part of the model, were reported and then subtracted. The strain is evaluated by dividing the subtracted value by the total length, 300 mm.

The summation of the supports horizontal reaction forces represents the total applied load. Thus, the stress is calculated by dividing the total force by the cross-sectional area, 70 x 9 mm^2.

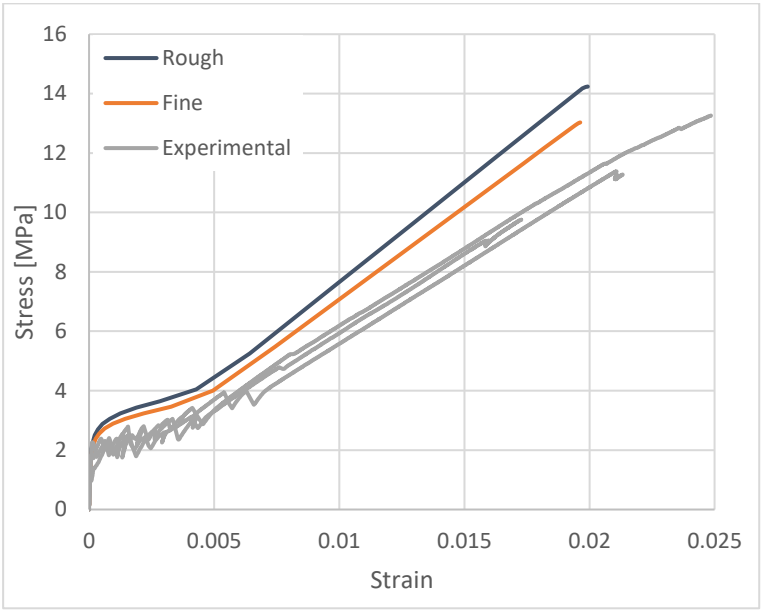

Figure 4.6 Stress vs. Strain response of the experimental results, and numerical modal A with "Fine" and "Rough" meshes, of FRCM composite, fabrics F4 and mortar M2

The simplified approach model gave good results, Figure 4.6, as the three branches of the trilinear response are delivered. The response followed the experimental transition phases, even though the second branch does not show the jumps of the stress transition between the mortar and the fabrics. It was expressed by a smooth curve behavior, which is explained in Figure 4.7 with the perfect homogenous numerical plastic strain. The first branch's stiffness was achieved, and the strain, and almost the stress, of the inflection point between the second and third branches.

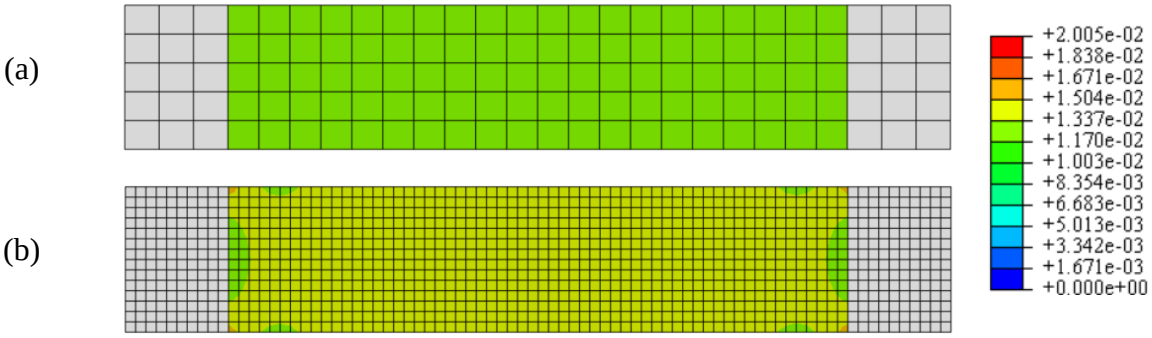

Figure 4.7 Plastic strain, max in-plane principal, contour plots at 1% strain of FRCM, fabrics F4 and mortar M2, model A, with "Rough" mesh (a); and "Fine" mesh (b) (with the same legend for both cases)

Regarding the meshes' performances, even with good results of the rough mesh, but the fine mesh provided the first peak closer to the experimental ones, the same as the final branch slope of the pure fabric's behavior.

Therefore, this modeling approach proved its validity, along with its simplicity and much less calculation cost time. Hence it can be used for general simplified approaches of the FRCM beam reinforcement.

4.3 Results of the Continuum Shell Model with Embedded Rebar Approach

In addition to the evaluation of the stress vs. strain results, the load application was the same as explained in section 4.2 for the modeling with model A approach.

4.3.1 M1-Based FRCM Model

As a first attempt, the tensile strength was evaluated from the experimental bending one, as explained in section 4.1.1, with a value of 6.31 MPa.

First, the modeling was performed on a rough mesh with a range, 10% to 100% of the MC2010 GF, in addition to the MC90 GF. Then modeling with a fine mesh was done with MC2010 GF ranging from 60% to 100%, and the MC90 one. The range was reduced in the fine mesh case since lower GF values could not provide the model's post-cracking response.

Figure 4.8 shows that GF's lower values provided a good response, especially in the 2nd branch where the peaks, and the strain of the transition to the 3rd branch are close to experimental ones. Nevertheless, the model's first cracking stress were almost two times the experimental one for all the GF range responses. While the results with a GF higher than 40%, including the MC90 representing 72% of the MC2010 GF, maintained the high stresses all over the 2nd branch and extending it to a higher strain value before the 3rd branch. Figure 4.9 shows

the plastic strain distribution with all GF values, which shows the rough mesh's problem in such representations. This might be related to the high cracking stress influence. In addition to the measurement that was at 1% strain, to the usage of one legend for the rough and fine mesh representations.

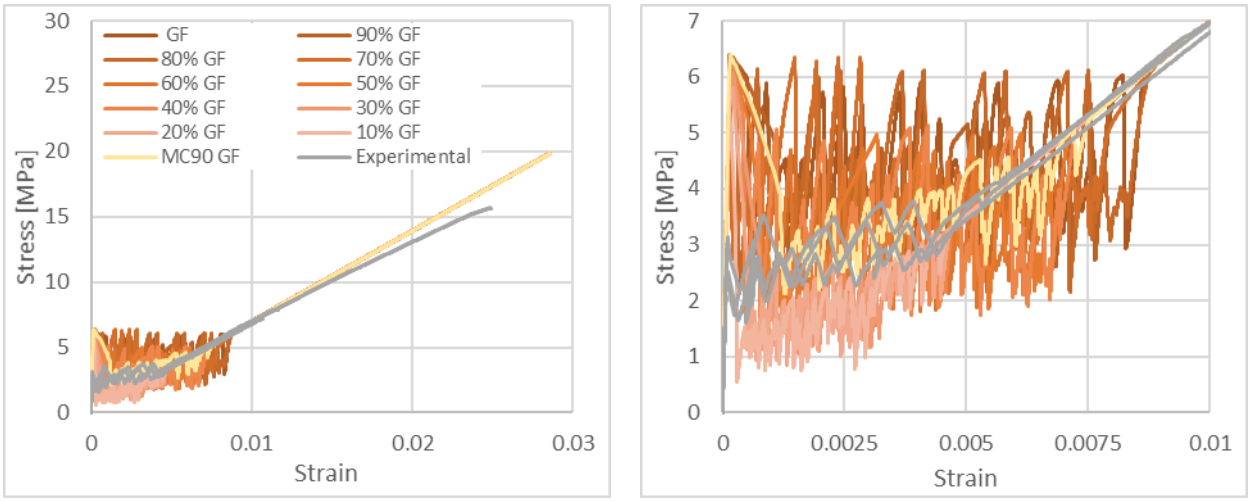

(a) (b)

Figure 4.8 FRCM composite model B "Rough" mesh and the experimental results of F4 fabrics and M1 mortar, with a tensile strength calculated from the bending tests, full response (a); and zoomed at the second branch (with the same legends) (b)

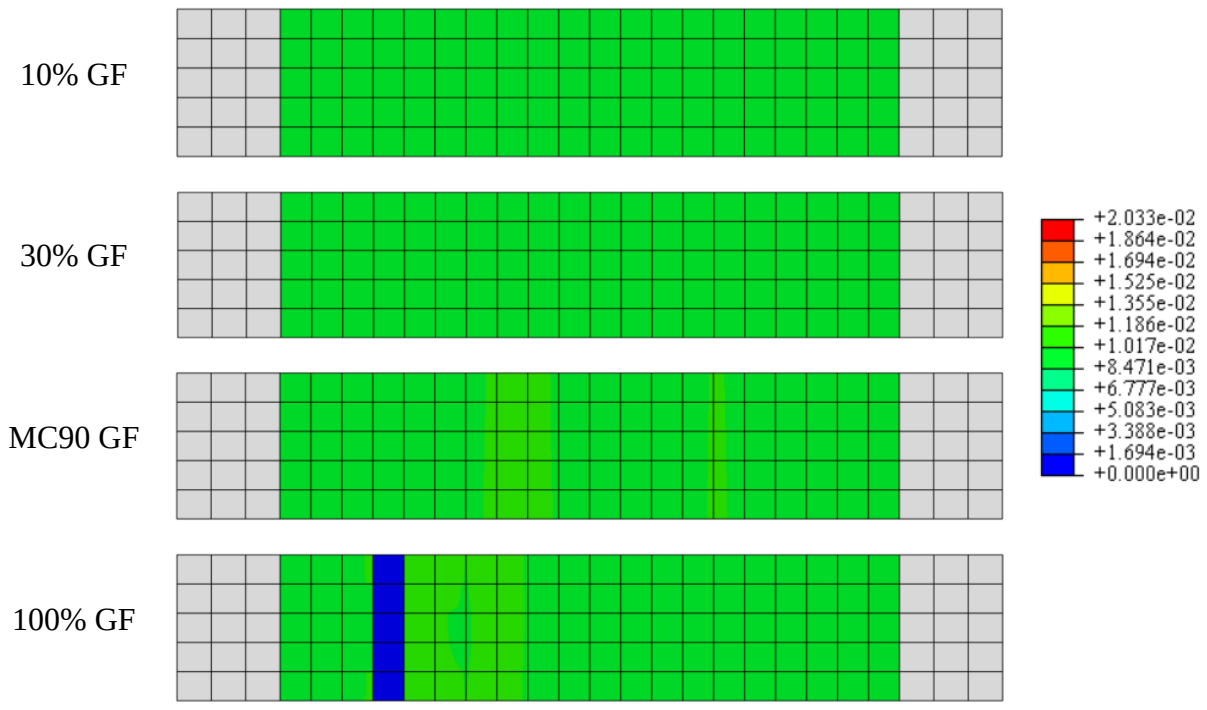

Figure 4.9 Plastic strain, max in-plane principal, contour plots at 1% strain of FRCM, fabrics F4 and mortar M1, model B, tensile strength from bending tests, with a "Rough" mesh, where GF is referred to as the MC2010 value (with the same legend for all cases)

To show that the numerical plastic strain distribution was not homogenous in the rough mesh as the simplified approach, a measurement at different strain was taken for what was

found a good GF value, 30% of the MC2010 case. Figure 4.10 shows the better plastic strain distribution and good evaluation.

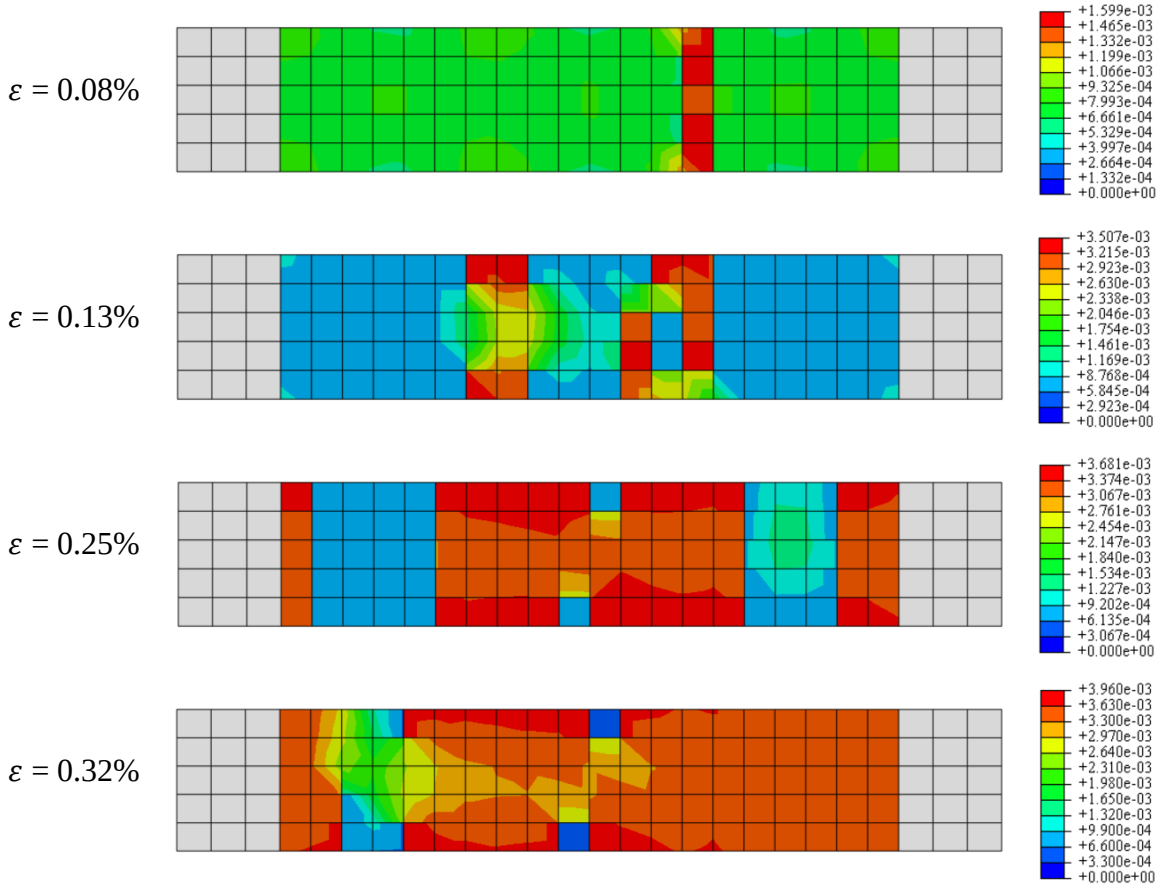

Figure 4.10 Plastic strain, max in-plane principal, contour plots at different strain values of FRCM, fabrics F4 and mortar M1, model B with 30% of MC2010 GF, and the tensile strength from bending tests, with a "Rough" mesh

The fine mesh of M1 FRCM could not replicate the experimental specimens' response, caused by the high f_{ct} value used, Figure 4.11. The cracking stress was higher and almost double the reference ones and maintained high in the 2nd branch. In addition to a different second branch response regarding its strain at the transition with the third one. As for higher values of GF to reach the MC2010 one, the response was losing the 2nd branch jumps, simplifying the stress transition between the mortar and fabrics to provide a simple linear branch as the model A one. But in this case because of the high tensile strength, it is very different from the experimental one, where model A response was able to give the same response with a simplified curve.

Figure 4.12 demonstrates the localized plastic strain's gradual loss by increasing the GF as it becomes closer to a uniform distribution. Moreover, the fine mesh provided a better cracking pattern, then the rough mesh model.

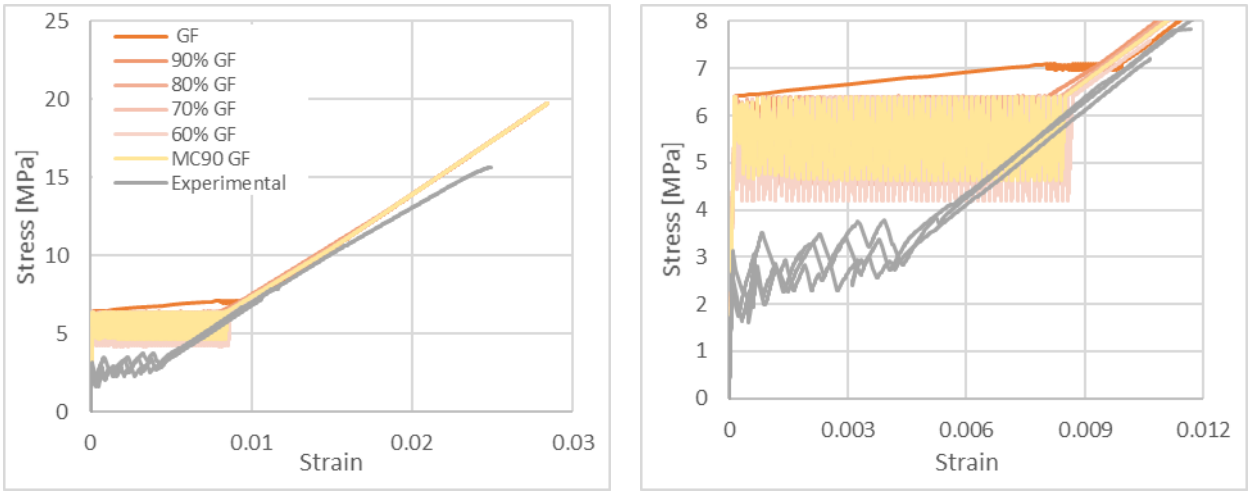

Figure 4.11 FRCM composite model B "Fine" mesh and the experimental results of F4 fabrics and M1 mortar, with a tensile strength calculated from the bending tests, full response (a); and zoomed at the second branch (with the same legends) (b)

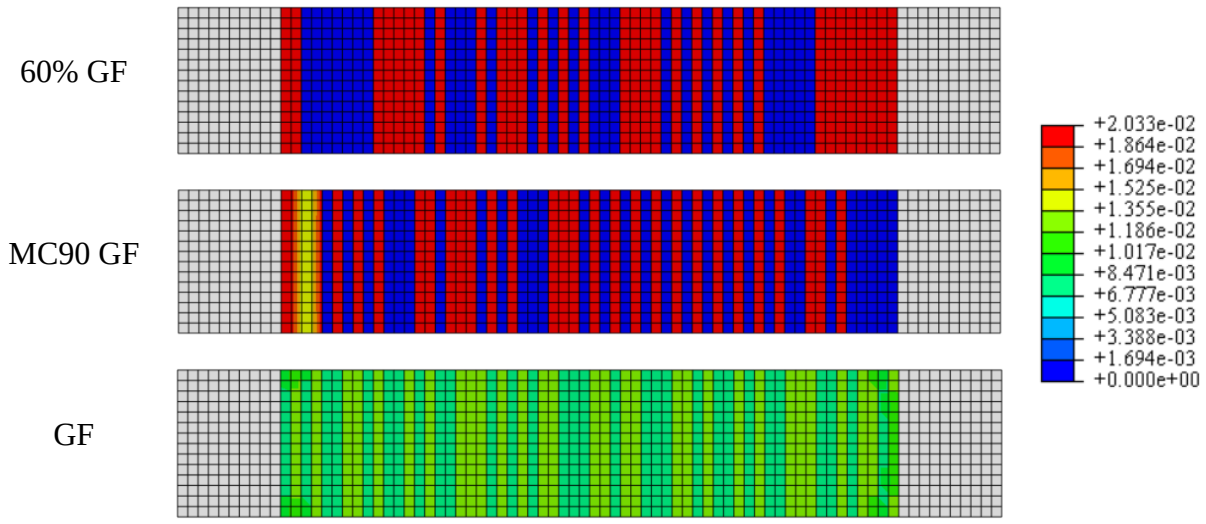

Figure 4.12 Plastic strain, max in-plane principal, contour plots at 1% strain of FRCM, fabrics F4 and mortar M1, model B, tensile strength from bending tests, with a "Fine" mesh, where GF is referred to as the MC2010 value (with the same legend for all cases)

Both the cases, fine and rough meshes, proved that the tensile strength used in the first attempt was overestimated; hence the one calculated from the compressive strength, equal to 4.59 MPa, should give better results, especially for the cases of small values of GF with a rough mesh, as the response was good enough, except the cracking stress value.

The model with the 4.59 MPa cracking strength and a rough mesh was executed with a lower range, 15% to 40% at 5% increment of MC2010 GF, hence without the MC90, since good results were provided previously at this range.

The rough mesh model results with the new cracking stress, Figure 4.13, shows an improvement in the model's response, as was able to deliver a closer cracking stress and maintain the stress range in the second branch close to the experimental one. This case showed that a GF between 25% and 35% was good value providing a similar response to the experimental one, especially with the strain at the end of the 2nd branch.

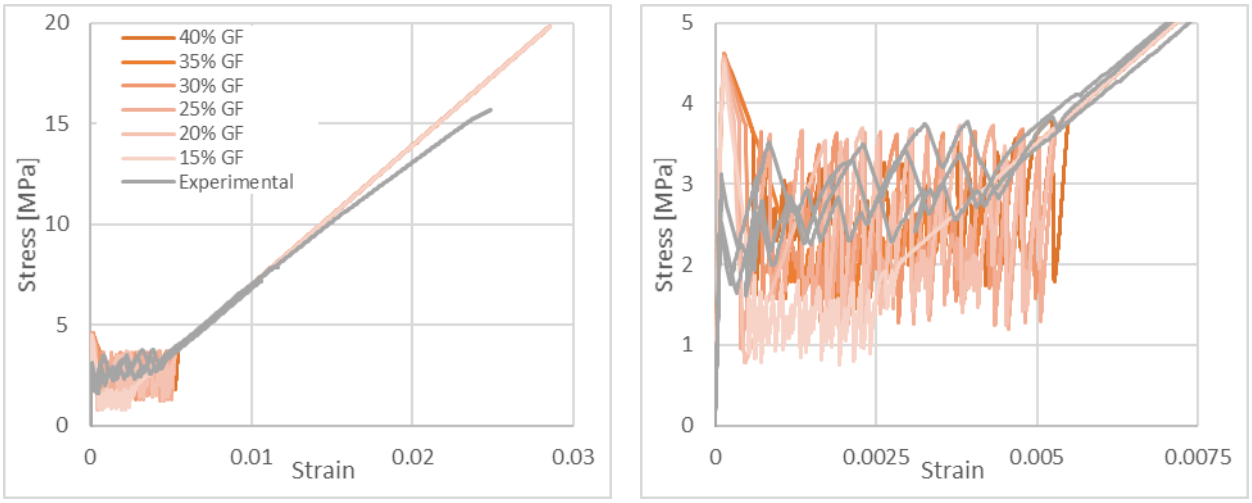

(a) (b)

Figure 4.13 FRCM composite model B "Rough" mesh and the experimental results of F4 fabrics and M1 mortar, with a tensile strength calculated from the compressive tests, full response (a); and zoomed at the second branch (with the same legends) (b)

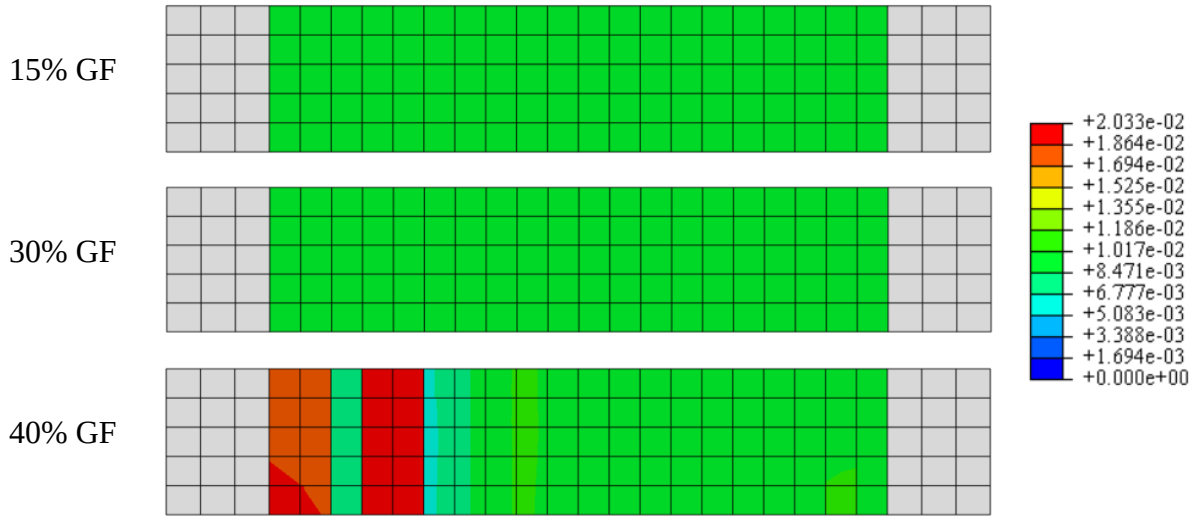

Figure 4.14 Plastic strain, max in-plane principal, contour plots at 1% strain of FRCM, fabrics F4 and mortar M1, model B, tensile strength from compressive tests, with a "Rough" mesh, where GF is referred to as the MC2010 value (with the same legend for all cases)

In Figure 4.14 the numerical plastic strain distribution plotted with the same legend and at the 1% strain as Figure 4.9 of the previous attempt, showed a general similar values of the plastic stain. While, with the plots of different legends and strain, Figure 4.15, of one GF case,

30% of MC2010, showed a better distribution and localization than the one with higher f_{ct}, Figure 4.10.

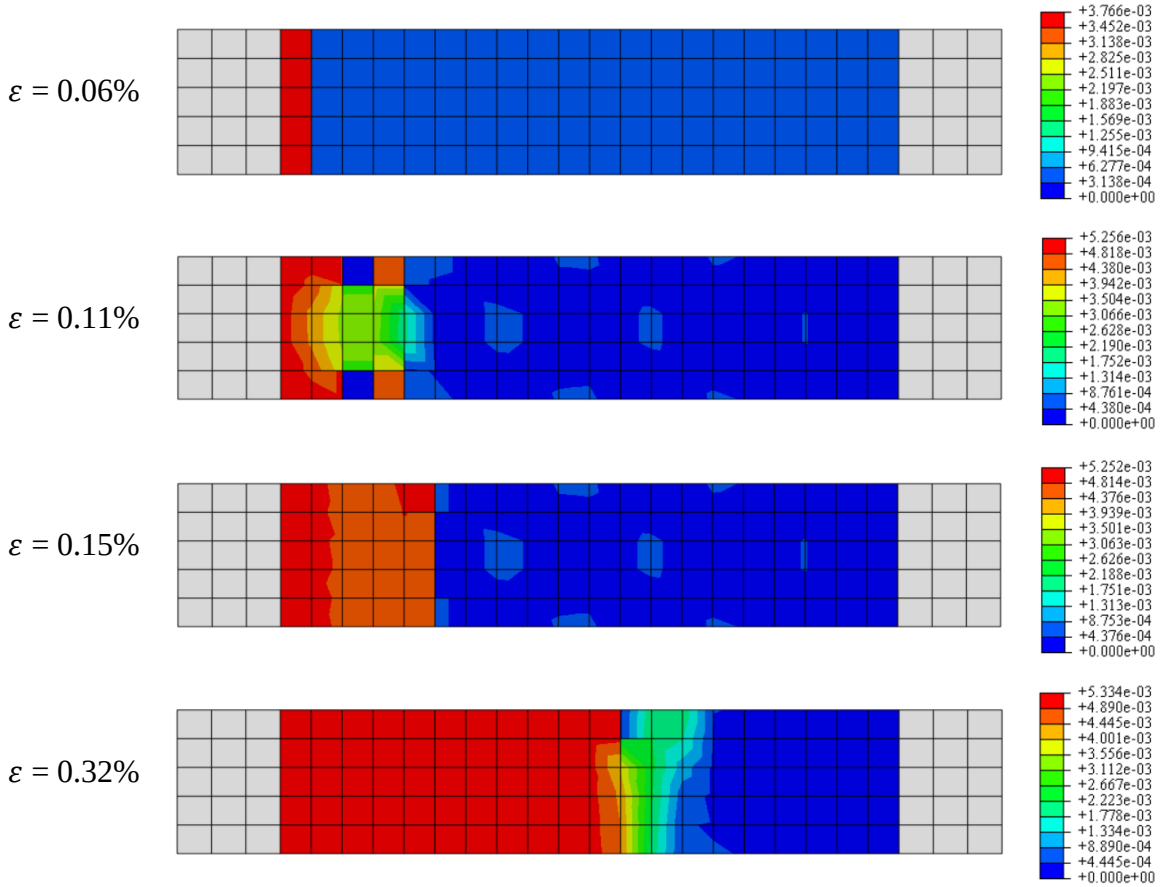

Figure 4.15 Plastic strain, max in-plane principal, contour plots at different strain values of FRCM, fabrics F4 and mortar M1, model B with 30% of MC2010 GF, and the tensile strength from compressive tests, with a "Rough" mesh

Figure 4.16 proves that the response with high cracking strength from bending tests had a much higher stress and with higher strain values at the end of the second branch. This compared with the lower strength value results, from the compressive tests, simulating better the experimental response. However, Figure 4.17 proves that the different tensile strength had some effects related to the numerical plastic strain distribution, as the model with the lower f_{ct} was able to give a better distribution.

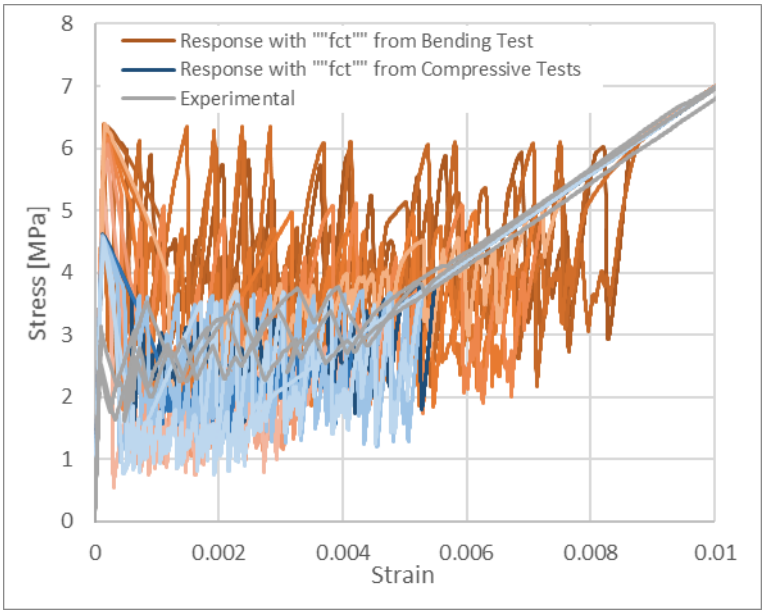

Figure 4.16 Stress vs. Strain comparison of "Rough" mesh models response with a tensile strength evaluated from bending or compressive tests of FRCM composite, F4 fabrics, and M1 mortar, zoomed at the second branch

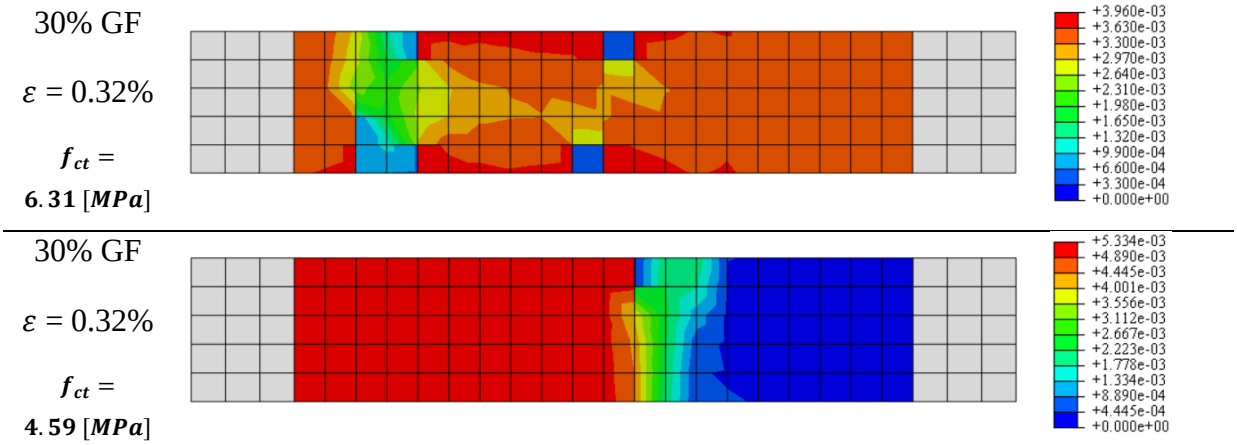

Figure 4.17 Plastic strain, max in-plane principal, contour plots at different strain of FRCM, fabrics F4 and mortar M1, model B, "Rough" mesh and 30% of MC2010 GF, comparing the model with tensile strength from bending tests (a); and the one from compressive tests (b)

The fine mesh of this model was implemented with a range of GF, 35% to 60% of the MC2010 one, with an increment of 5%, as the lower values could not give the full response, and with the higher values the 2nd branch was being more simplified and incorrect. As shown in Figure 4.18, this fine mesh results confirm that this model is better represented with a more rough mesh, like the one performed before, as this mesh was giving a different second branch response, higher values of stress and strain, same as the fine mesh case with the higher tensile strength.

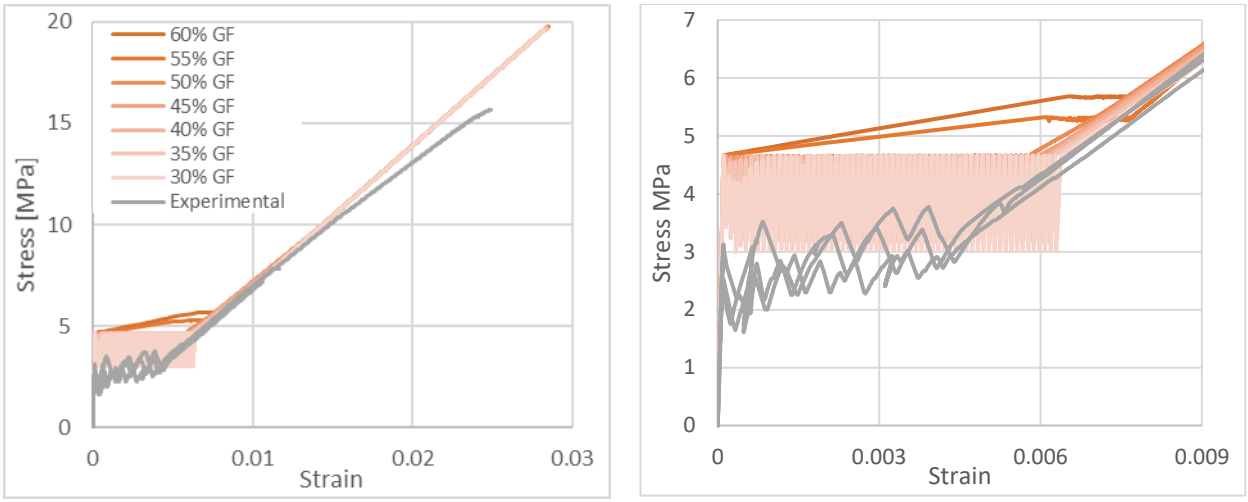

(a) (b)

Figure 4.18 FRCM composite model B "Fine" mesh and the experimental results of F4 fabrics and M1 mortar, with a tensile strength calculated from the compressive tests, full response (a); and zoomed at the second branch (with the same legends) (b)

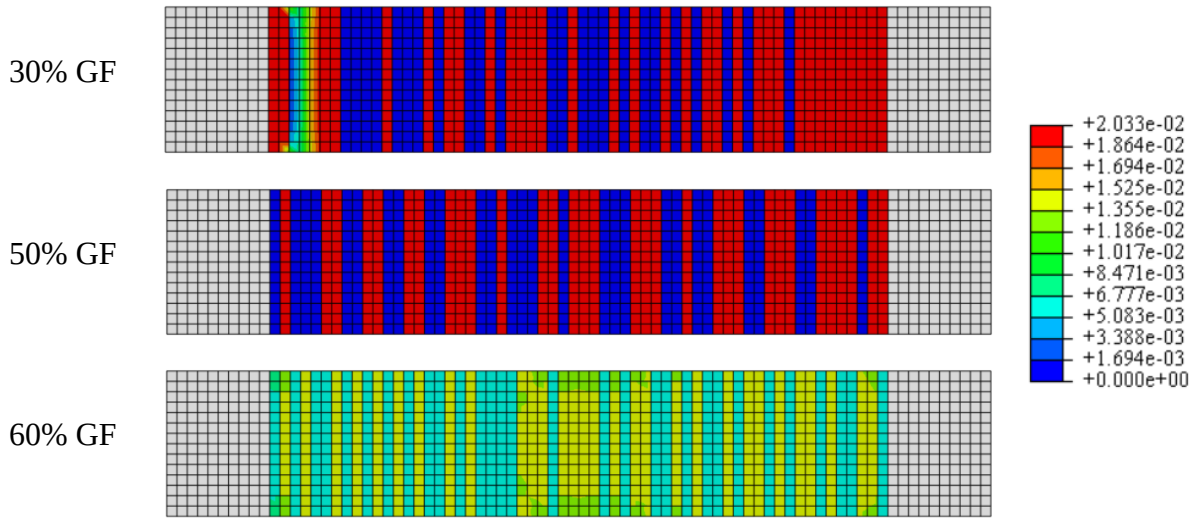

Figure 4.19 Plastic strain, max in-plane principal, contour plots at 1% strain of FRCM, fabrics F4 and mortar M1, model B, tensile strength from compressive tests, with a "Fine" mesh, with 30% of MC2010 GF (a); 50% of MC2010 GF (b); and 60% of MC2010 GF (c)

While, referring to the plastic strains, Figure 4.19, the fine meshes provided a better localized results and tended to diffuse it more with higher GF values. This was not enough to choose the fine mesh, as the stress-strain plots showed a very different results, in addition to the higher calculation cost time with the fine meshes.

To better highlight, the comparison with the different models concerning the cracking strength value, Figure 4.20, confirms that the value evaluated from the bending tests was highly overestimated.

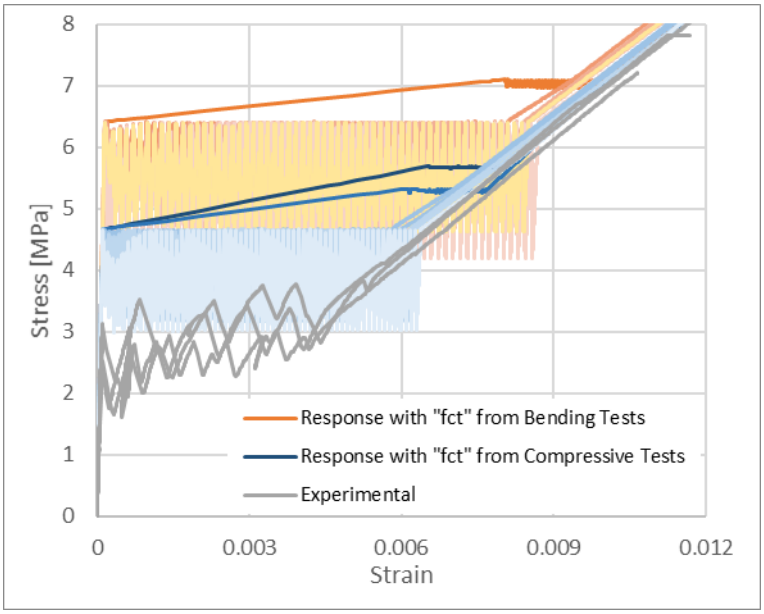

Figure 4.20 Stress vs. Strain comparison of "Fine" mesh models response with a tensile strength evaluated from bending or compressive tests, of FRCM composite, F4 fabrics, and M1 mortar, zoomed at the second branch

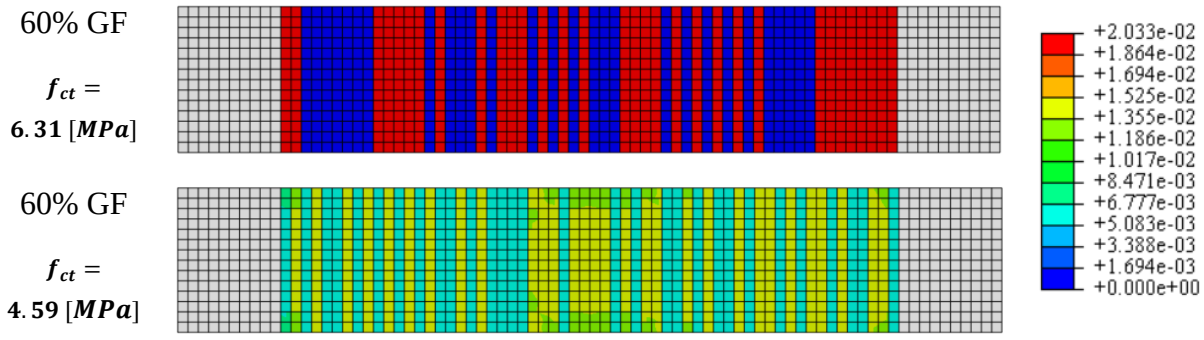

Figure 4.21 Plastic strain, max in-plane principal, contour plots at 1% strain of FRCM, fabrics F4 and mortar M1, model B, "Fine" mesh and 30% of MC2010 GF, comparing the model with tensile strength from bending tests (a); and the one from compressive tests (b) (with same legends for both cases)

An interesting comparison in Figure 4.21 is a lower localizing values distributed with the same GF and lower f_{ct}.

Figure 4.22 confirms the rough mesh's better response, compared with the fine one, as it better fits the experimental results.

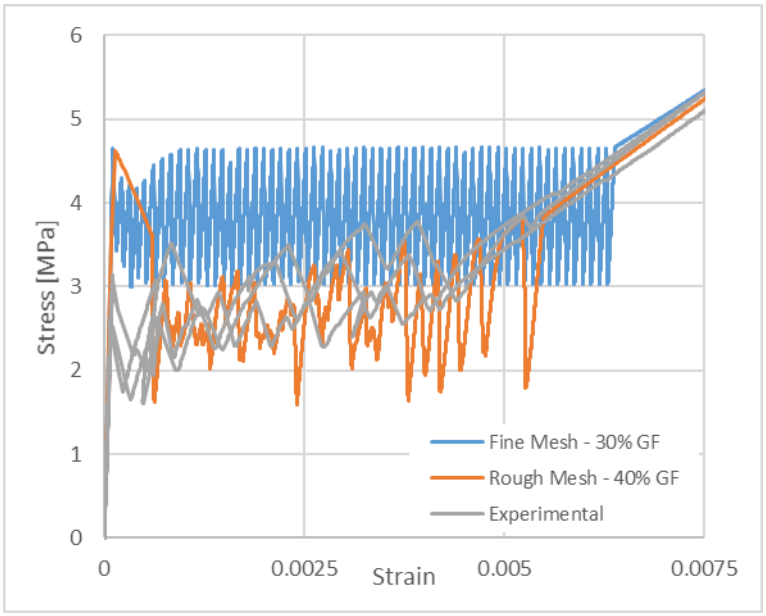

Figure 4.22 "Rough" and "Fine" meshes best responses compared with the experimental ones, of FRCM composites, model B, F4 fabrics and M1 mortar with the tensile strength evaluated from compressive tests, zoomed at the second branch

Therefore, the best method to model the FRCM composite with F4 fabrics and M1 mortar, using a continuum shell model with embedded rebar approach, model B, was with a mesh of 15 x 15 mm^2 element size, a cracking strength calculated from the compressive tests, equal to 4.59 MPa, and finally a fracture energy value with 40% of the MC2010 value, 0.066 N/mm.

4.3.2 M2-Based FRCM Model

This model was created according to the details explained in section 4.1.1, with the same loading and results extraction as the previous models.

The rough mesh model performed with eleven different GF parameters, from 10% to 100% of the MC2010 value, 0.152 N/mm and the MC90, 0.086 N/mm. While the fine mesh model was done with only three values, 20%,25%, and 30% of the MC2010 value, since lower values failed at the cracking stress, and higher values gave unsuitable results.

Figure 4.23 of the rough mesh model shows promising results with GFs ranging from 30% to 50% of the MC2010, as they were able to give good peak stress values. Also, the end of the 2^{nd} branch had a strain value close to the experimental one.

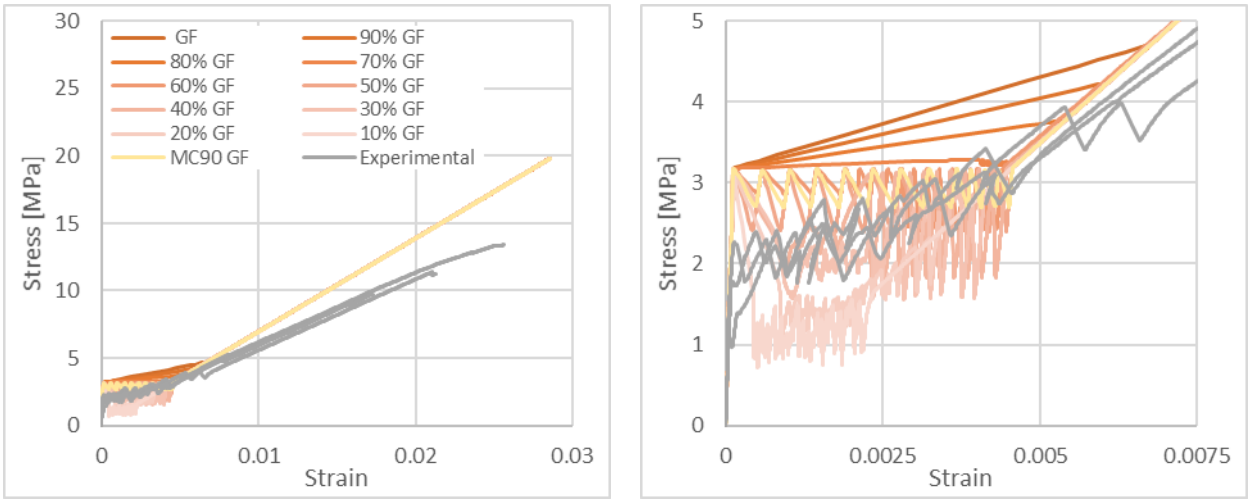

(a) (b)

Figure 4.23 FRCM composite model B "Rough" mesh and the experimental results of F4 fabrics and M2 mortar, full response (a); and zoomed at the second branch (with the same legends) (b)

Dissimilar to the fine mesh model of the FRCM with mortar M1, the response of the one with mortar M2 was well-replicated with the experimental one, probably this was caused by the better tensile strength estimation for this different mortar. As Figure 4.24 shows that the model with a 20% GF of the MC2010 gave almost perfect results. Where the 25% and 30% responses proved that their GF value is high enough to simplify the 2nd branch and lose the good behavior with the experimental one.

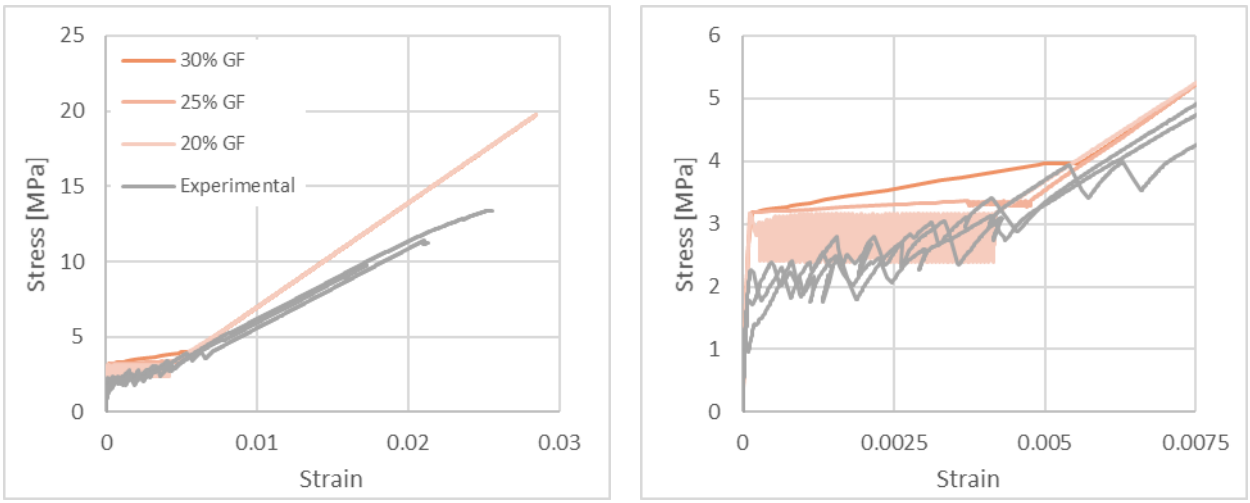

(a) (b)

Figure 4.24 FRCM composite model B "Fine" mesh and the experimental results of F4 fabrics and M2 mortar, full response (a); and zoomed at the second branch (with the same legends) (b)

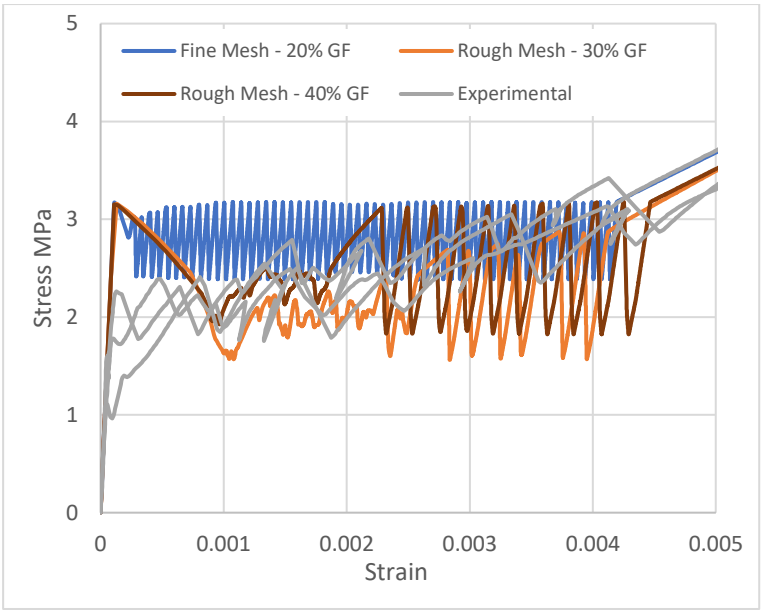

Figure 4.25 "Rough" and "Fine" meshes best responses compared with the experimental ones, of FRCM composites, model B, F4 fabrics and M2 mortar, zoomed at the second branch

Figure 4.25 illustrates that the rough mesh results represent the FRCM composite even better than the fine mesh one, and this can be explained by the high dependence of the results with GF on the mesh. Thus, the rough mesh was chosen to model the FRCM composite for the following modeling of the beam reinforcement, with two advantages. The first is the excellent response compared with the experimental one, and the second and important one is taking less than a quarter of the calculation time required for the fine mesh.

Therefore, the best method to model the FRCM composite of F4 fabrics and mortar M2, with the continuum shell with embedded rebars approach, was with a rough mesh, 15 x 15 mm size elements, and a fracture energy value, 0.0608 N/mm, which was 40% of the MC2010.

Finally, as a final comparison between the two different modeling approaches, "A" and "B", the plastic strain distribution comparison presented with diverse GF values, at 1% strain. In Figure 4.27, the fine mesh gave a good cracking simulation, proving the weak representation of the homogenous model cracking pattern in comparison with the different GF values with the one-layer reinforced model. While for the rough mesh model "B", Figure 4.26, due to the chosen legend maximum and minimum values, it is not possible to appreciate the different numerical plastic strain distribution that represent the crack pattern for both models. In addition to the fact that at 1% strain it is quite normal for such a mesh to have an almost uniform distribution. So, in Figure 4.28 a different legend was selected for the best fitting GF case, a

40% of the MC2010 value, of the model “B” rough mesh at different strains, which shows a better cracking pattern.

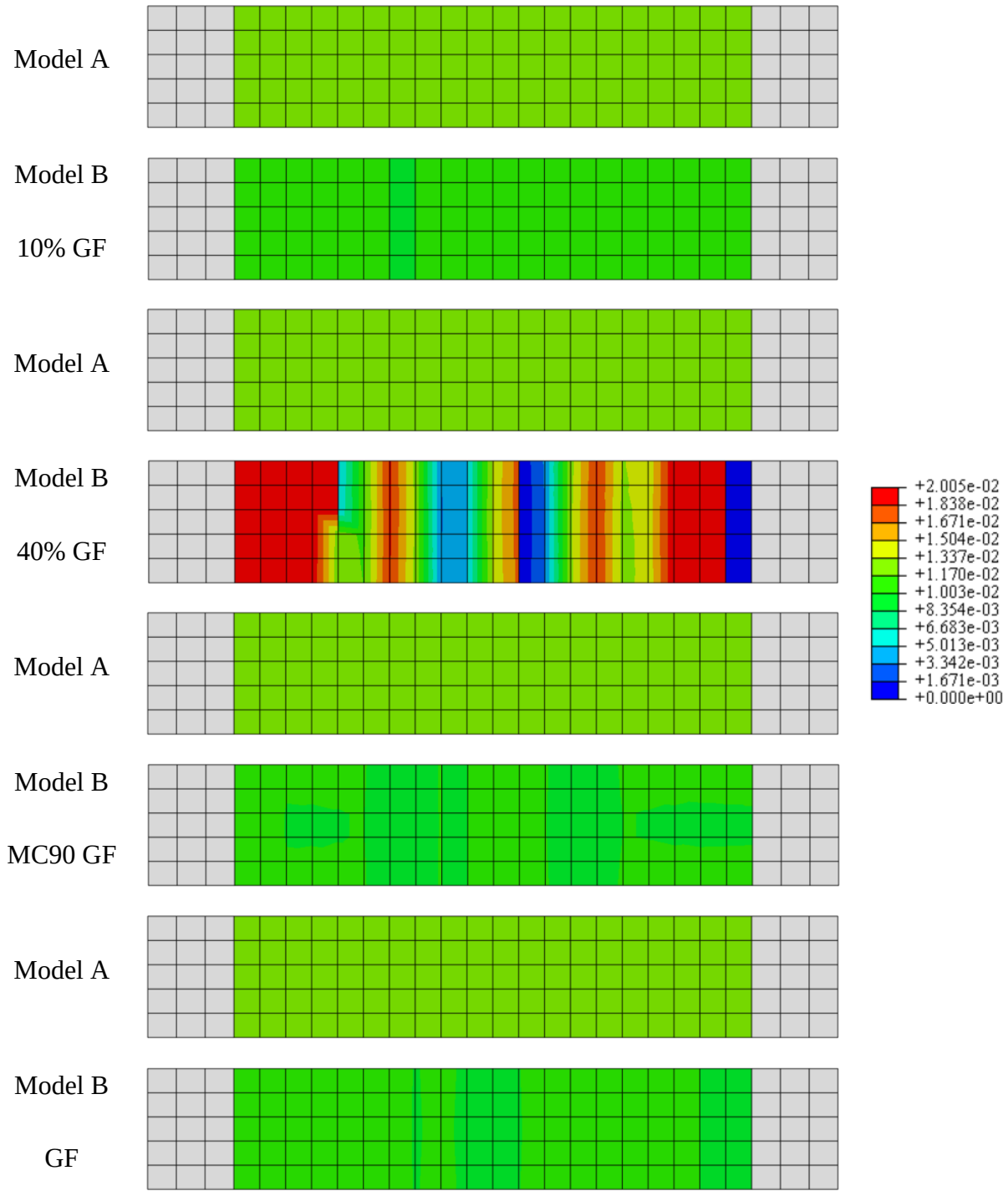

Figure 4.26 Plastic strain, max in-plane principal, contour plots at 1% strain of FRCM, fabrics F4 and mortar M2, with a "Rough" mesh, with model A compared in each figure with model B (with the same legends for all cases)

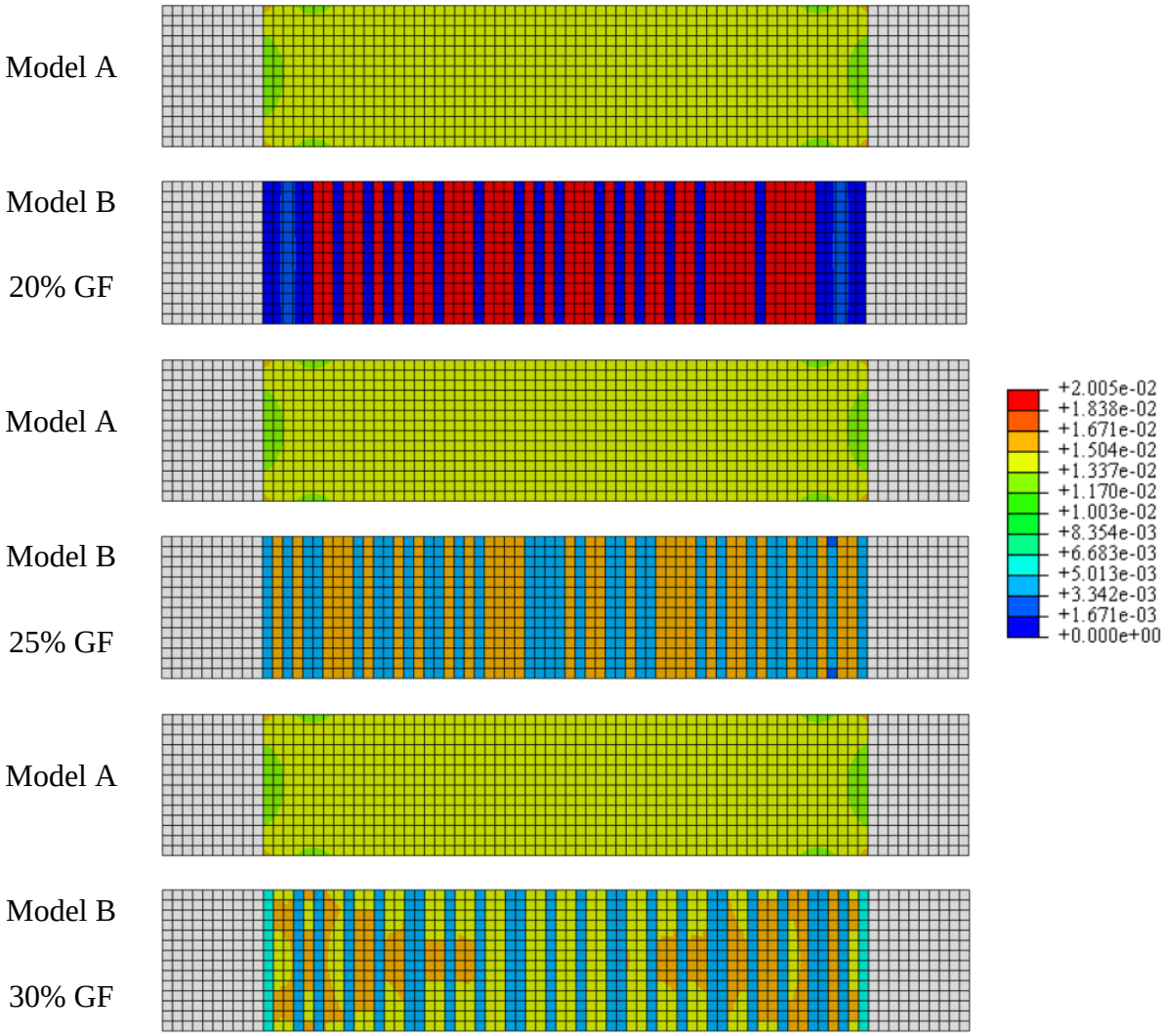

Figure 4.27 Plastic strain, max in-plane principal, contour plots at 1% strain of FRCM, fabrics F4 and mortar M2, with a "Fine" mesh, with model A, compared in each figure with model B (with the same legends for all cases)

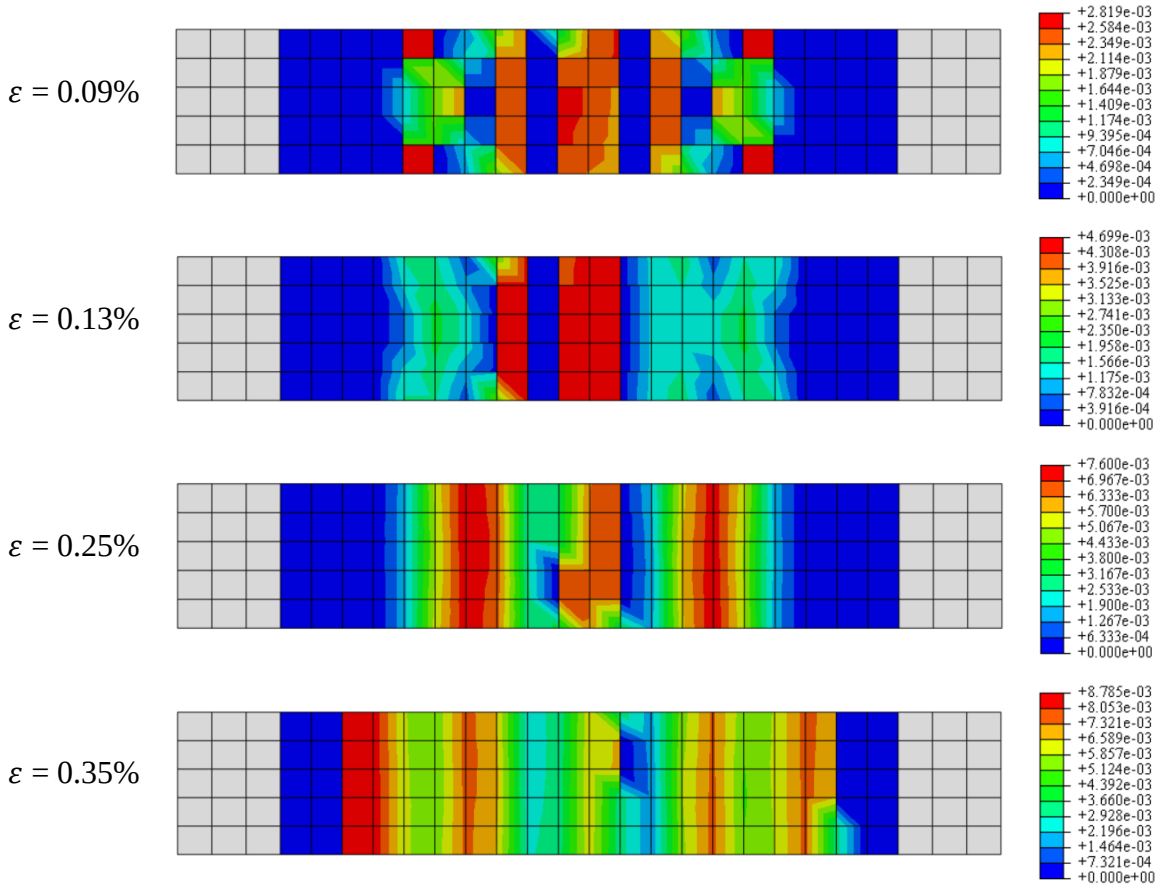

Figure 4.28 Plastic strain, max in-plane principal, contour plots at different strain values of FRCM, fabrics F4 and mortar M2, with a "Rough" mesh, with model B using a GF of 40% of the MC2010 value

5 NUMERICAL MODELING OF SFRC NOTCHED BEAMS

5.1 CONSTITUTIVE LAWS

The SFRC has a complex behavior, different from the one of a standard reinforced concrete. This is due to its post-elastic mechanical behavior, which is related to the presence of the micro-fibers that allow a stress transition providing a high ductility to the beam.

In order to numerically simulate this material behavior, it is possible to start from the experimental characterization results. For this reason, this research used the data from another experimental campaign, explained in section 3.2, of the SFRC notched beam experiments, in which the crack opening diameter was represented by the notch opening displacement.

The constitutive tensile laws were evaluated with two different methods. The first one was using the previous experimental results and the Model Code 2010 provisions to obtain the multi-linear laws, in this first case, four different laws can be obtained in according to various curing ages and the statistical evaluation method (average or characteristic). While, the second method, which was provided from another research [12] uses the results of two full-scale beam tests, evaluating the laws by means of an inverse plane-section analysis. The compressive laws were obtained using the Model Code 2010 provisions for the plain concrete.

5.1.1 Constitutive Laws Evaluated from the Notched Beam Experimental Data

The Model Code method to evaluate the tensile law of an SFRC is divided into two main parts. The first part, simulating the plain normal weight uncracked concrete behavior, is calculated with three main branches, elastic (up to 90% f_{ct}), post-elastic till the peak, and a softening branch. The second part is the post-cracking law related to the fiber reinforcement, through the residual stresses at specific crack openings (0.5-2.5 mm), evaluated with the linear model from [11], starting from the notched beam's data results. The particular criteria to join the curves to get the final law is defined from the standards. This was done for two different curing ages, 34 days and around 167-220 days, and both with two different statistical values used, mean and characteristic.

The most important parameter to be calculated was the modulus of elasticity, using the formula of the plain concrete [11], equation (4), which was found equal to $38.65 * 10^3$ MPa.

$$E = E_0 * \alpha_E * \left(\frac{f_{cm}}{10}\right)^{\frac{1}{3}} \quad (4)$$

Where, E_0 is equal to $21.5 * 10^3$ MPa, α_E taken as 1, and f_{cm} provided from a cubic compression test (58.09 MPa).

Since the first branch of the law is purely elastic, it was evaluated by the strain and slope of the simplified line, which is the modulus of elasticity, equation (5), arriving at the first point considered without any plastic strain with 90% of the tensile strength.

$$\sigma = E * \varepsilon \quad (5)$$

The tensile strength was calculated from the flexural strength experimental data in Table 3.2, using the formula proposed by the Model Code 2010 [11], equation (6), with a suggested α value of 0.06, h representing the depth of the beam, 150 mm, and f_{ctf} was taken according to the curing age, 34 or 167, and a mean or a characteristic value.

$$f_{ct} = f_{ctf} * \frac{\alpha * h^{0.7}}{1 + \alpha * h^{0.7}} \quad (6)$$

The second branch was defined until the tensile strength, arriving at a strain value of 0.00015, equation (7).

$$\sigma = f_{\frac{ctm}{k}} * \left(1 - 0.1 * \frac{0.00015 - \varepsilon}{0.00015 - 0.9 * \left(\frac{f_{\frac{ctm}{k}}}{E}\right)} \right) \quad (7)$$

The third branch was the plain concrete softening branch, where, at some point, this branch was intersected with the second part of the law, evaluated due to the presence of the short fibers. The softening will reach a 20% value of the tensile strength, with a strain value calculated in equation (8), where GF was calculated as in equation (2) (0.151 N/mm).

$$\varepsilon_Q = \frac{GF}{f_{\frac{ctm}{k}}} + \left(0.00015 - \frac{0.8 * f_{\frac{ctm}{k}}}{E} \right) \quad (8)$$

The post-cracking linear model was then evaluated using the results of the notched beam experiments, as instructed in the Model Code 2010. This branch was a line with two main points at the Crack Mouth Opening Displacement, CMOD, of 0.5 and 2.5 mm, with stress f_{Fts} and f_{Ftu} that were directly evaluated, in equations (9) and (10), from the residual flexural strength of the experiments, $f_{R,1}$ and $f_{R,3}$. For this reason, the experiment in [10] was an essential database for this research and was needed to develop such constitutive laws, allowing the tracking of the stress at specific required values of the crack's opening.

$$f_{Fts} = 0.45 * f_{R,1} \quad (9)$$

$$f_{Ftu} = f_{Fts} - \frac{w_u}{CMOD_3}\left(f_{Fts} - 0.5 * f_{R,3} + 0.2 * f_{R,1}\right) \quad (10)$$

Where in this case, w_u is the maximum accepted crack opening is equal to $CMOD_3$ (2.5 mm).

To intersect the line of the second part with the 3rd branch of the plain concrete law, which was evaluated with a stress-strain relation, the CMOD had to be converted to strain. The conversion as suggested by the Model Code 2010, was done by dividing with the characteristic length (l_{cs}), which can be equal to the depth of the beam, 150 mm, but having a 25 mm notch at the mid-section, gave an l_{cs} equal to 125 mm.

Finally, after both the parts are evaluated, and represented in stress-strain, the intersection was found with the plain concrete's softening branch and the extension of the linear model line. Then the rest of the softening branch is deleted. Figure 5.1 is an example of the law with 34 curing days and mean values, showing the two different constitutive models' intersection.

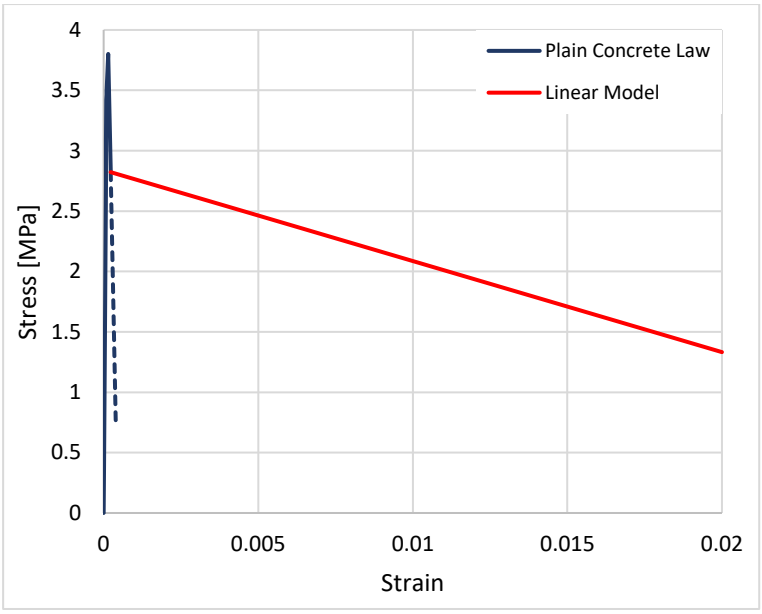

Figure 5.1 34m SFRC constitutive law, with the removed line represented as dashed

Figure 5.2 represents all four of the identified multilinear tensile laws of the SFRC material, in terms of stress-strain.

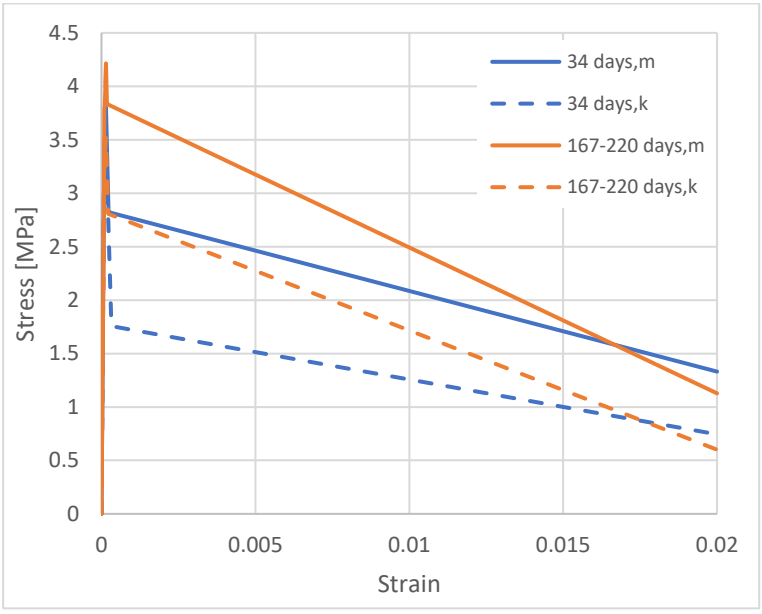

Figure 5.2 Constitutive laws of SFRC with different ages

In general, the compressive behavior of the SFRC can be represented by the constitutive law of the uncracked normal-weight concrete since fibers affect mainly the tensile one. Equation (11), from [11], defines all the compressive behavior of the concrete, with the compressive strength taken from the cubic compression test experiments, and found with a mean value 58.09 MPa, and a characteristic one 50.09 MPa.

$$\sigma_C = f_{\frac{cm}{k}} * \left(\frac{k * \eta - \eta^2}{1 + (k-2) * \eta} \right) \tag{11}$$

Equation (11) is used until a maximum strain, suggested by [11], of a value 3.4, related as the other parameters to the concrete grade C50, with:

- $k = 1.66$, is the plasticity number.
- $\eta = \varepsilon_C / \varepsilon_{C1}$, is the ratio of the strain over the strain at maximum compressive stress.
- $\varepsilon_{C1} = 2.6$, the strain at maximum compressive stress.

Figure 5.3 shows the full compressive laws, mean and characteristic, were after the strain limit suggested by the code, a fictitious value was added just to reach a stress failure value.

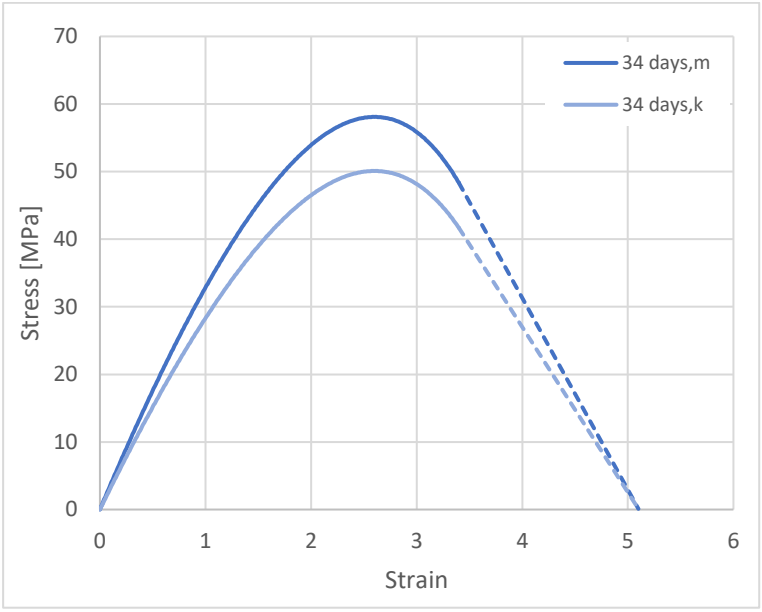

Figure 5.3 Compression constitutive law, mean or characteristic

5.1.2 Identified Laws from the Inverse Plane-Section Analysis

The previous laws, even with their tensile stress catch and post-peak description, lack the actual simulation of the cracking behavior, since as shown in the plot of the experimental results in Figure 3.5, a hardening branch is present, which description is absent in the previous laws.

Two laws were provided from other ongoing research, which is the proceeding of [12], shown in Figure 5.4, identified using an inverse plane-section analysis, using the experimental data of the SFRC four-points bending beams, BF1 and BF2.

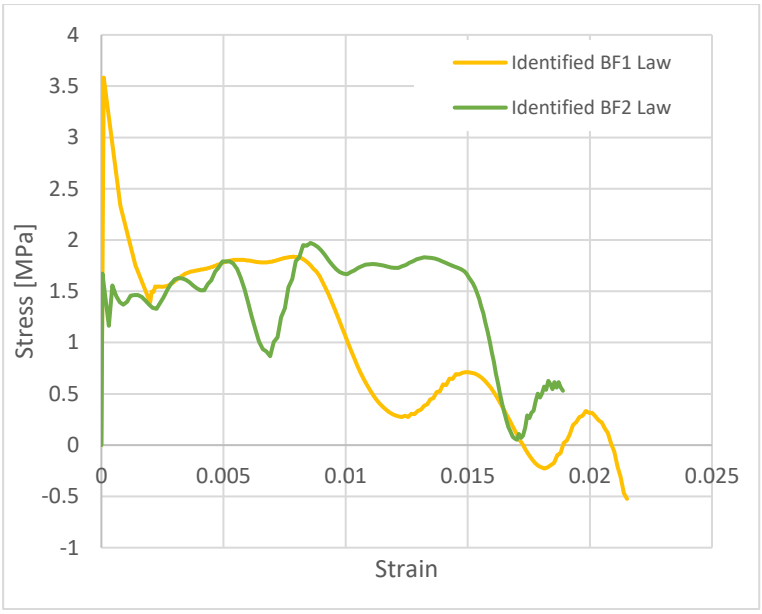

Figure 5.4 BF1 and BF2 tensile identified laws

The identified BF1 and BF2 laws were simplified, for the ABAQUS input, with a multilinear law able to fit the peak and the inflection points, Figure 5.5 & Figure 5.6. It was able to fix the identified BF2, where its peak was very low compared to the BF1 and all the previous laws. In addition to neglecting the last parts of the curves, BF1 negative part, and the new hardening segment in BF2.

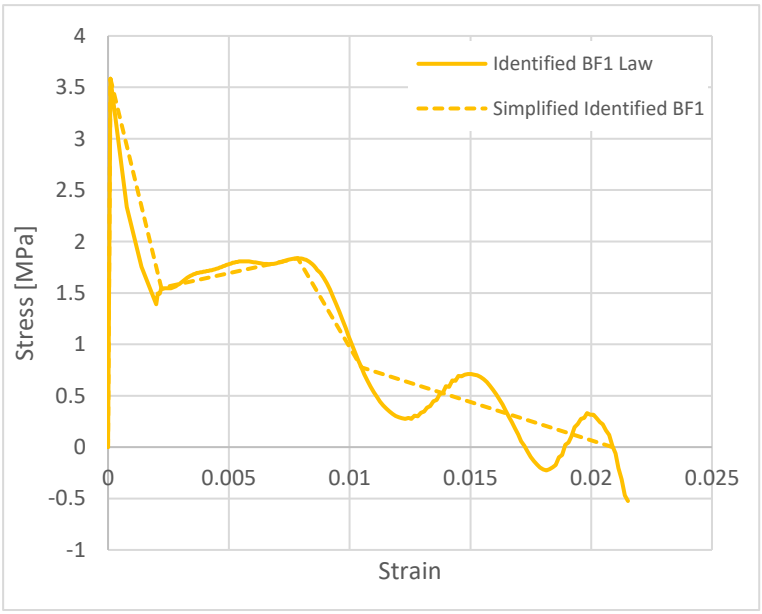

Figure 5.5 Simplified BF1 law curve to multilinear

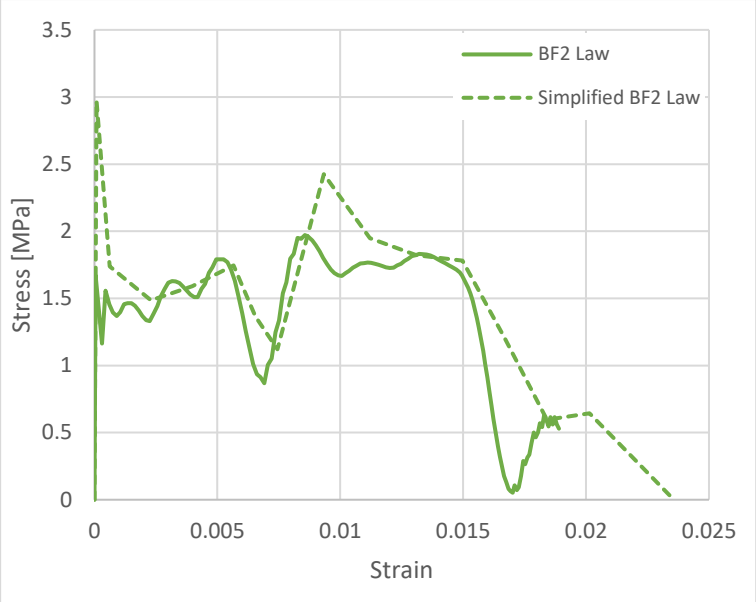

Figure 5.6 Modified and Simplified BF2 law curve to multilinear

5.2 ABAQUS MODELING

5.2.1 The Notched Beam ABAQUS Model

The notched beam was modeled as a 2D 150 x 600 mm^2 element in ABAQUS, provided from the research in [10], as a three-point loading beam. The loads were applied as a displacement control on steel cylinders to avoid stress concentration, perfectly simulating the experimental results. The model had been defined in plane stress state, with 150 mm thickness.

The beam's material was described with elastic and CDP behaviors to simulate the SFRC, with a solid homogenous section. The elastic behavior is defined with the modulus of elasticity computed in the previous section, 38.650 GPa, and a Poisson's ratio of 0.2. The plasticity section of the CDP was defined with the same parameter's values shown in Table 4.1 of the FRCM mortar, except for the viscosity parameter defined as zero in this model.

The compressive and tensile behaviors in the CDP were defined with the stress and corresponding to the end of the elastic branch, taken from the previous section's constitutive laws. However, some modifications were made to the laws to define them in ABAQUS by removing all the branches related to the elastic behavior of the SFRC until the tensile strength considered as 90% of the peak, and translating the rest of the law, Figure 5.7and Figure 5.8.

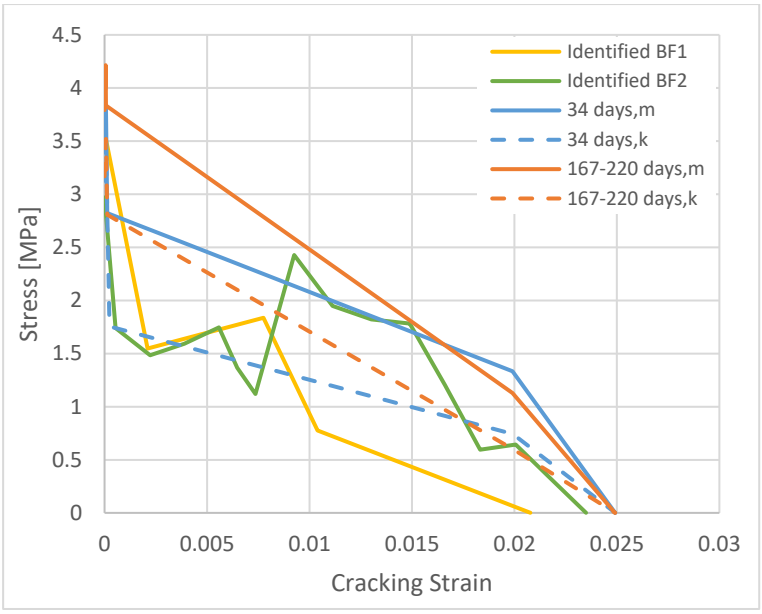

Figure 5.7 CDP tensile behavior of SFRC with different age, average (m) or characteristic (k), identified BF1 & BF2

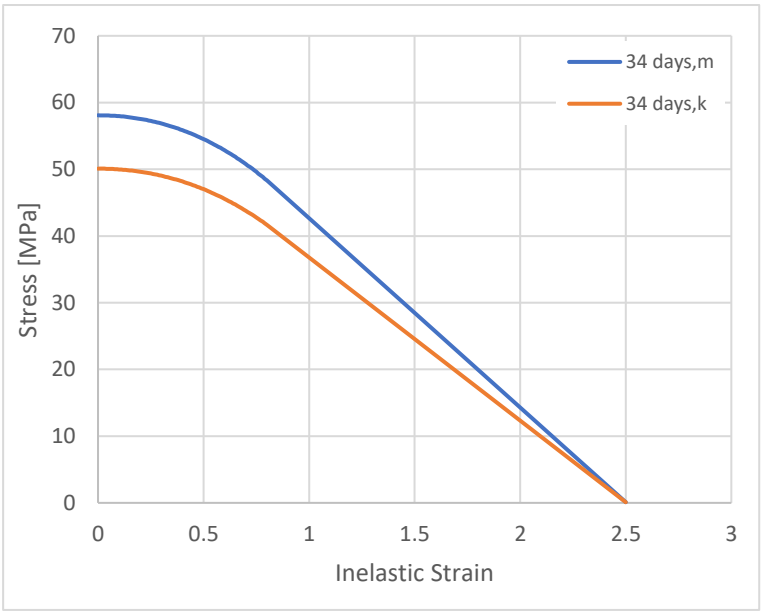

Figure 5.8 CDP compressive behavior of SFRC with 34 curing days, average (m) or characteristic (k)

The steel cylinders were defined with a perfectly elastic behavior by a modulus of elasticity 210 GPa and a 0.2 Poisson's ratio, with a diameter of 30 mm. They were placed one on the top middle of the beam in correspondence to the load application knife, and two on the bottom, 50 mm from the left and right beam boundaries, to simulate the supports. The interaction between the cylinders and the beam was defined with a tangential law, with a 0.5 friction coefficient, and a hard contact in the normal direction.

The notch at the bottom side was modeled as an XFEM segment [7] 25 mm deep. In addition to the vertical supports, the horizontal translation was fixed at the crack tip in order to respect the symmetry of the response. The CMOD was measured by taking the relative displacement between the two of the bottom nodes of the notch.

The model was meshed with a four-node bilinear plane stress quadrilateral (CPS4) mesh element type, of a size of 2.5 mm, that varies to increase in the not sections, as the left and right unsupported sides, as shown in Figure 5.9.

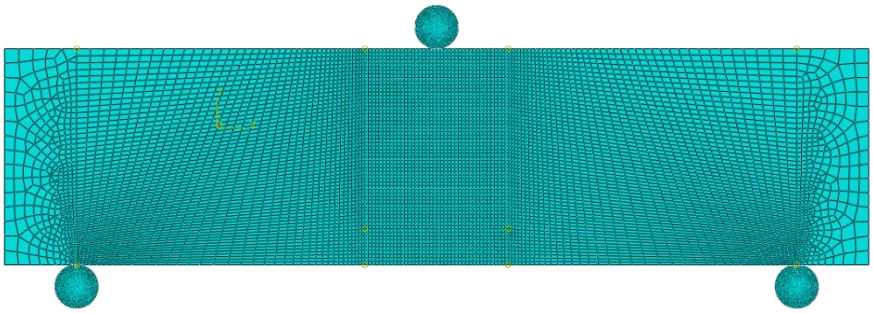

Figure 5.9 Notched three-points beam, ABAQUS model mesh

5.2.2 CDP Tensile Behavior's Input Methods

The CDP tool in ABAQUS allows various methods of input for tensile behavior. The first one was shown in the previous section, which was the cracking stress-strain full behavior. The second method was the cracking stress- crack displacement input. While the third method was the use of the cracking stress value and the fracture energy GF. The numerical analysis was done with the three different inputs to choose the method with the best response for the following modeling of the full-scale four-points beam.

The GF tensile input was done to evaluate laws with different curing age, excluding the identified laws. The GF value (0.151 N/mm) was the same for different ages and evaluated in 5.1.1, using equation (2). The tensile strength values, in Table 5.1, were calculated using equation (6) from the experimental database in Table 3.2.

	34 days, m	**34 days, k**	**167-220 days, m**	**167-220 days, k**
f_{ct}	3.80	3.47	4.21	3.52

Table 5.1 Tensile strength values for different age concrete, mean (m) or characteristic (k), in MPa

The crack displacement input was evaluated differently for the two different laws, the MC2010 and the identified laws. In the case of MC2010, since as explained in 5.1.1 section,

the second part was calculated from the linear model using the crack opening, while the plain concrete part was using strain, therefore to transform the behavior to crack displacement, the strain of the plain concrete part was multiplied by the mesh size, 2.5 mm. Where for the identified laws, evaluated differently, the transformation was done with the multiplication by the characteristic length l_{cs}, 150 mm, the depth of the beams tested under the four-point bending test configuration. It is also interesting to notice that 150 mm was also the approximate crack distance observed at the end of the tests. The CDP tensile behaviors for all the laws are shown in Figure 5.10.

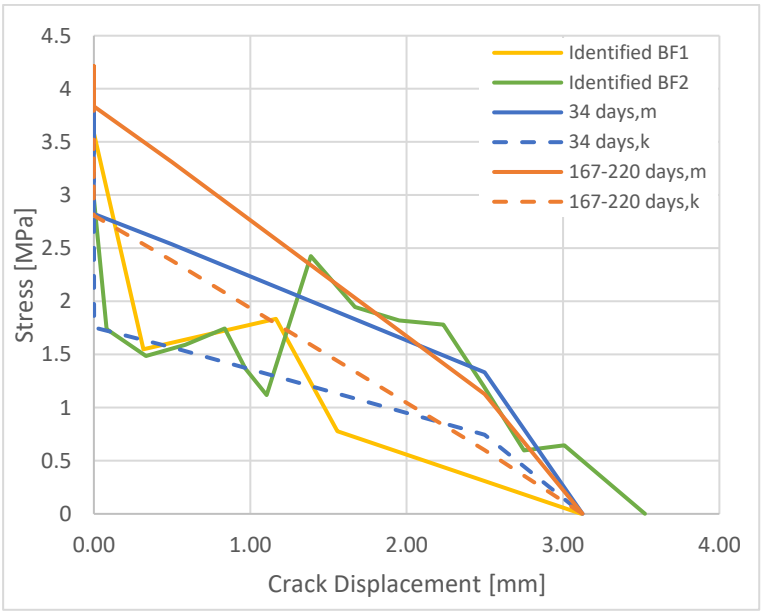

Figure 5.10 CDP tensile behaviors with stress and crack displacement input

ABAQUS transforms the strain into the crack displacement before its calculations by multiplying its values to around 2.5 mm. Thus, an exciting input was to perform the calculation of dividing the crack displacement by 2.5 mm and using it as a strain input. It was referred as strain-new or strain*, which allowed a check if the mesh element's size was enough for the model to regularize the behavior over the meshed model, as the strain* should give the same results. Note that this tensile behavior input, strain* shown in Figure 5.11, has different values of the whole identified strain input, and only for the linear model part of the MC2010 laws.

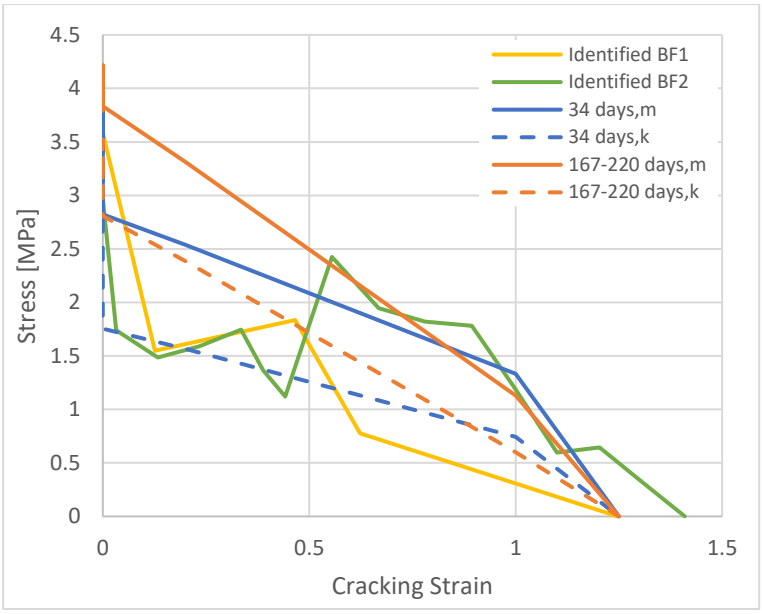

*Figure 5.11 CDP tensile behaviors with stress and cracking strain input, evaluated as strain**

5.2.3 Results of the Notched Beam Model

The model was controlled by increasing the vertical displacement, so the time increment value is equal to the displacement load in the mid-section, measured in mm.

The results were plotted on the experimental data, Figure 3.5, allowing a direct comparison with the numerical analysis response. Thus, they were presented in terms of stress vs. CMOD. The stress was calculated with equation (12), where M is the internal moment at the middle of the beam, y is the distance from the neutral axis, which is considered half the depth without the notch, 62.5 mm, and I is the moment of inertia.

$$\sigma = \frac{M * y}{I} \tag{12}$$

To highlight the different methods of CDP tensile behavior definitions in ABAQUS, first, the graphs were reported as the same law with different inputs. Then with the chosen best method the results were plotted with its input and different constitutive laws. In addition to these graphical plots, the plastic strain contour plots, in maximum in-plane principal, from ABAQUS were represented at the same and significant displacement load values, allowing another comparison aspect.

The 34 curing days law of average and characteristic values delivered different graded results, Figure 5.12, according to the tensile behavior definition. The results with the tensile behavior defined with the original strain caught the peak stress and the first softening branch

slope in the case of the mean values, Figure 5.12(a); however, it did not describe the full behavior with the hardening branch and was led to failure at a slight value of CMOD, due to the high localization of the behavior. In contrast, the characteristic one did not even reach the peak. In the case of strain* or displacement of tensile definition, which gave the same results as expected, proving that the mesh size was right for the regularization of the behavior. With the mean law, regardless of the much higher and delayed stress peak, the curves were able to describe the full behavior, also considering the simplified softening slope. In comparison, the characteristic law in Figure 5.12(b) provided a better, stress peak value close to the experimental ones, with the same condition of a simplified softening slope. Moreover, this simplification of the softening branch was caused by the evaluation of the linear model, defining this branch, as only two residual points from the experiments used to define such complicated after post-peak behavior. Thus, a main drawback of the MC2010 laws was the incapability of describing this hardening post-peak branch mainly due to the absence of stress evaluated values at the lower crack opening point (less than 0.5 mm). The fracture energy method proved that it was not suitable for this kind of modeling, where it resulted in a curve that almost did not relate to the experimental results, in both cases, Figure 5.12(a) and (b). In fact, in general, the GF method can only be used for plain concrete.

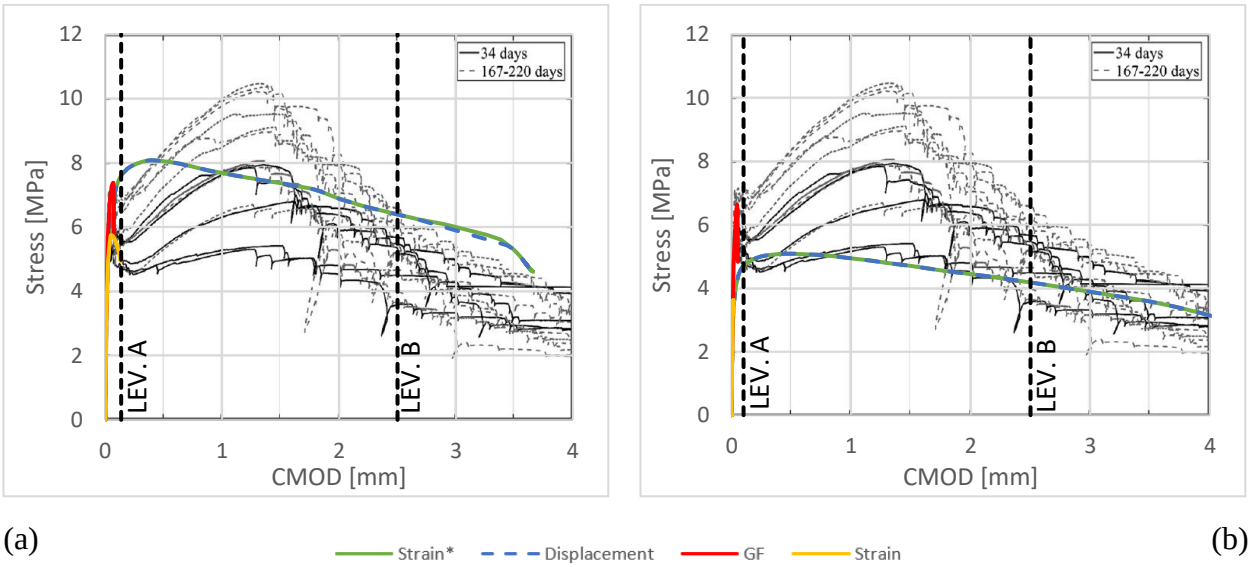

Figure 5.12 Stress vs. CMOD results with different CDP tensile definitions, of 34 days, m (a); and 34 days, k (b) (with the same legends)

The high tensile strength of the (167-220 days, m) law caused a very high stress peak of the displacement, or strain*, around one and a half higher than the experimental results, Figure 5.13 (a). The case of the characteristic values, Figure 5.13(b), delivered a closer stress peak value. Like the previous case, the strain input method highly localizes the cracking behavior,

but even with a good peak it was unable to provide good behavior. As for the GF responses, it has proved its non-functionality for such behaviors again.

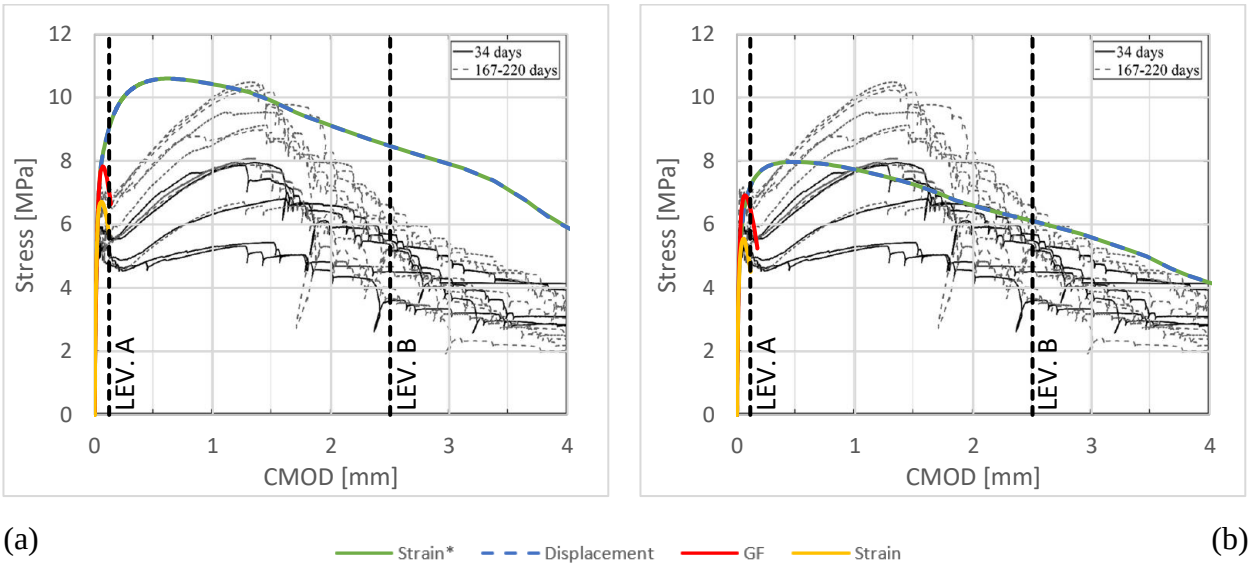

Figure 5.13 Stress vs. CMOD results with different CDP tensile definitions, of 167-220 days, m (a); and 34 days, k (b) (with the same legends)

The use of the inverse laws were expected to give a better response, since their constitutive laws were able to describe the experimental response with a better post-peak behavior. The same tensile behavior methods were used, except the GF that was removed due to its impractical results, while the strain input, even with its unusable response, was used to prove that the model was better regularizing with the displacement or strain* definitions. Figure 5.14 shows that both results did not correctly fit the experimental curves as expected, mainly because these laws were evaluated from the four points bending beams experiments, not the notched one. Despite that, the identified laws showed a better post-peak response description, unlike the very simplified responses of MC2010 provisions.

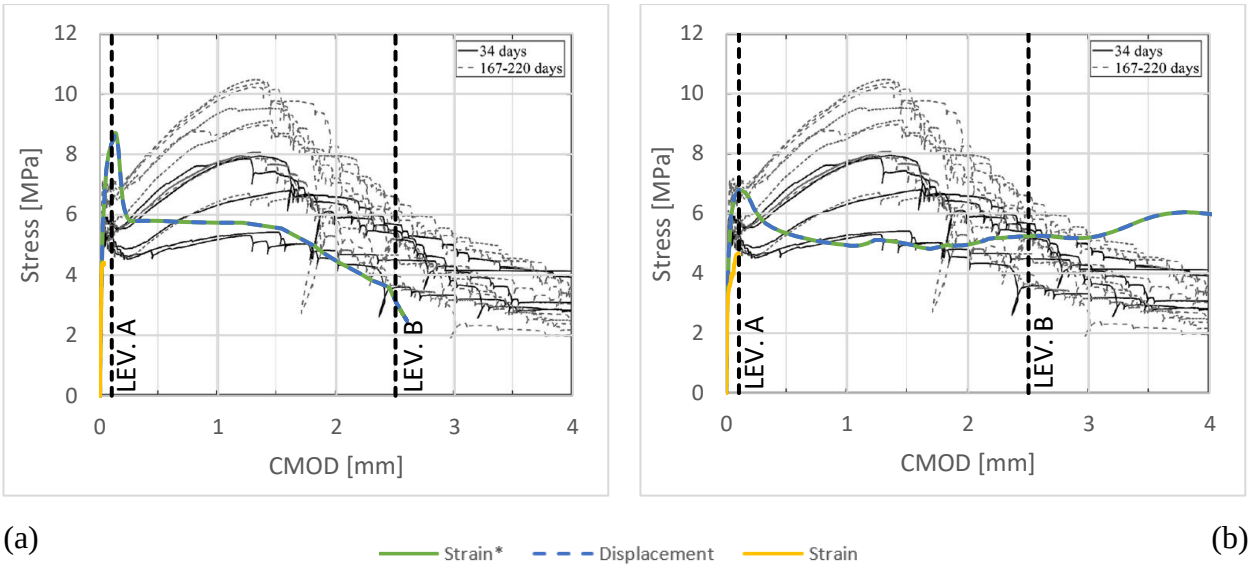

Figure 5.14 Stress vs. CMOD results with different CDP tensile definitions of the identified laws, BF1 (a); and BF2(b) (with the same legends)

The dashed lines in the plots, Figure 5.12, Figure 5.13, and Figure 5.14, at level A they are representing the point of failure of the response with strain defined input. While at level B it is a CMOD of 2.5 mm representing the exact stress value evaluated with the MC2010 provisions, and a post-peak softening position. At these levels, contour plots are presented in three figures. The first, where the 34 days with mean values law was chosen, with the three inputs, strain, displacement, and strain* at the two different levels, Figure 5.15. While the second and third figures, Figure 5.17 & Figure 5.18, show all the laws with displacement defined tensile behavior at the two different levels.

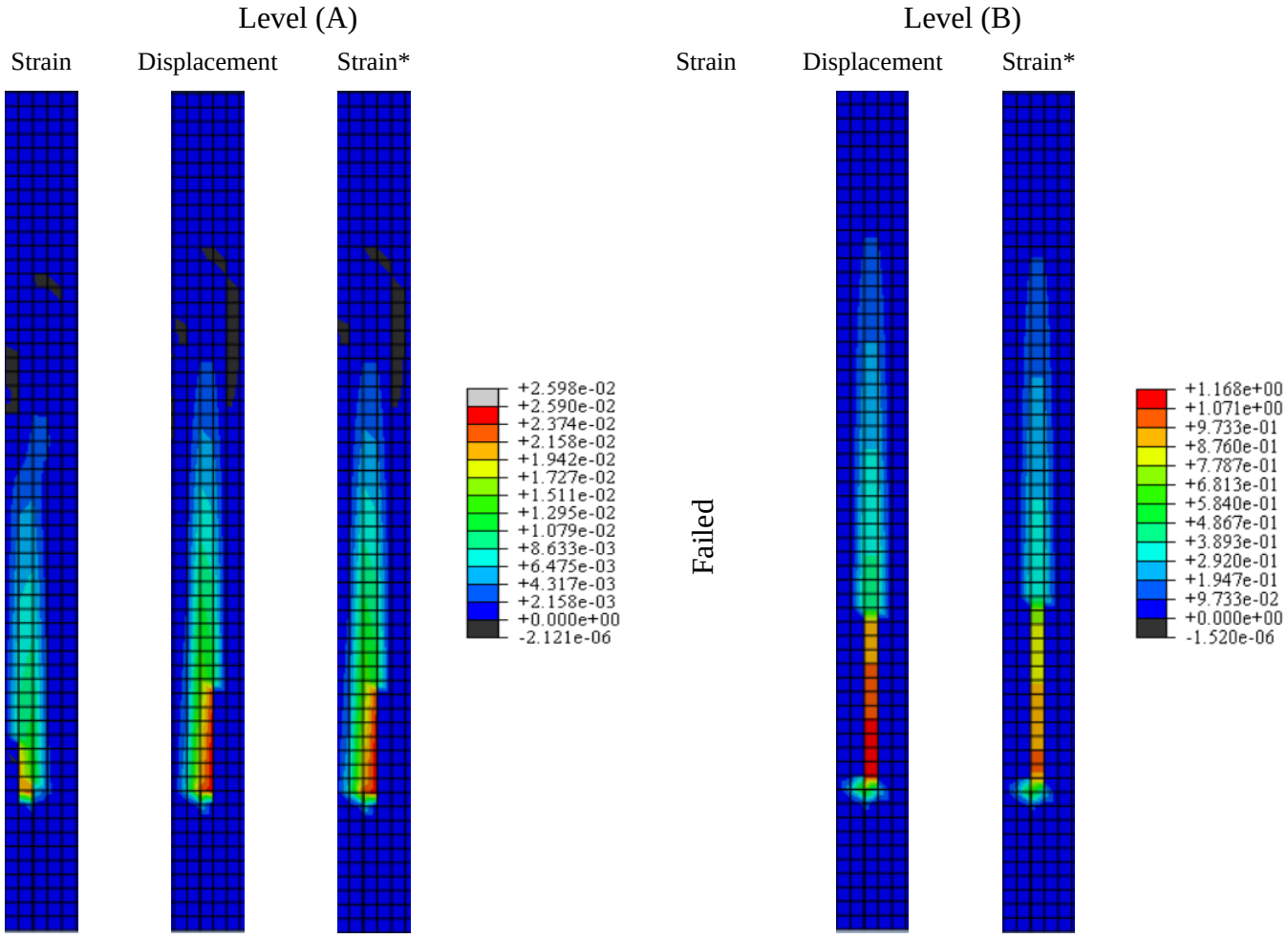

Figure 5.15 Plastic strain, max in-plane principal, contour plots of the model in the notch zone, with 34 days, m law at two levels (A) and (B) (with the same legend for each level), with different tensile behavior definition

The models that were expressed with a displacement or strain* CDP tensile behavior were all able to provide a full-beam response as the experimental ones; even though, in some cases, they were not able to deliver a good correspondence of the peak branch. Therefore, the SFRC beam models will be expressed with a displacement tensile definition to provide a good response.

For this research's proceeding work, as these tensile behavior definitions will be used to define models of the FRCM reinforced SFRC beam's full-scale experiments, a comparison of the laws with the same tensile behavior description was necessary, Figure 5.16.

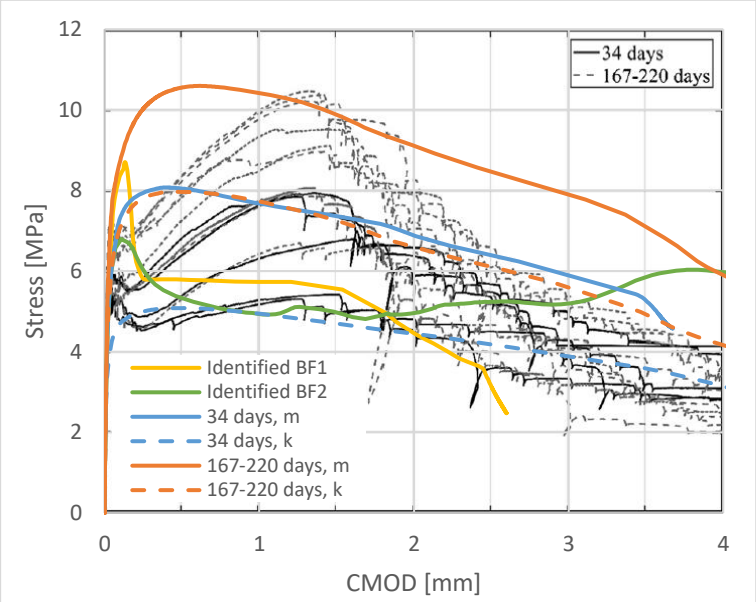

Figure 5.16 Stress vs. CMOD response of different constitutive laws with cracking displacement for the CDP tensile behavior definition

Finally, with the law of the 167-220 curing days with mean values delivering a different response than the experimental one, and the characteristic one giving a response similar to the (34 days, m), the MC2010 167-220 laws were considered ineffectual for the later modeling of SFRC beams.

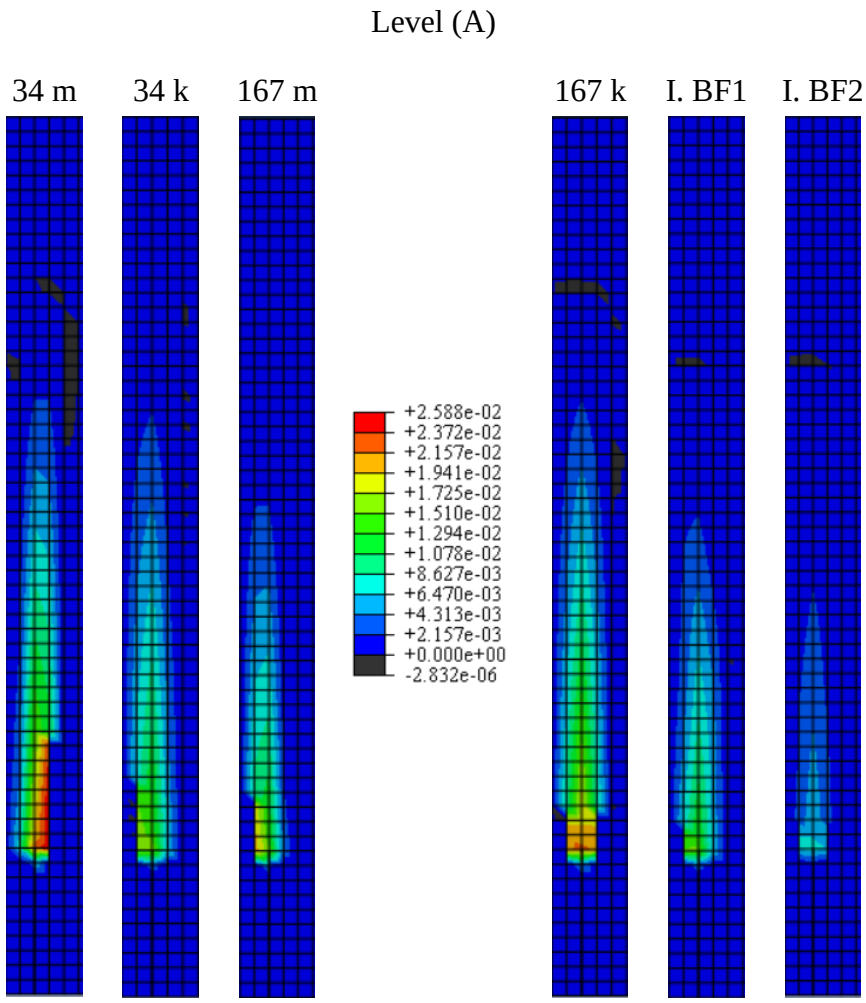

Figure 5.17 Plastic strain, max in-plane principal, contour plots of the model in the notch zone, at level (A), (with the same legend for all the models), with tensile behavior defined with cracking displacement, for laws of 34 days, m (1); 34 days, k (2); 167-220 days, m (3); 167-220 days, k (4); identified BF1 (5); and identified BF2 (6)

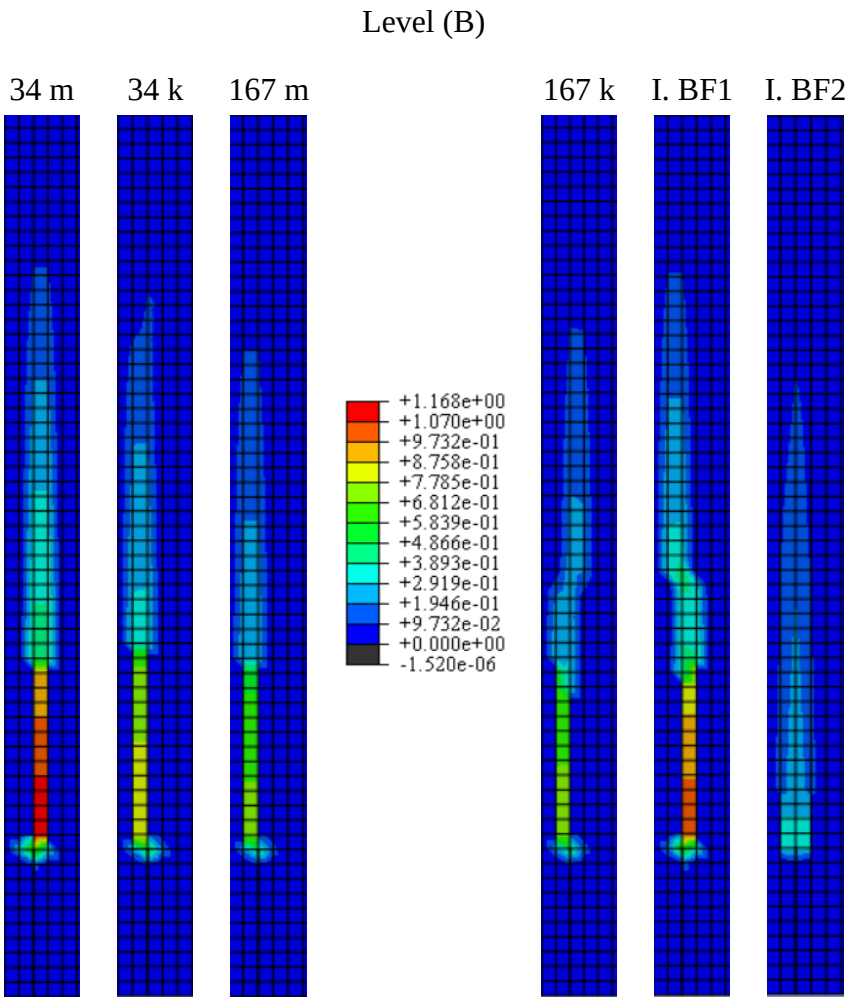

Figure 5.18 Plastic strain, max in-plane principal, contour plots of the model in the notch zone, at level (B), (with the same legend for all the models), with tensile behavior defined with cracking displacement, for laws of 34 days, m (1); 34 days, k (2); 167-220 days, m (3); 167-220 days, k (4); identified BF1 (5); and identified BF2 (6)

6 NUMERICAL MODELING OF A REINFORCED SFRC FOUR POINTS BEAM

6.1 PRE-DAMAGED BEAM

The previous section's constitutive laws choice were defined for the four-point SFRC beam to simulate the experiments in [11] of the pre-damaged case, and obtain a similar response to be used in the following section of the application of the FRCM reinforcement.

6.1.1 SFRC Four Points Bending Beam ABAQUS Model

The beam was modeled as a 3D deformable elements in ABAQUS, 350 x 1450 x150 mm^3 with a 1350 mm span, which are the same dimensions of the experimental ones and as explained in 3.3.1. In addition to the four cylinders, 30 mm diameter, two at the top for the load knives, 450 mm apart, and two at the bottom for the supports, 50 mm from the end. Both the beam and cylinders were modeled as solid homogenous sections.

The material elasticity, CDP plasticity, and compressive behavior definitions of the beam and the elastic cylinders were described same as the notched beam model, 5.2.1. The viscosity parameter, described in 4.1.1, was slightly increased from zero up to a range between $1x10^{-6}$ and $1x10^{-5}$, in some cases especially with the models with the MC2010 laws. Since this model is more complex and this parameter is required to allow the full response delivery, increasing the model stability, by the increasing of the dimension of the plastic strain distribution.

The post-elastic tensile behavior in CDP is defined in stress-displacement. Thus, the MC2010 laws, only the plain concrete branch, transformation from strain to displacement was different with respect to the previous one since it depends on the mesh size. In this case, the strain is converted by multiplying it to 25 mm, representing the mesh element size in the middle part of the beam (the zone where the inelastic process takes place). The identified laws were maintained the same since their transformation depends on the beam depth and the experimental crack distance, which was 150 mm. The tensile behavior inputs of the various laws are shown in Figure 6.1.

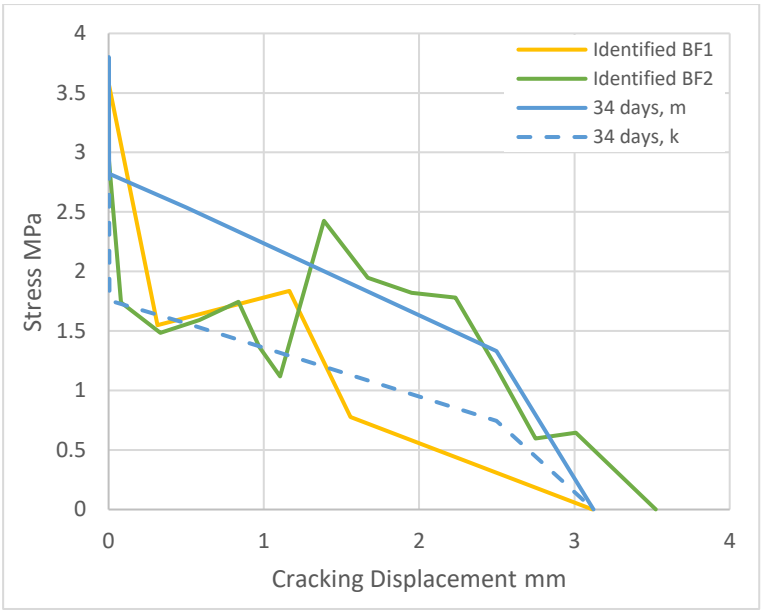

Figure 6.1 CDP tensile behavior definition of the laws used for the SFRC four points bending beam

The contact interaction between the cylinders and the beam was modeled with the same parameters as in the notched beam model in 5.2.1.

The supports of the beam were placed in the center lines of the two bottom cylinders, in all directions. In addition another horizontal support was placed in the bottom middle node of the beam prevents any beam sliding (point 2 of Figure 6.2). The displacement were applied at the top cylinders' center lines to simulate the experimental displacement control method, with an amplitude equal to double the step time increment. The supports and loads application on the beam scheme are shown in Figure 6.2.

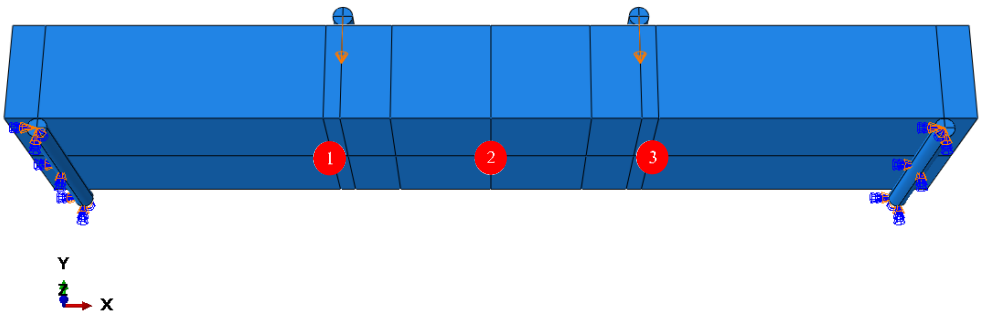

Figure 6.2 Four Points Bending Beam ABAQUS model scheme with loads and supports (with a slight rotation around the x-axis and a perspective view)

The model was meshed with a standard 3D Stress eight-node linear brick with reduced integration (C3D8R) mesh element type. In the longitudinal cross-section the mesh size ranges

from 25 mm side, in the middle part, to the edges with a 75 mm base and 25 mm height rectangular elements. The cylinders were also meshed with a 7.5 mm, approximately, polygons sides. Whereas for the whole model in the width direction, the element mesh size was 50 mm. The full meshed model is depicted in Figure 6.3.

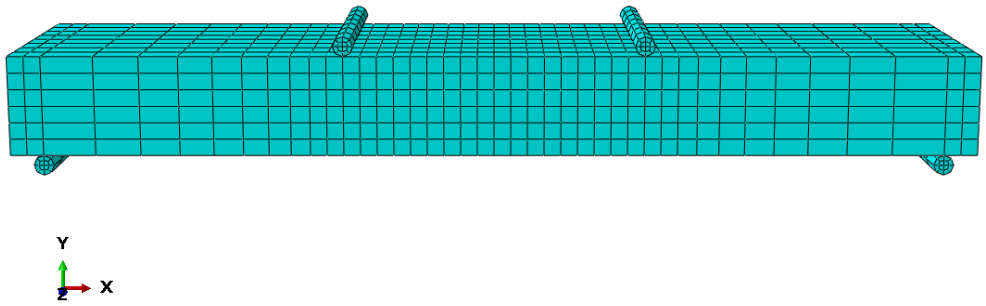

Figure 6.3 Four Points Bending Beam meshed ABAQUS model (with a slight rotation around the x-axis and a perspective view)

6.1.2 The Response with Different Constitutive Laws Models

The results of the model were extracted in two different representations. The first one was the total applied load, equal to double the reaction force of one support, plotted against the beam's mid-span deflection, measured at the red point 2 in Figure 6.2. The second one is the moment, evaluated at the mid-span vs. COD, obtained from the model by the relative horizontal displacement, in the x-axis direction, of the two nodes located in the mid-width, at a 500mm span in the middle of the beam (points 1&3 in Figure 6.2), similarly as to what was done in the experimental measurements shown in Figure 3.6 (a).

The response with the identified BF1 law was very different from the experimental results, Figure 6.4. There was around an increase of the peak load of about 50%, and, in general, a different response path, thus, the check and the modification of this law were necessary. The slope of the first branch in Figure 6.4 (a), related to the stiffness of the elastic zone, was different from the experimental one, which was caused by a slight experimental error at the beginning of the load application at the cylinders, where Figure 6.4 (b) proves that the first branch slope was correctly obtained.

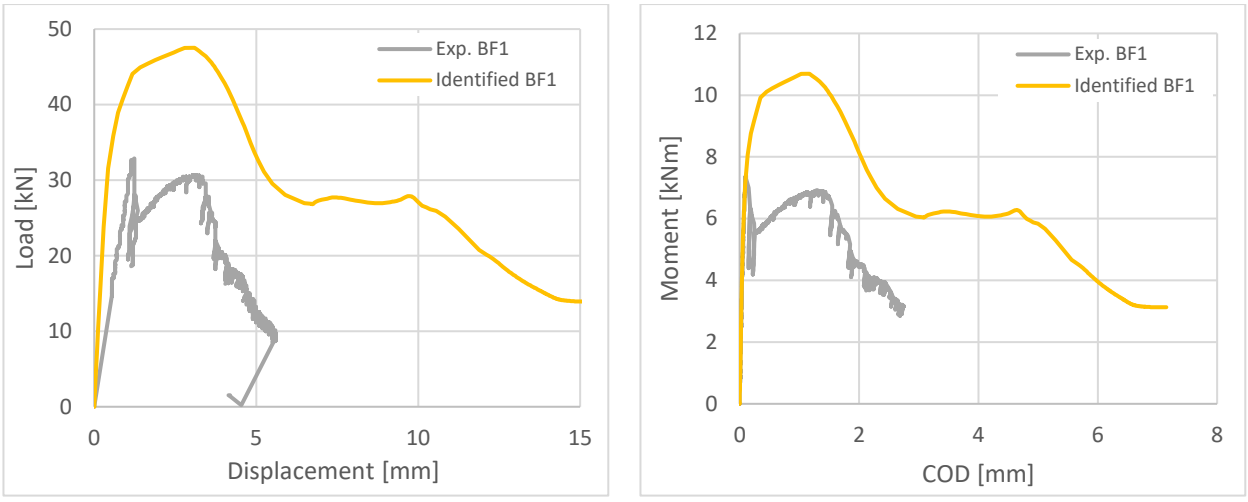

(a) (b)

Figure 6.4 SFRC beam with Identified BF1 law, results of load vs. mid-span displacement(a); and Moment vs. COD (b)

As shown in Figure 6.5, the identified BF2 gave better results than the previous one. However, the peak load was still higher than the experimental one, and the final softening branch was initiated at a higher displacement.

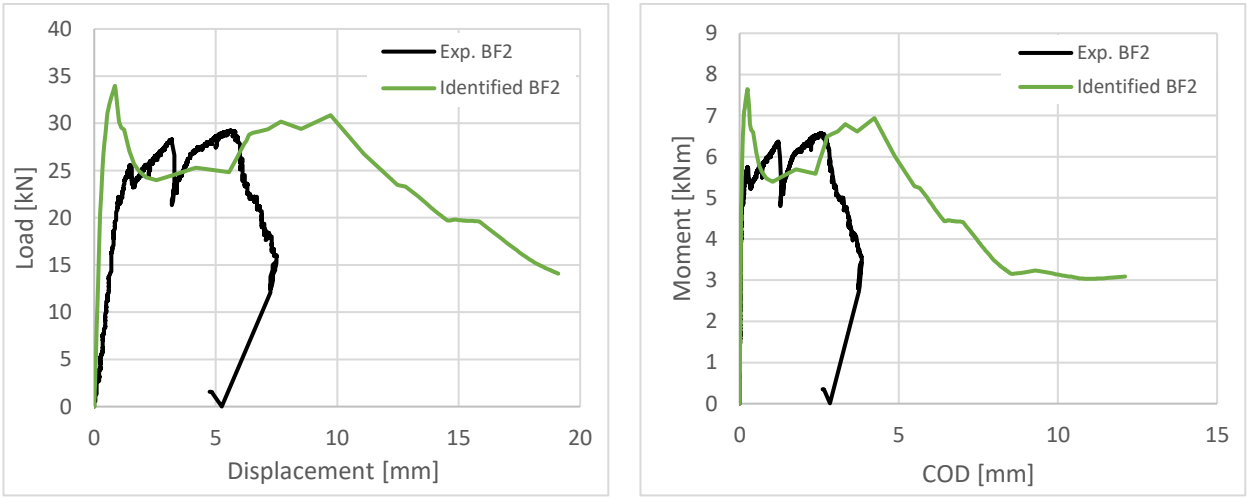

(a) (b)

Figure 6.5 SFRC beam with Identified BF2 law, results of load vs. mid-span displacement(a); and Moment vs. COD (b)

As for the MC2010 laws with 34 days, mean and characteristic, Figure 6.6, the first branch, compared with both the experimental specimen's results, was well replicated as they almost shared the same load peak value. Nevertheless, the softening branch for the characteristic one was better even with its simplified line, unlike the mean one, since the weird post-peak behavior is only provided because of the viscosity parameter, wherein lower values of it, the model was

failing at the load peak. Noting that, both laws required a viscosity parameter of $1x10^{-5}$ to give a full post-cracking response.

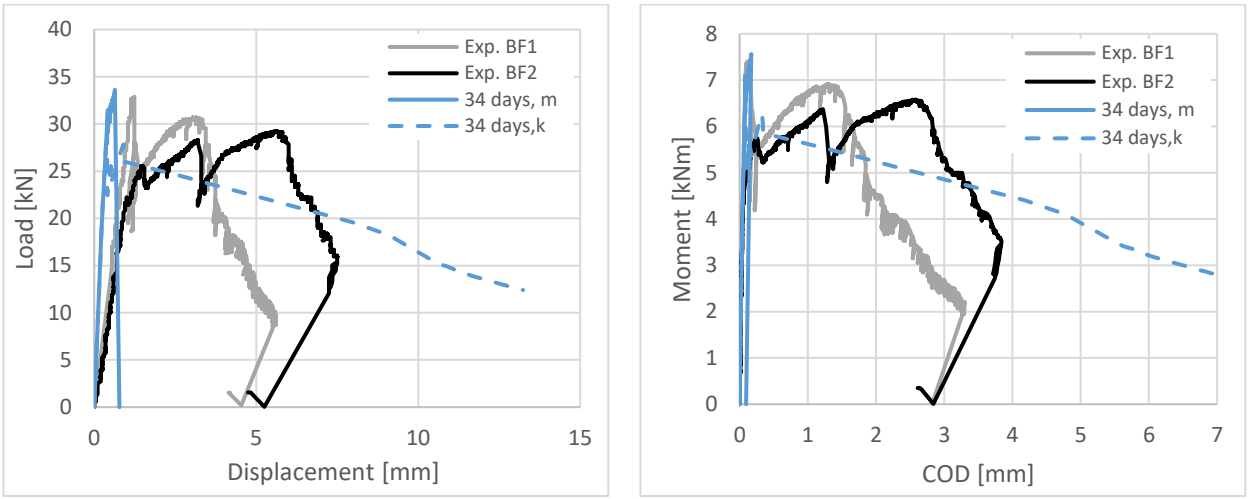

(a) (b)

Figure 6.6 SFRC beam with MC2010 laws, 34 days mean(m) and characteristic(k) values, results of load vs. mid-span displacement(a); and Moment vs. COD (b)

Therefore, according to the presented results, the MC2010 produced laws were removed from the following simulations because of their simplified and incoherent softening branch, which was due to the use of only two residual points to create the linear model branch. The high load peaks demonstrated that the constitutive law post-cracking branch was not steep enough for the identified laws, providing the model with higher energy. Thus, some modifications were performed to these laws to obtain a better-suited results.

6.1.3 Identified Laws Post-Cracking Branch Modifications

Given that the MC2010 laws were able to better simulate the peak load value and somehow the beginning of the post-cracking response, it seemed that ABAQUS would simulate better the results if the law a plain concrete post-tensile strength branch. Hence, the best modification method was by introducing a new first post-peak branch for the identified laws, instead of the existing one.

The modification was done using the approach shown in 5.1.1, to the simplified identified laws, Figure 5.5 & Figure 5.6. The second branch stats from the same tensile strength value, but the post branch slope was developed by joining the peak stress with the point of 20% of the tensile strength with a strain value calculated in equation (8), using the same parameters of the MC2010 laws case since they were the same material. This new branch was then cut and joined at the intersection with the third branch of the simplified identified laws. The new modified

laws and the original ones are plotted in Figure 6.7 and Figure 6.8 (a), and better illustrated (b). this approach is a better simulation of the stress reduction (jump), related to the crack formation and it prevents, in the numerical results, a re-distribution of the stresses that causes the reaching of an peak load too much higher than the experimental one.

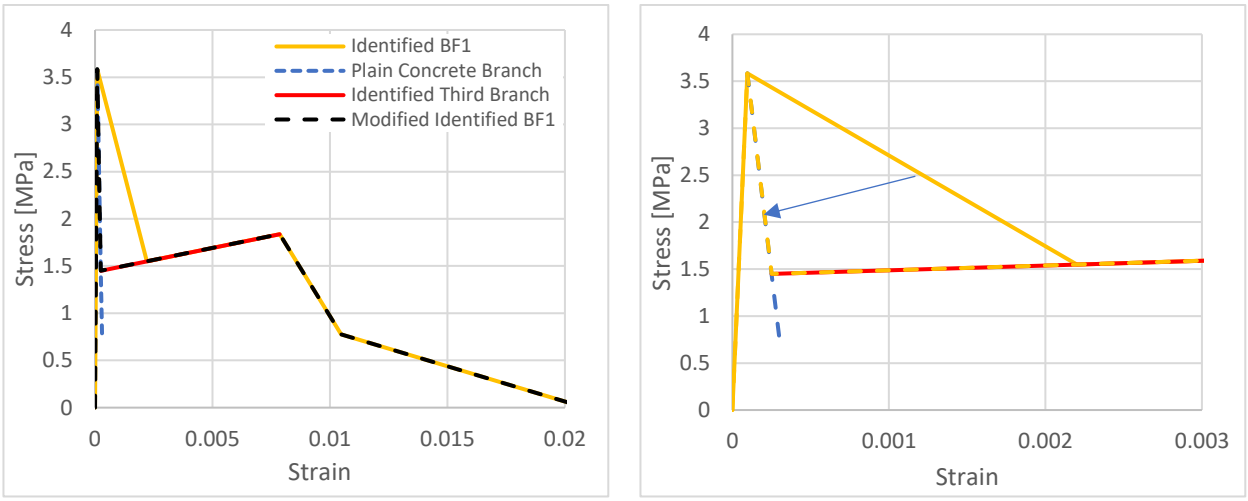

(a) (b)

Figure 6.7 Modified identified BF1 law, with a plain concrete post-cracking branch (a); and zoomed to the modified part (with the same legends) (b)

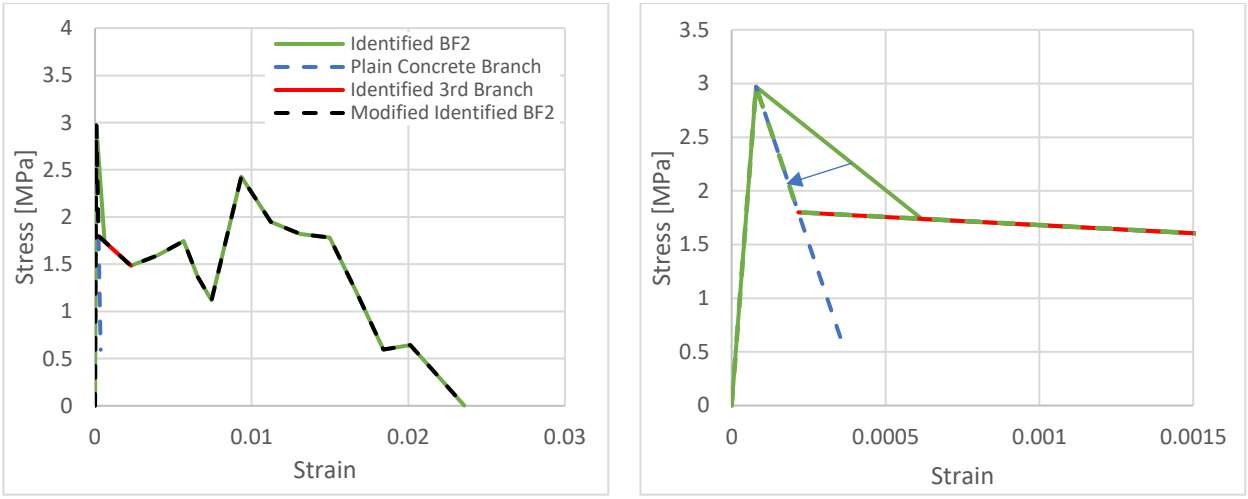

(a) (b)

Figure 6.8 Modified identified BF2 law, with a plain concrete post-cracking branch (a); and zoomed to the modified part (with the same legends) (b)

The modification of the identified BF1 gave excellent results, Figure 6.9, as the peak load value was similar to the experimental one, in addition to the first post-cracking branch and followed by the hardening. Hence, the model was able to replicate the experimental beam results with a response of the same path, which was convenient for the following modeling of the reinforced beam.

On the other side, the modification of the identified BF2 law was not that successful, Figure 6.10, even though the load peak was perfectly captured with a short part of the following branch, but then the response's final softening branch was delayed to a displacement of around 90 mm, Figure 6.10 (a), while the experimental one had it around a 6 mm value.

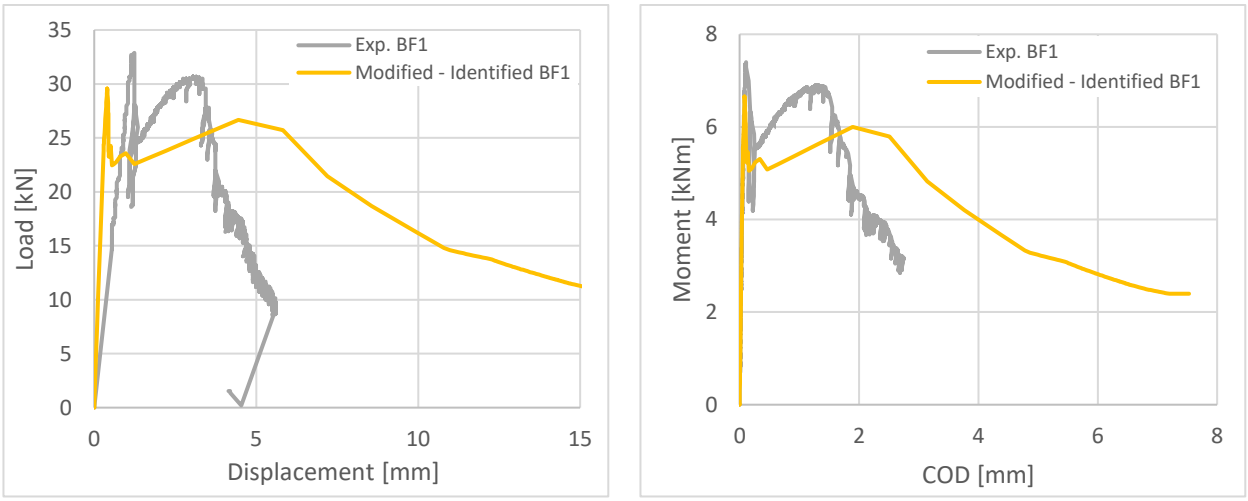

(a) (b)

Figure 6.9 SFRC beam with the modified Identified BF1 law, with a plain concrete post-cracking branch, results of load vs. mid-span displacement(a); and Moment vs. COD (b)

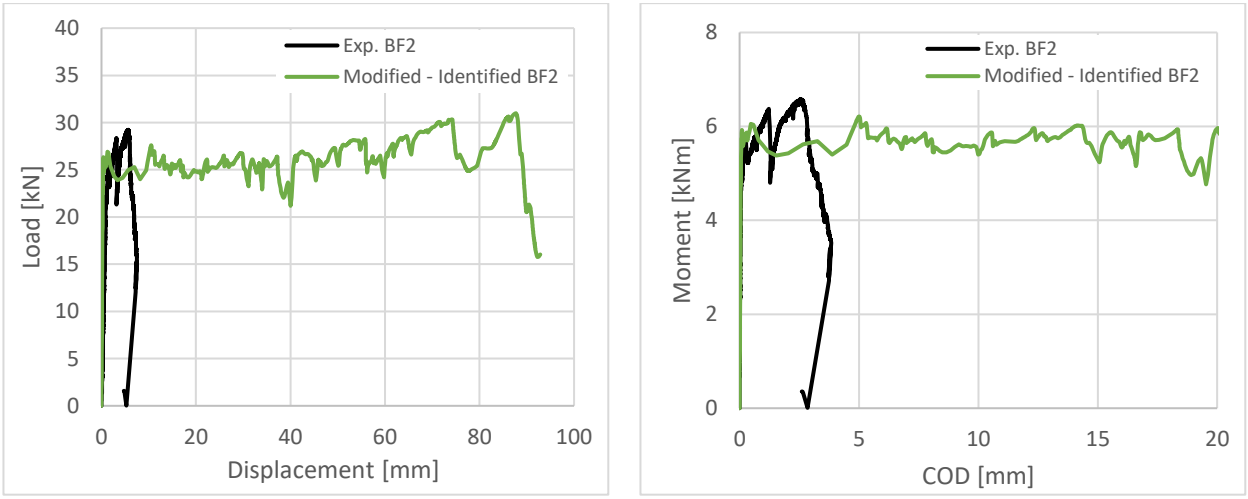

(a) (b)

Figure 6.10 SFRC beam with the modified Identified BF2 law, with a plain concrete post-cracking branch, results of load vs. mid-span displacement(a); and Moment vs. COD zoomed to the first 20 mm (b)

A new modification was introduced to the modified identified BF2 law, as it proved a good first response, and the issue was the delayed softening branch. A partial reduction of the law's strain was made, forcing the early start of the softening, using the ligament crack length, with a value equal to the depth of the beam, 150 mm. This was done because the ABAQUS regularization works only for the softening phases. So, due to the quite horizontal second part

of the stress-displacement identified BF2 law, it was necessary to change the numerical characteristic length, increasing the inelastic process zone.

The first part of the response was well replicated; hence the new modification was done after the plain concrete branch. Moreover, as seen in Figure 6.8 (a), the final softening branch started around a 1.5% strain, which was reduced while maintaining the branch after it unchanged. The modification was done by dividing the strain values by the lcs of 150 mm, only between 0.02% and 1.5% strains, without affecting any other part of the law. Figure 6.11 shows the new modification performed. This l_{cs} value was taken equal to the one representing both the crack experimental distance and the width of the section, describing the dimension of the inelastic process zone.

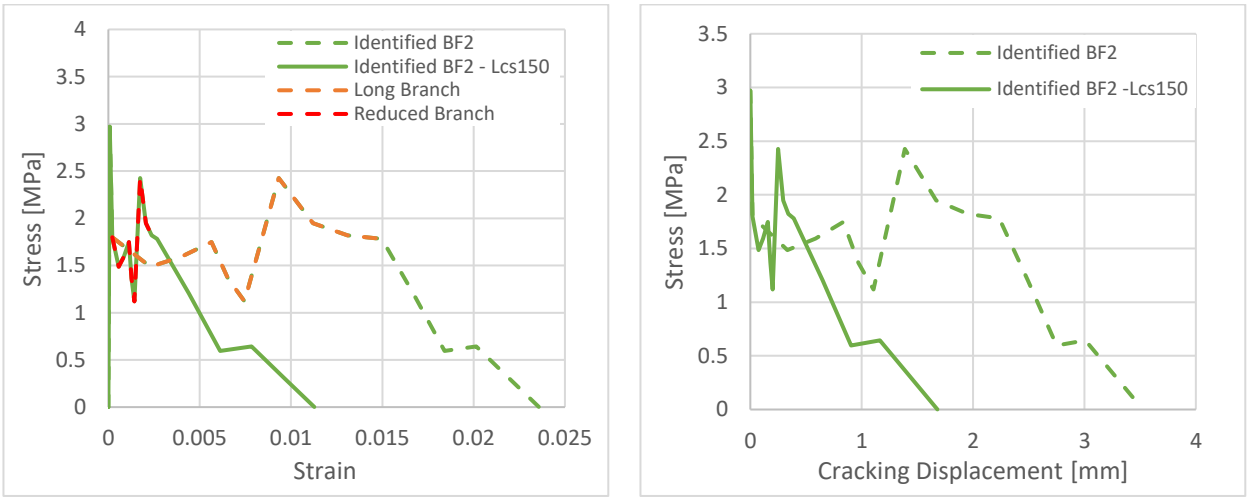

(a) (b)

Figure 6.11 The partial modification with lcs 150 mm of the identified BF2 law stress vs. strain (a); and its CDP tensile behavior new input stress vs. cracking displacement (b)

The results of the shortening of the identified BF2 law was entirely efficient, as the model delivered a similar response to the experimental one, Figure 6.12, even with a slight difference of the shortening branch start and slope, but was still considered with a good and suitable results for the following modeling of the reinforced beam.

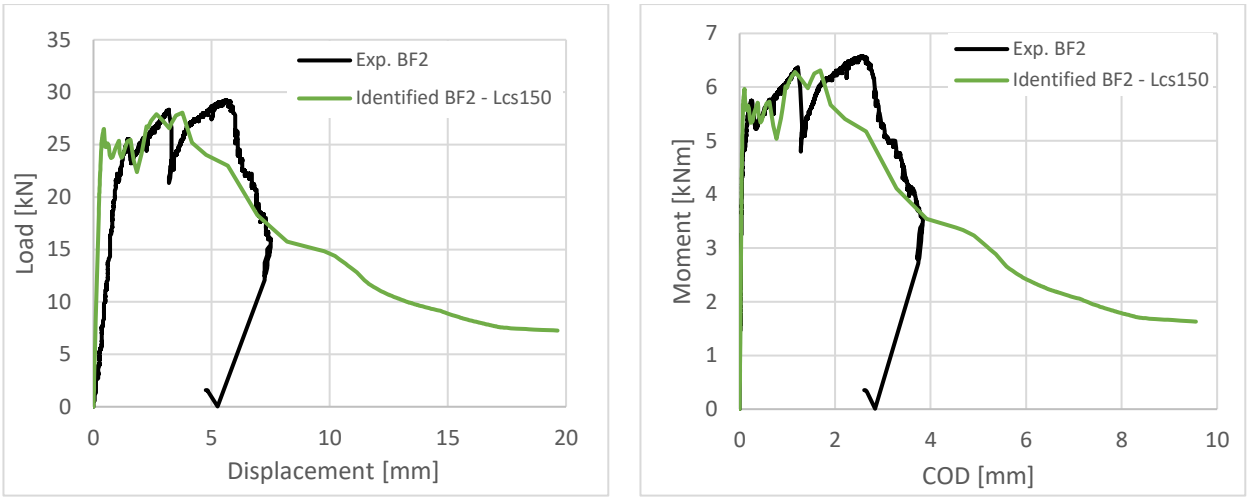

(a) (b)

Figure 6.12 SFRC beam with the modified Identified BF2 law, with a partial shortening with lcs 150 mm, results of load vs. mid-span displacement(a); and Moment vs. COD (b)

Figure 6.13 and Figure 6.14 present the plastic strain contour lines at the point of failure of the experimental beams, BF1 and BF2, respectively. The figures prove that the models' modified laws were also able to deliver a perfect simulation of the cracking pattern, with an approximate cracking distance of 100 mm for the BF1 case and between 75 and 100 mm for the BF2 model.

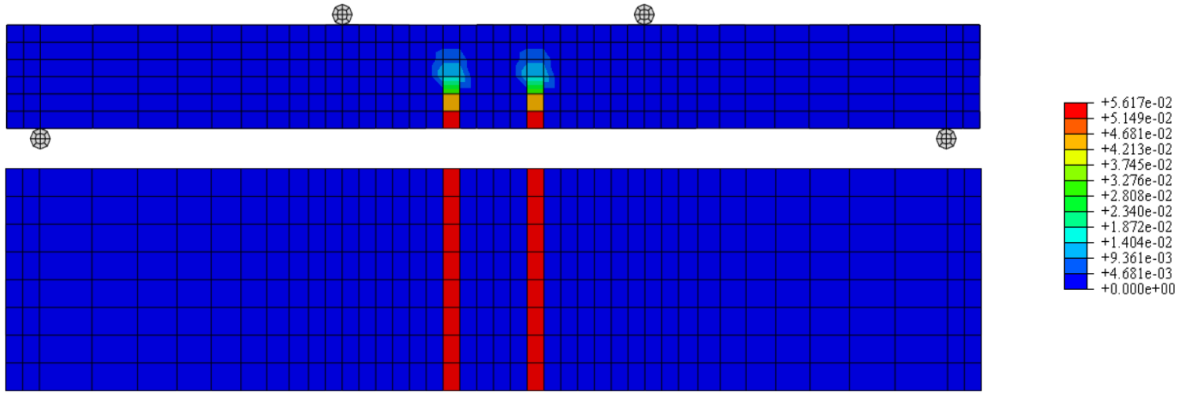

Figure 6.13 Plastic strain, of max principal, of the four points bending beam model with the modified BF1 law, at around 5.5 mm mid-span displacement

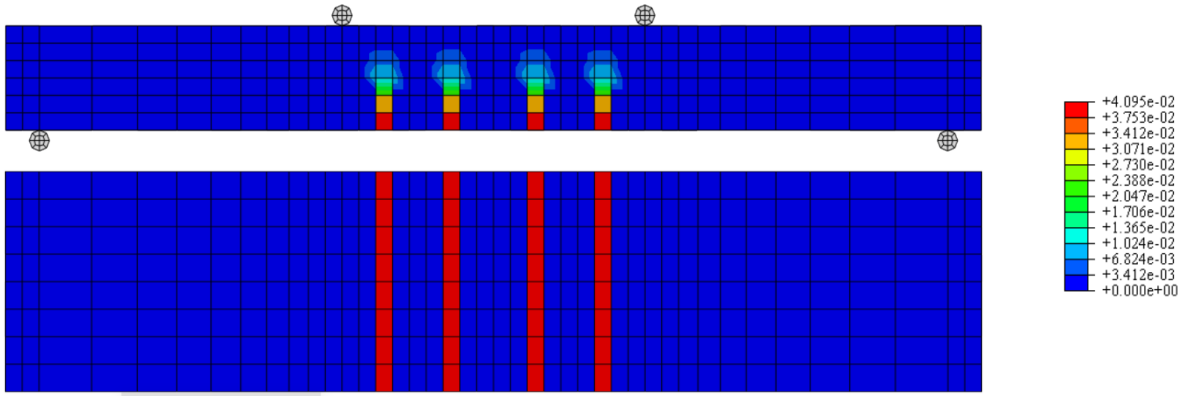

Figure 6.14 Plastic strain, of max principal, of the four points bending beam model with the modified BF2 law, at around 8 mm mid-span displacement

6.2 Reinforced Undamaged Beam

To appreciate the beneficial effects of the FRCM reinforced on the SFRC beam, a model was created with the beam's full capacity and was defined by the two modified identified laws, BF1 and BF2. Hence this model was not simulating the reinforced beam's response in the experimental research [12]. As in that case, the beam was pre-damaged, modeled in this research's previous section, 6.1, and then reinforced, with a residual capacity of the beam.

This modeling was performed to highlight the different strength of the undamaged beam reinforced with FRCM composite, and since it was difficult to model a reinforced damaged and deflected beam.

6.2.1 FRCM Reinforced Beam Model

A 350 x 1200 mm^2 FRCM composite, with fabrics F4 and mortar M2, of 20 mm thickness, was applied to the bottom side of the beam, same as in the experiment of [12]. The reinforcement was constrained with a surface-to-surface tie since, in the experiments, it was considered a perfect contact due to the hydro-scarification of the beam.

The reinforcement was modeled in two different approaches, same as in its uniaxial tensile test modeling, 4.1.1. Model A, with a homogenous material approach with solid section in this case, and model B, as a continuum shell model with embedded rebar approach.

Since model A was defined by the revised ACK, which depends on the thickness of the section, previously 9 mm, a newly revised law was provided, with the same definition and a thickness of 20 mm in Figure 6.15. This model was meshed same as the beam with a standard

3D Stress eight-node linear brick with reduced integration (C3D8R) mesh element, and as before in 4.2, with a size of squared 15 mm sides.

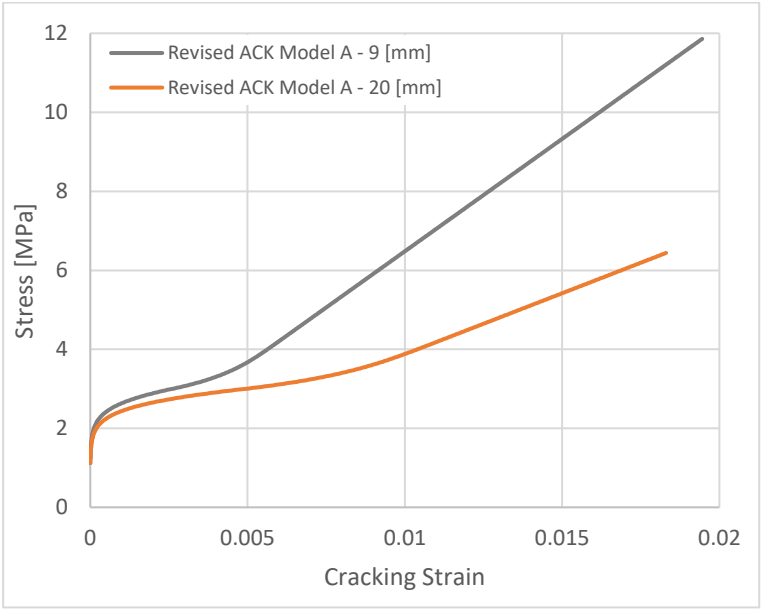

Figure 6.15 The revised ACK laws of a 9 and 20 mm thickness composites

Model B was defined the same as before, a homogenous shell section, with a fracture energy value of 0.0608 N/mm, representing 40% of the MC2010 value as chosen in 4.3.2, and a mesh of a squared 15 mm sides, both as decided in 4.3.2. The mesh element type of this model was an eight-node quadrilateral continuum shell with reduced integration (SC8R).

Figure 6.16 shows the reinforced beam model, with the same four points bending beam model of the previous section and the attached FRCM reinforcement.

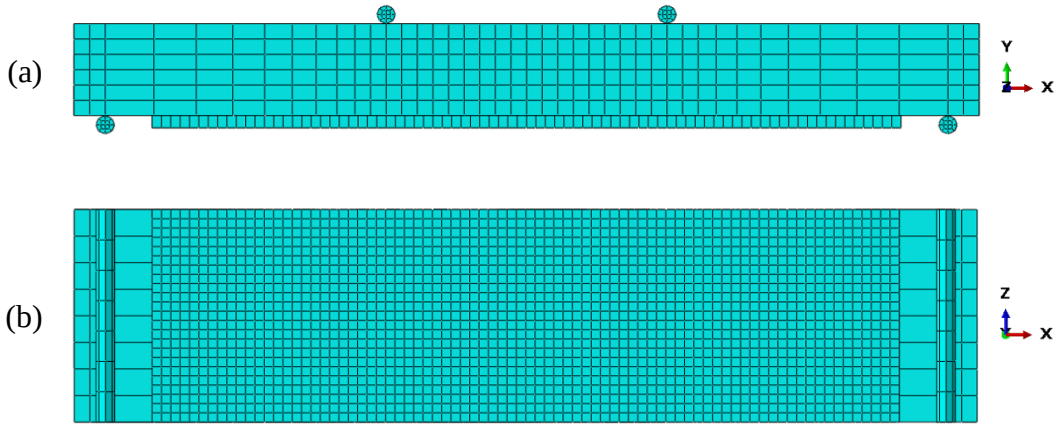

Figure 6.16 FRCM reinforced four points bending beam meshed ABAQUS model scheme, of the front view (a); and the bottom view (b)

6.2.2 Beam Reinforcement FRCM with Model Approaches A & B

The models were performed with the same displacement loading as in 6.1, where the difference is the Crack Opening Displacement COD extraction from the model done same as before, but from the FRCM nodes, with the exact coordinates of the previous case, simulating the displacement measurement of the experiments, Figure 3.6.

The response of the identified BF1 model, Figure 6.17, shows an increase in the load peak by 30% and 40%, with FRCM model A and B, respectively, proving the model's efficiency to demonstrate the capacity improvement. Due to the reinforcement, a higher load value of the hardening was achieved, similar in both models. Noting that the rest of the response was removed since the increased slope was describing the plain fabrics one, then it was after the beam's failure. In this case, the issue was the softening branch absence at the end of the response, as the model was not able to simulate a strength reduction of the whole system.

On the other hand, a good response was delivered by the model of identified BF2 with model A reinforcement, a reduction in the strength presenting a softening branch, was obtained at high displacement values. Dissimilar to the one with model B that had a similar behavior as the same approach with the identified BF1, where similarly the branch at the end related to the fabrics had to be removed. The cracking loads were also higher by more than 40% of the beam one, with both A and B models, Figure 6.18.

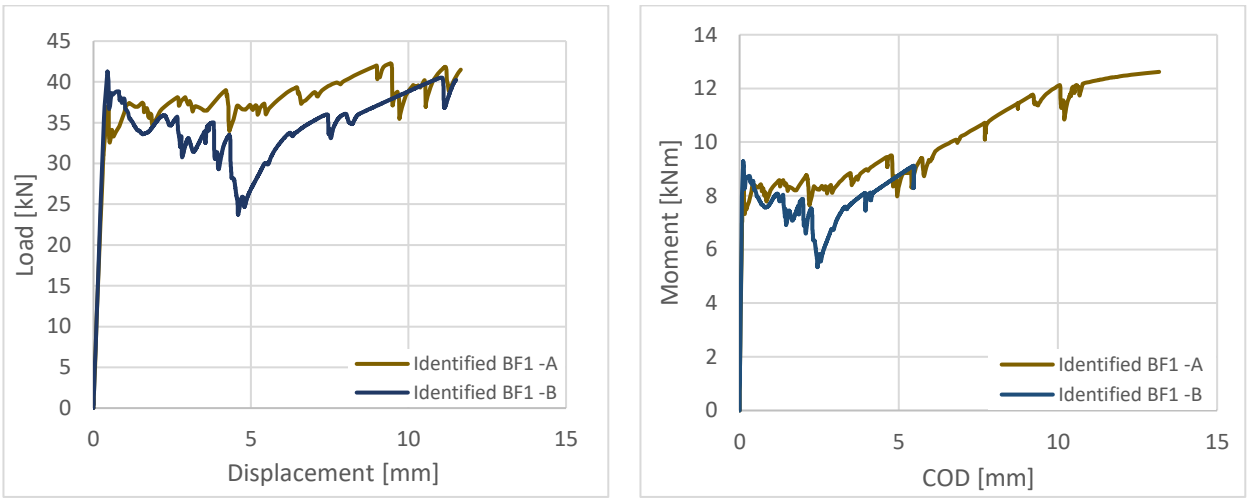

(a) (b)

Figure 6.17 Reinforced SFRC beam, undamaged with identified BF1 law, with FRCM of F4 fabrics & M2 Mortar, defined with model "A" or "B", results of load vs. mid-span displacement (a); and moment vs. COD (b)

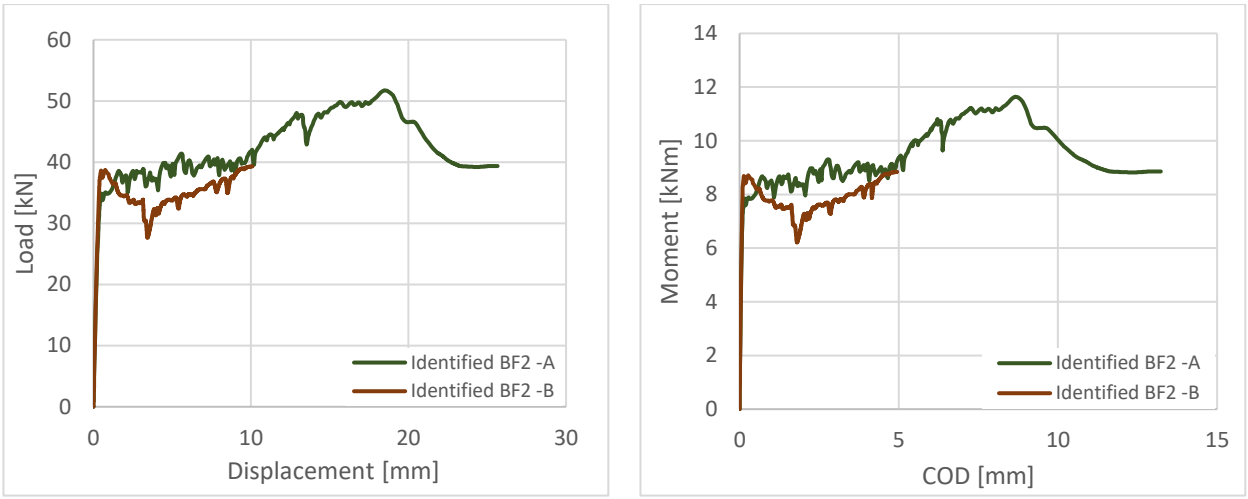

(a) (b)

Figure 6.18 Reinforced SFRC beam, undamaged with identified BF2 law, with FRCM of F4 fabrics & M2 Mortar, defined with model "A" or "B", results of load vs. mid-span displacement (a); and moment vs. COD (b)

Therefore, the homogenous model provided better results, describing a post-cracking response with a hardening behavior that gave a higher capacity, without any numerical problem. Then a softening branch, describing the whole system's final capacity reduction. The problem was with the delayed softening, allowing a more flattened response, a lower load peak, and a softening initiations at higher displacement values due to the high reinforcement stiffness.

6.2.3 FRCM Stiffness Variation with a Crack Distribution Factor

The use of the experimental response of the FRCM, obtained in direct tension does not correctly replicate the response when the composite material is applied to a concrete surface. This is caused by a different crack pattern (cracks are closer in the tensile test while they have a great distance in the real application).

So, the stiffness increase simulates the response of a zone between two cracks in which the mortar is considered not cracked.

The critical point was calibrating a good factor value that delivers the best response. Some options can be used regarding the diverse values of the characteristic length.

The first one was to double the stiffness, since the cracks are spread almost according to the fabrics spacing, 38 mm, then multiplying it by 76 mm to deliver half the cracks, localizing one crack in every two spacings.

The second, which was from the design of structures Eurocode 2 (EC2) [14], suggesting a value around 114 mm, so a value of 110 mm was used. This value was computed to what is usually done for the standard steel meshes in thin concrete.

The third was related to the model's depth, which was 170 mm because of the FRCM reinforcement layer.

A fourth option, which was more practical and related to the existing beam results, was to follow the SFRC beam results of crack spacing. This case was checked using Figure 6.13 and Figure 6.14, which showed around 100 mm and 75 mm for the BF1 and BF2 beams crack spacing, respectively. Hence, since this one was closer to the values of the first and second cases, it was neglected.

Therefore, three different lcs were used to increase the stiffness, wherein the homogenous model it was done by transforming the revised ACK behavior to crack displacement, multiplying by the fabrics spacing, 38 mm, and then dividing by the ligament length. While in the case of model "B", the young moduli of the fabrics, both warp, and weft, were directly multiplied by the lcs and divided by the spacing. Figure 6.19 illustrates the effects of the two different models' stiffness variation, with the uniaxial tensile loading test modeling.

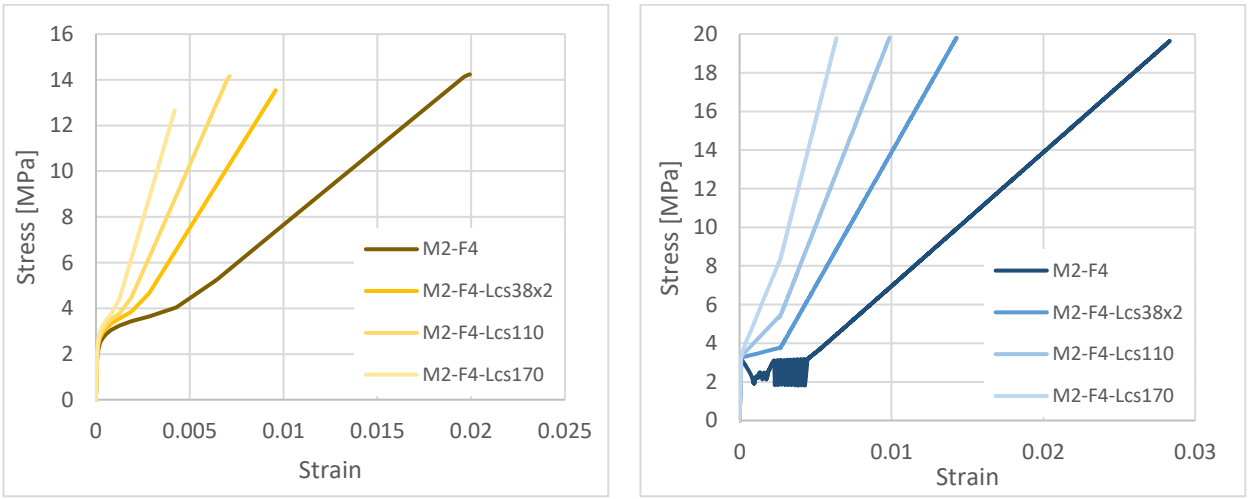

Figure 6.19 Stiffness variation of FRCM's fabrics, fabrics F4 & mortar M2, uniaxial tensile test modeling with models "A" (a); and model "B" (b)

Figure 6.20 and Figure 6.21 show the effect of stiffness variation, proving that the post-peak response depends on the fabrics. The results of the BF1 reinforced with a model "A" composite showed better response with the increase of the stiffness, as a softening branch can

be seen, Figure 6.20 (a). Similarly, with a better improvement, BF2 with model A, Figure 6.21 (a), with the purpose of this modification was perfectly achieved, with the greater localizing of the cracks leading to an earlier softening branch.

While the model “B” responses, even with an evident change of the results, were still unable to fully describe the reinforced beam post-cracking response due to numerical convergence problem, with a final part strictly related to the fabrics, Figure 6.20 (b) and Figure 6.21 (b).

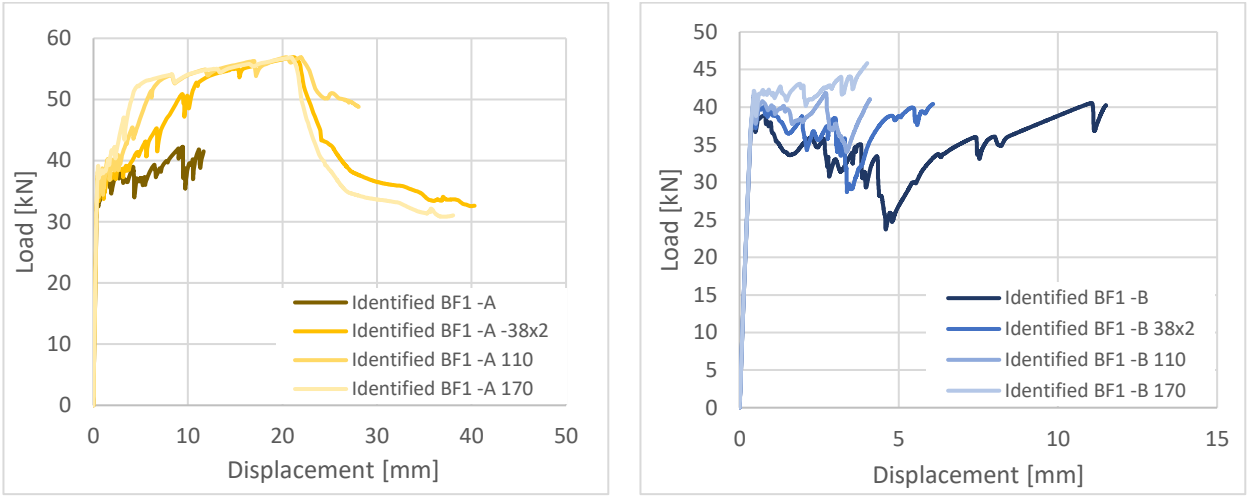

(a) (b)

Figure 6.20 Stiffness variation of FRCM’s fabrics, fabrics F4 & mortar M2, reinforced to the undamaged SFRC beam with identified BF1 law, load vs. mid-span displacement with FRCM model "A" (a); and model "B” (b)

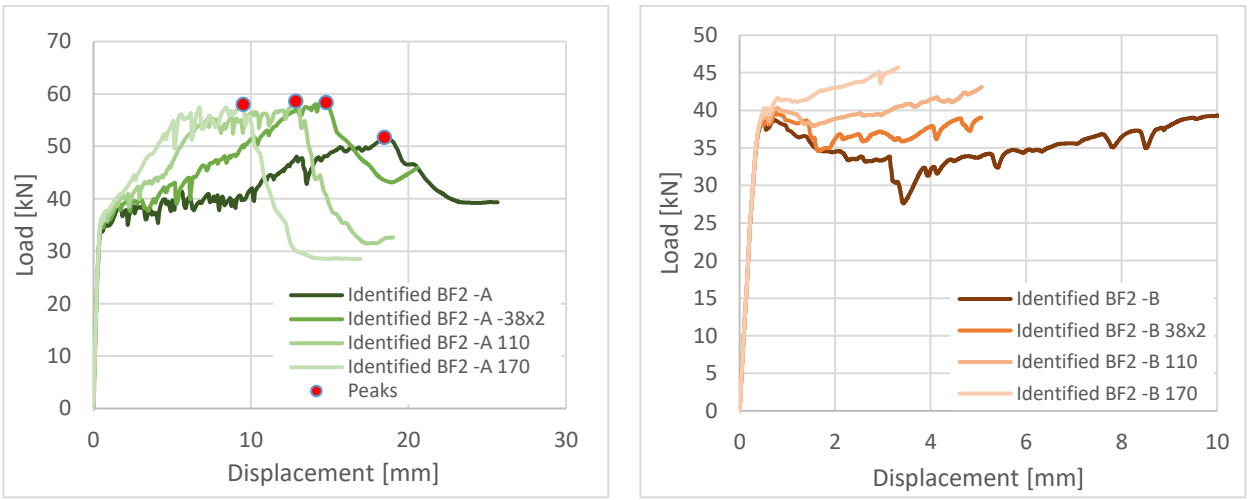

(a) (b)

Figure 6.21 Stiffness variation of FRCM’s fabrics, fabrics F4 & mortar M2, reinforced to the undamaged SFRC beam with identified BF2 law, load vs. mid-span displacement with FRCM model "A" (a); and model "B” (b)

Figure 6.21 (a), which gave the best results, has the peaks pointed out as with higher stiffness their loads value gradually increased and was at lower displacements, which was mainly related to the revised ACK, whereas the load peaks are strictly related to the fabrics.

The comparison with the different reinforcement models, modified with the same lcs, for the models with identified BF1 and BF2 laws were highlighted in Figure 6.22, Figure 6.23, Figure 6.24, Figure 6.25, Figure 6.26, and Figure 6.27 with the load vs. mid-span displacement and moment vs. crack opening displacement.

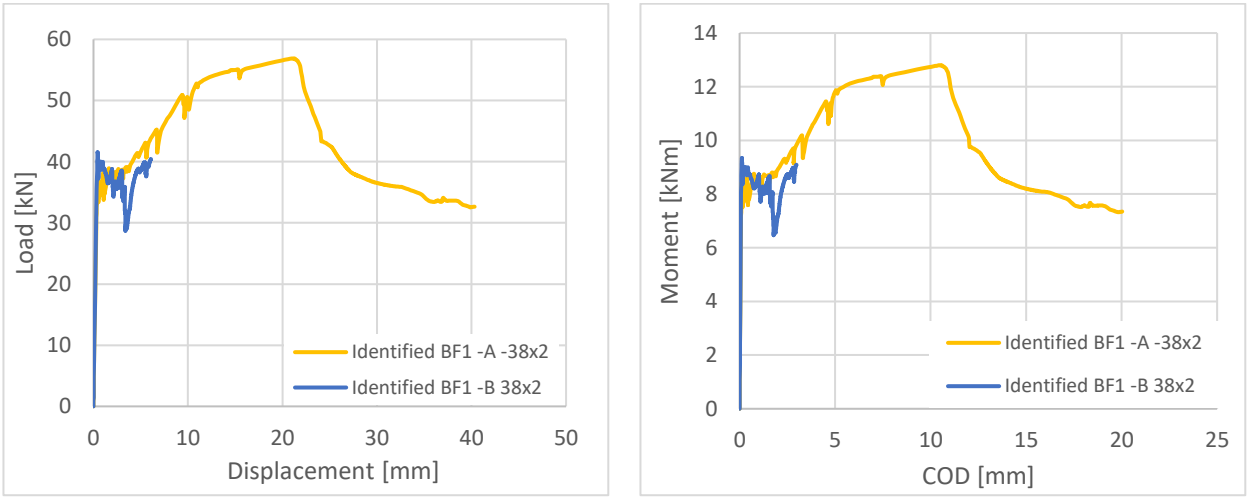

(a) (b)

Figure 6.22 FRCM model "A" and "B" comparison with lcs 38x2 stiffness modifier, reinforced to the undamaged beam with identified BF1 law, load vs. mid-span displacement (a); and moment vs. COD (b)

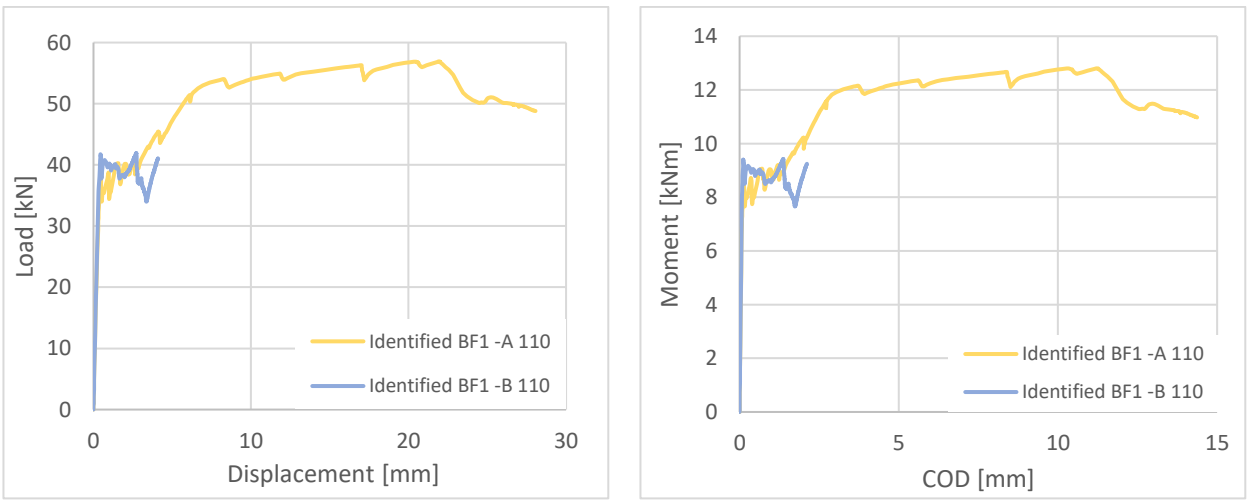

(a) (b)

Figure 6.23 FRCM model "A" and "B" comparison with lcs 110 stiffness modifier, reinforced to the undamaged beam with identified BF1 law, load vs. mid-span displacement (a); and moment vs. COD (b)

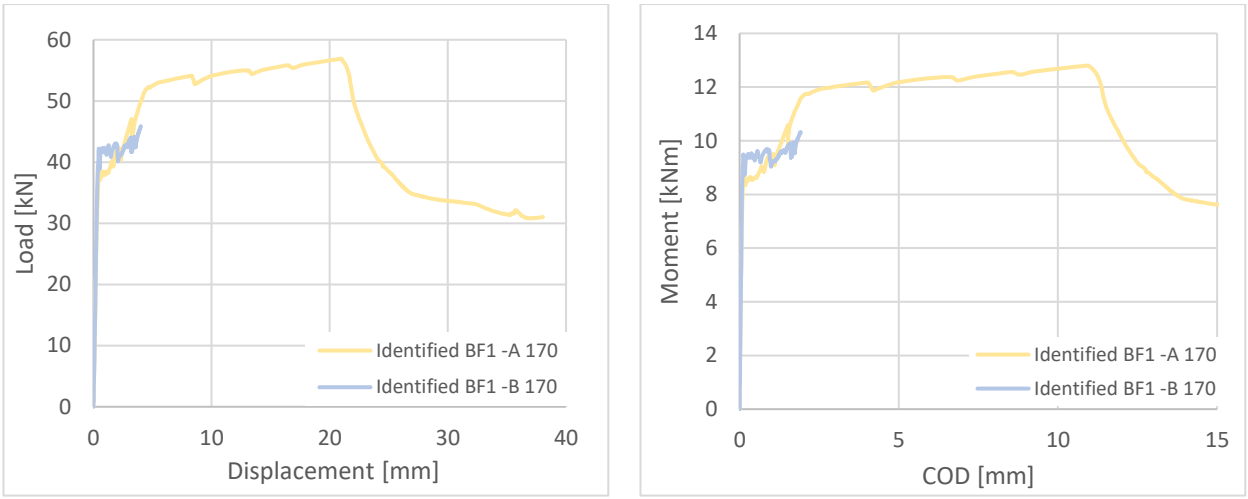

(a) (b)

Figure 6.24 FRCM model "A" and "B" comparison with lcs 170 stiffness modifier, reinforced to the undamaged beam with identified BF1 law, load vs. mid-span displacement (a); and moment vs. COD (b)

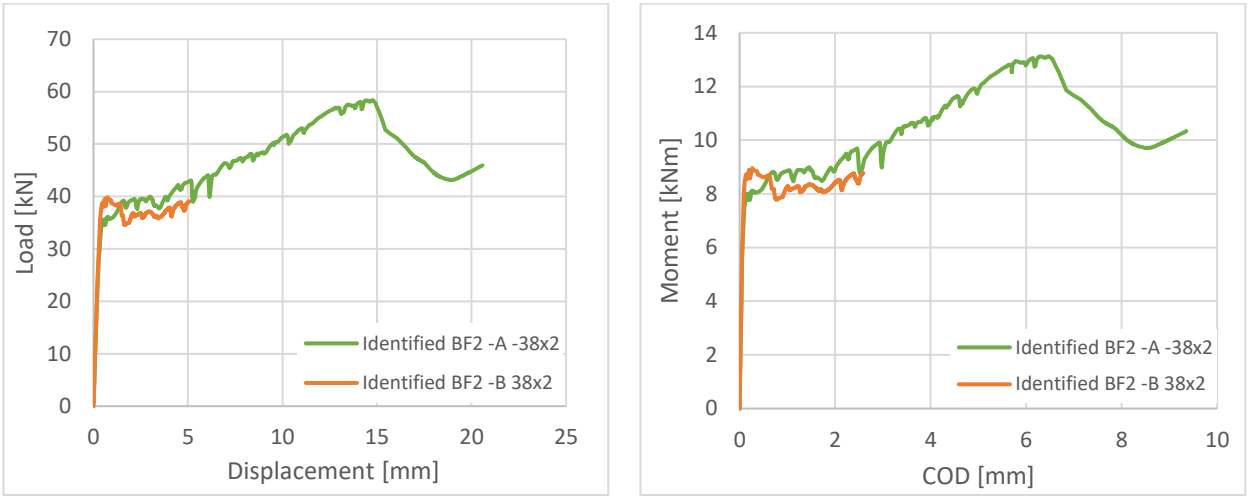

(a) (b)

Figure 6.25 FRCM model "A" and "B" comparison with lcs 38x2 stiffness modifier, reinforced to the undamaged beam with identified BF2 law, load vs. mid-span displacement (a); and moment vs. COD (b)

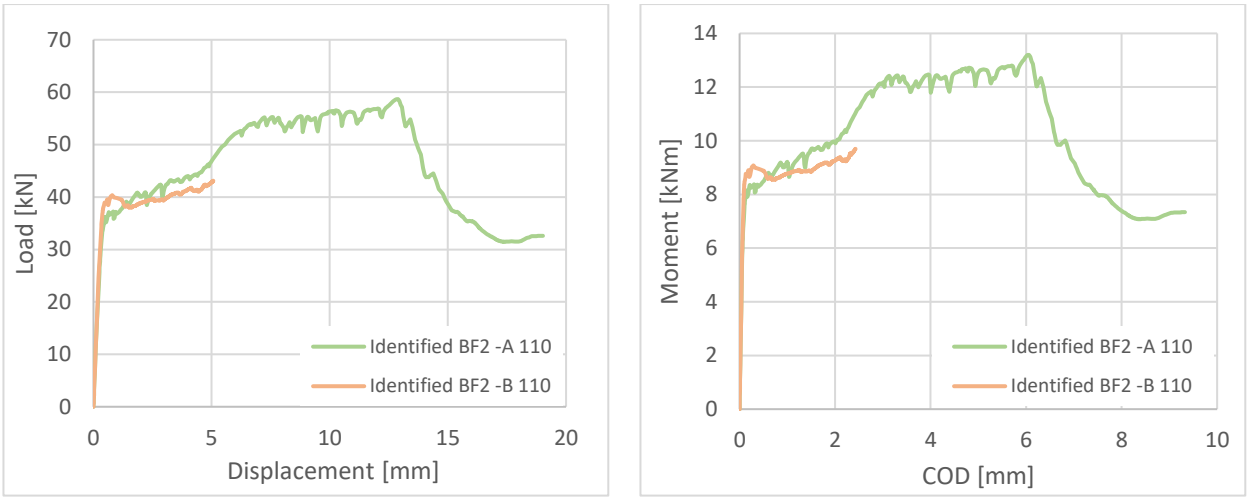

(a) (b)

Figure 6.26 FRCM model "A" and "B" comparison with lcs 110 stiffness modifier, reinforced to the undamaged beam with identified BF2 law, load vs. mid-span displacement (a); and moment vs. COD (b)

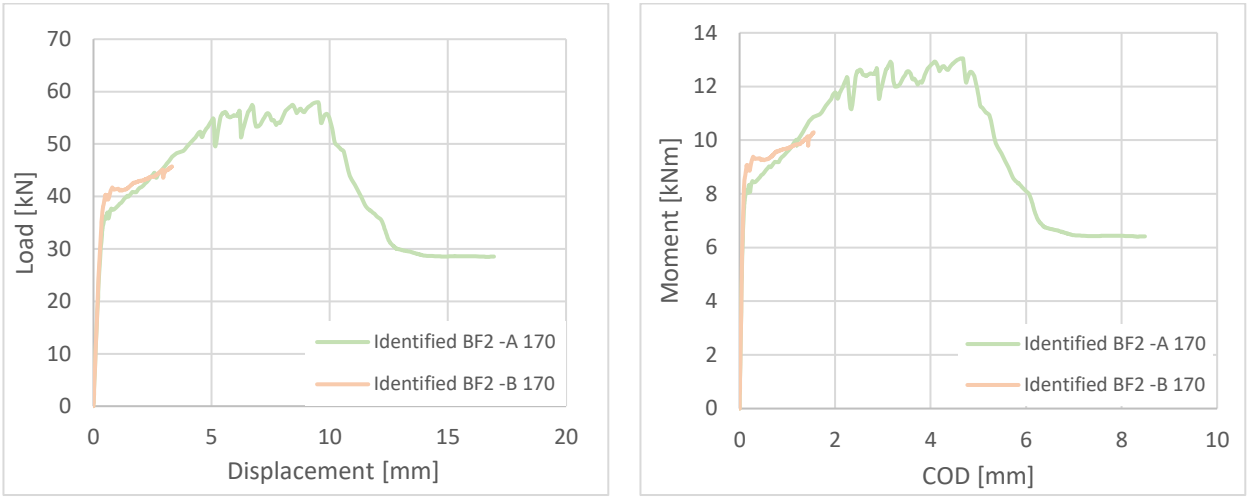

(a) (b)

Figure 6.27 FRCM model "A" and "B" comparison with lcs 170 stiffness modifier, reinforced to the undamaged beam with identified BF2 law, load vs. mid-span displacement (a); and moment vs. COD (b)

The plastic strain was checked at the end of the reinforced beam's response, for both reinforcement models of BF1 and BF2, at the primary stiffness and with the modified case of lcs equal to 110 mm, since it showed the most convenient results.

The exciting point achieved with both the beams and both models "A" and "B" was that the cracking in the beam was always affecting the FRCM cracking (see for example Figure 6.28 plastic strain distribution).

It was proved that due to the stiffness increase of the fabrics, model “A” could better localize the cracks, as with BF1, Figure 6.28 and, the plastic strain diffusion was reduced in Figure 6.29. The same, and with better results, BF2 case with the two main cracks, Figure 6.32 were reduced to one crack, Figure 6.33, a high localization explaining the better earlier start of the softening branch, in addition to its significant higher peak, Figure 6.21 (a).

However, model B reinforcement, Figure 6.30 and Figure 6.31 with BF1, Figure 6.34 and Figure 6.35 with BF2, did not support any significant meaning, except the fact that the crack was following the beam’s one, even with the stiffness increase, no better results were provided.

Finally, as a conclusion of this section, the model A reinforcement, in such modeling cases, was better a better simulation of the response, even in terms of crack’s pattern, and this was mainly due to the excellent behavior description of the analytical model, and to the modification introduced with a characteristic length of 110 mm, to increase the fabrics’ stiffness and the numerical crack distance.

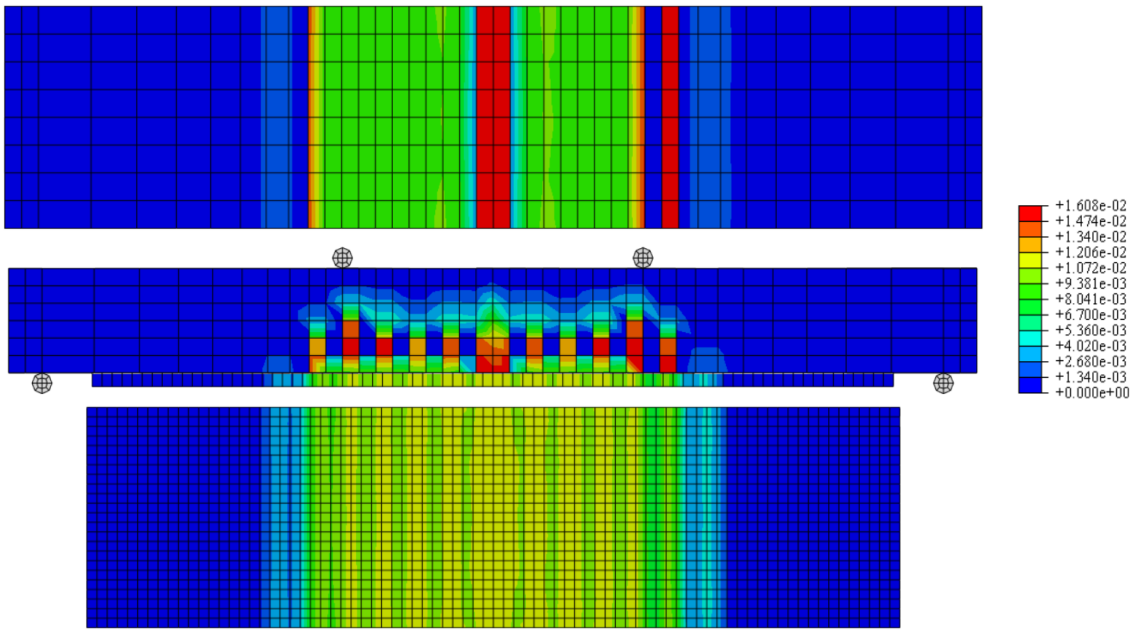

Figure 6.28 Plastic Strain, of max principal, of the SFRC beam model defined by the identified BF1 law, reinforced with FRCM, F4 fabrics, and M2 mortar, defined with model A

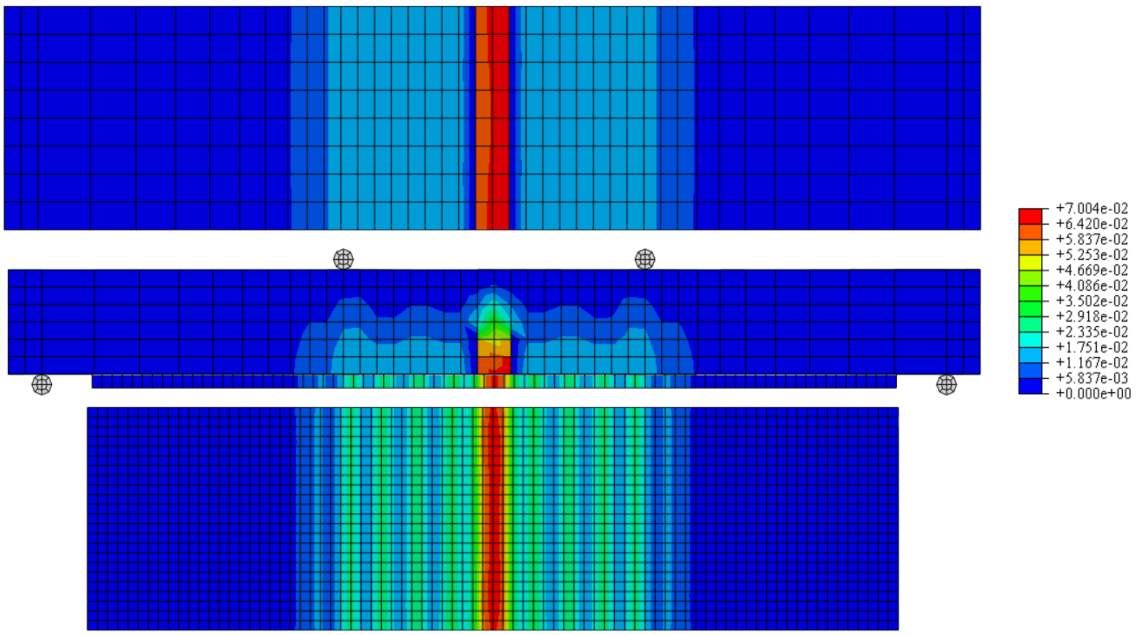

Figure 6.29 Plastic Strain, of max principal, of the SFRC beam model defined by the identified BF1 law, reinforced with FRCM, F4 fabrics, and M2 mortar, defined with model A stiffness modified with lcs 110 mm

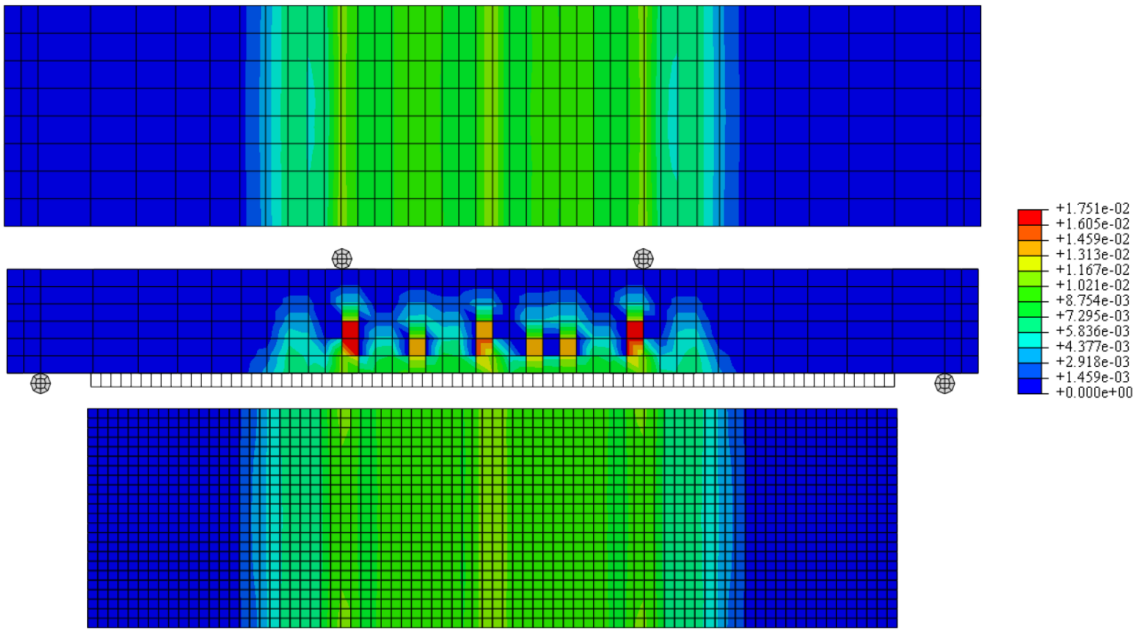

Figure 6.30 Plastic Strain, of max principal, of the SFRC beam model defined by the identified BF1 law, reinforced with FRCM, F4 fabrics, and M2 mortar, defined with model B

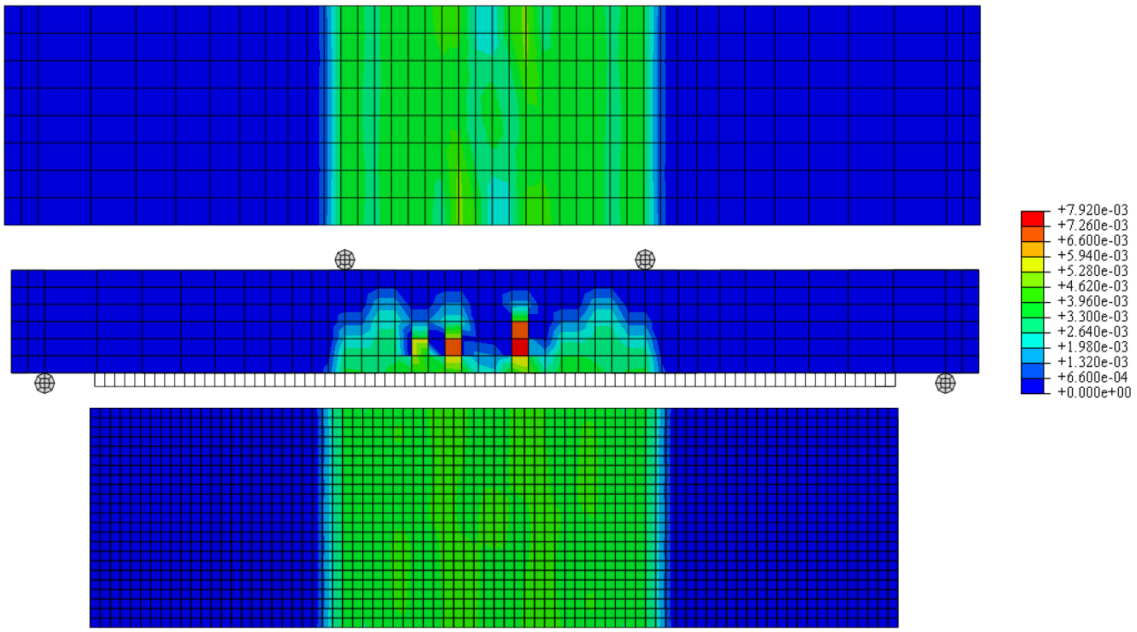

Figure 6.31 Plastic Strain, of max principal, of the SFRC beam model defined by the identified BF1 law, reinforced with FRCM, F4 fabrics, and M2 mortar, defined with model B stiffness modified with lcs 110 mm

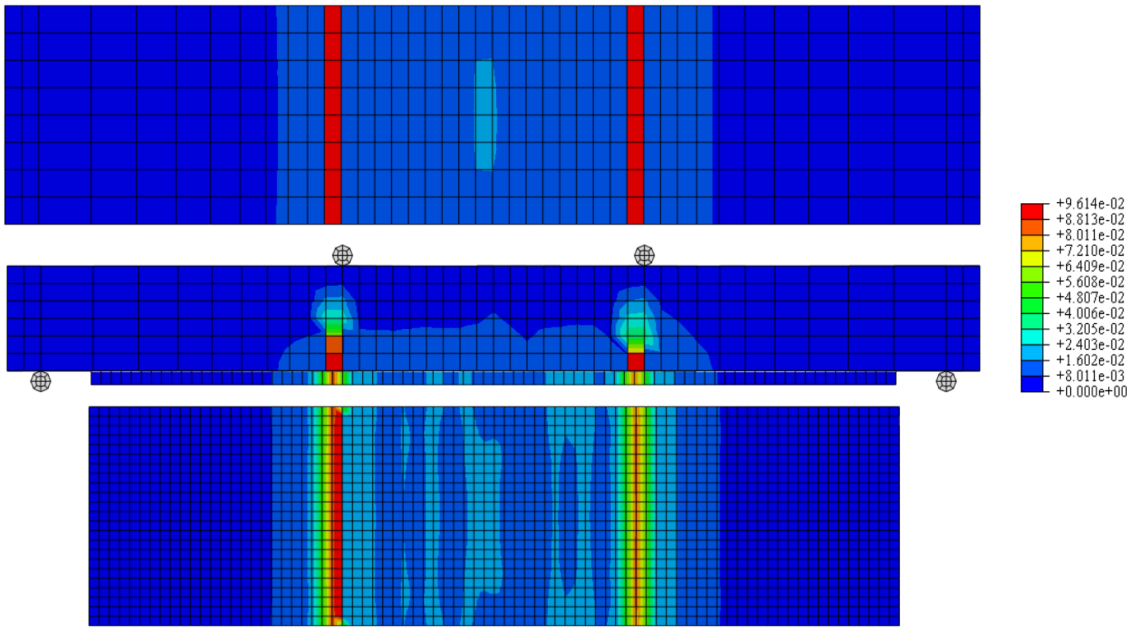

Figure 6.32 Plastic Strain, of max principal, of the SFRC beam model defined by the identified BF2 law, reinforced with FRCM, F4 fabrics, and M2 mortar, defined with model A

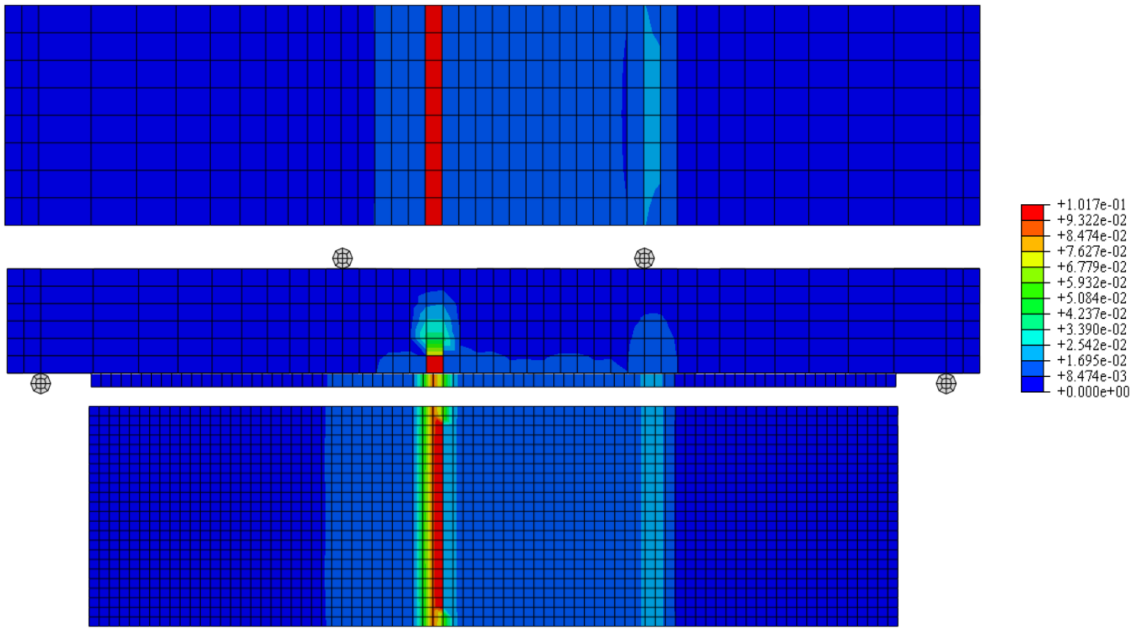

Figure 6.33 Plastic Strain, of max principal, of the SFRC beam model defined by the identified BF2 law, reinforced with FRCM, F4 fabrics, and M2 mortar, defined with model A stiffness modified with lcs 110 mm

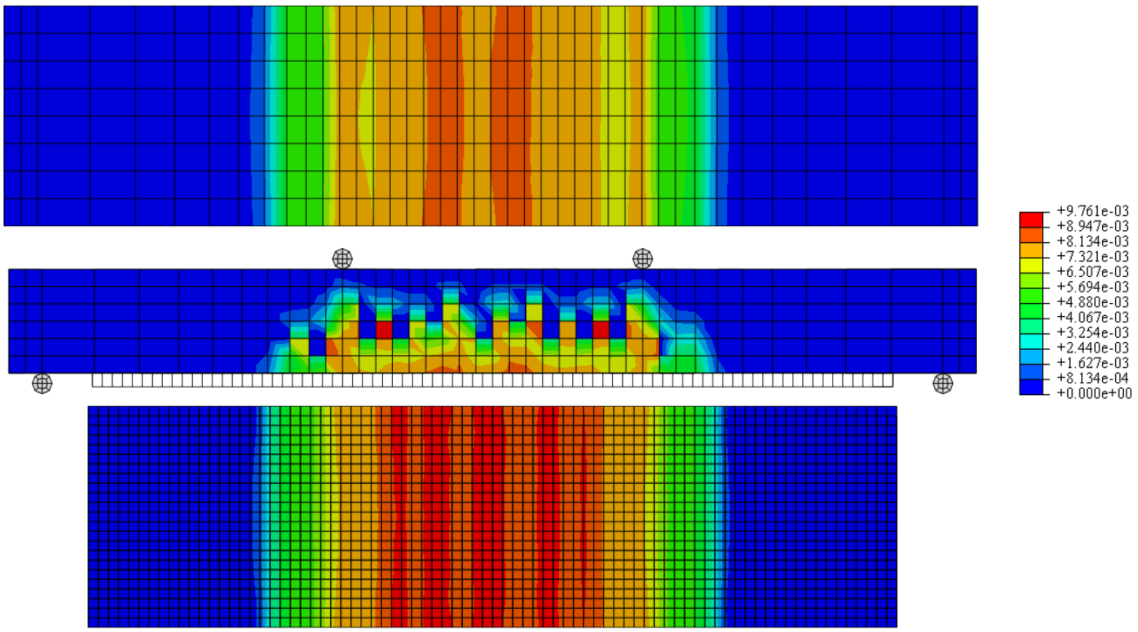

Figure 6.34 Plastic Strain, of max principal, of the SFRC beam model defined by the identified BF2 law, reinforced with FRCM, F4 fabrics, and M2 mortar, defined with model B

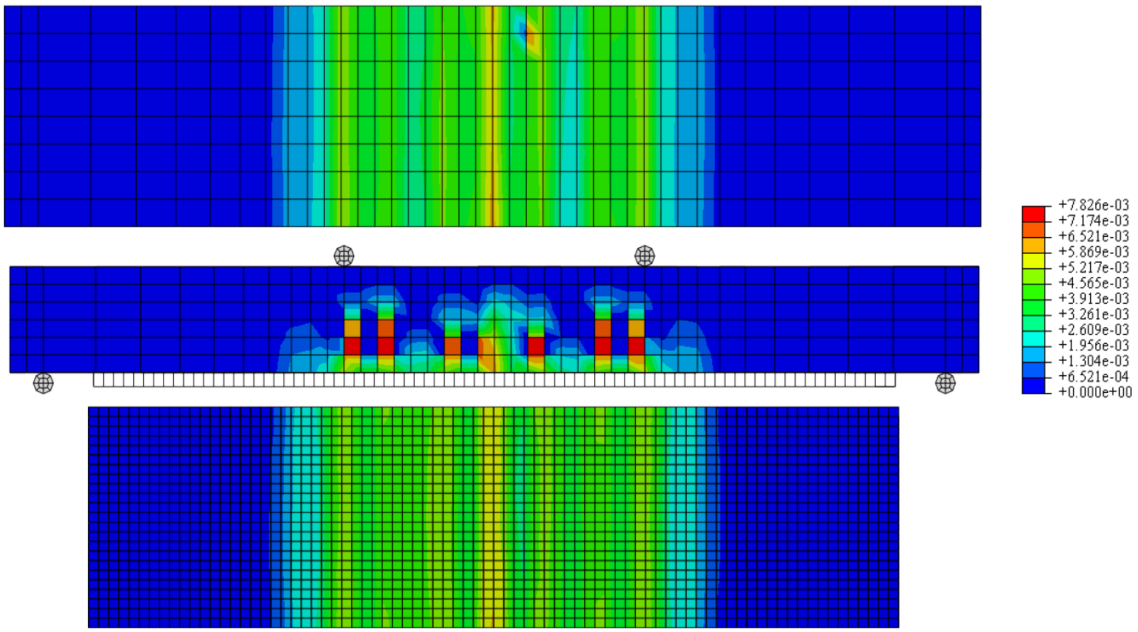

Figure 6.35 Plastic Strain, of max principal, of the SFRC beam model defined by the identified BF2 law, reinforced with FRCM, F4 fabrics, and M2 mortar, defined with model B stiffness modified with lcs 110 mm

6.3 A Simplified Approach for the Pre-Damaged FRCM-Reinforced Beam

The modeling of a pre-damaged and retrofitted beam is a critical task. Hence, a simplified approach was carried out to give a rough simulation of the retrofitted pre-damaged beam 3.3.2. This could be a starting point for further research based on defining the correct pre-damaged beam behavior

This approach was performed on the beam with the final identified BF2 law and reinforced with the model A FRCM, with a modified stiffness by two lcs values, 110 and 170 mm. This model definition was chosen since it gave the best results, with a well-positioned peak and softening branch.

The middle 500 mm part, noted by B in Figure 6.36, was defined with a residual tensile capacity, extracted from the stress – cracking strain regularized on the mesh, strain*, taken from a rough estimation of the plastic strain of this part, at the end of the numerical response with the identified BF2 law in 6.1.3, Figure 6.14. The values were taken at a mid-span displacement of the model equal to the failure one of the experimental BF2 beam, around 7.5 mm, and then correlated with its stress-strain tensile behavior Figure 6.37. To avoid complex calculations for such a simple approach, the law was assumed to maintain the same initial stiffness (no stiffness damage was considered). Therefore, the obtained stress – cracking strain in Figure 6.38(a) is the shifting of the end of the curve up to zero stress.

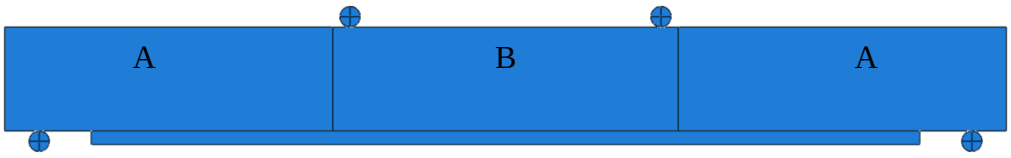

Figure 6.36 The pre-damaged beam scheme with its divided parts of full tensile capacity, A, and the residual one, B

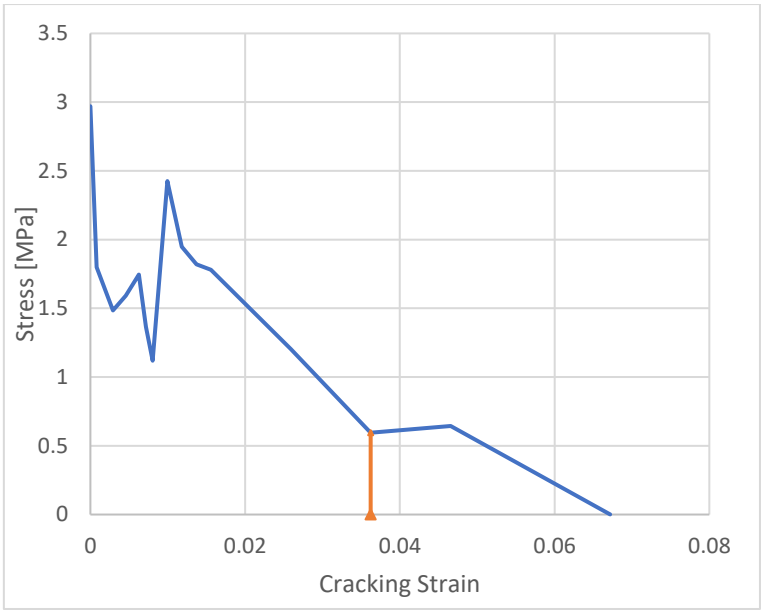

Figure 6.37 The plastic strain projection from the identified BF2 results on the mesh regularized stress – cracking strain behavior (strain), at a mid-span displacement of around 7.5 mm, representing the failure point of the experimental BF2 beam*

The compressive behavior of the damaged part B was defined with the full capacity for simplicity and due to its minor effects in such simulations. Part A was defined with the full capacity of both tensile and compressive behaviors, Figure 6.38.

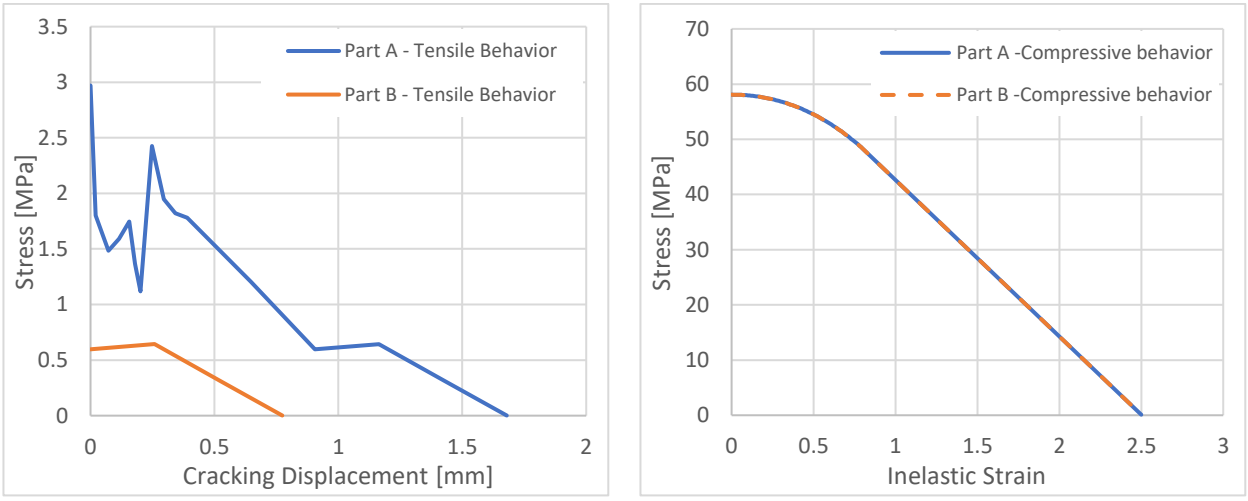

(a) (b)

Figure 6.38 The inelastic behaviors definition of the full capacity parts A and damaged one B, with stress vs. cracking displacement tensile behavior (a); and stress vs. inelastic strain compressive behavior (b)

Figure 6.39 shows acceptable results of the simplified approach, as both cases were able to follow the experimental BF2 response with its transition phases, and most importantly, with the peak value.

These good responses confirm that the choosing of a correct characteristic length helps in the correct experiment reproduction. In this case the 110 and 170 mm lengths represent the experimentally observed crack distance and the depth of the retrofitted (SFRC + FRCM) section, respectively.

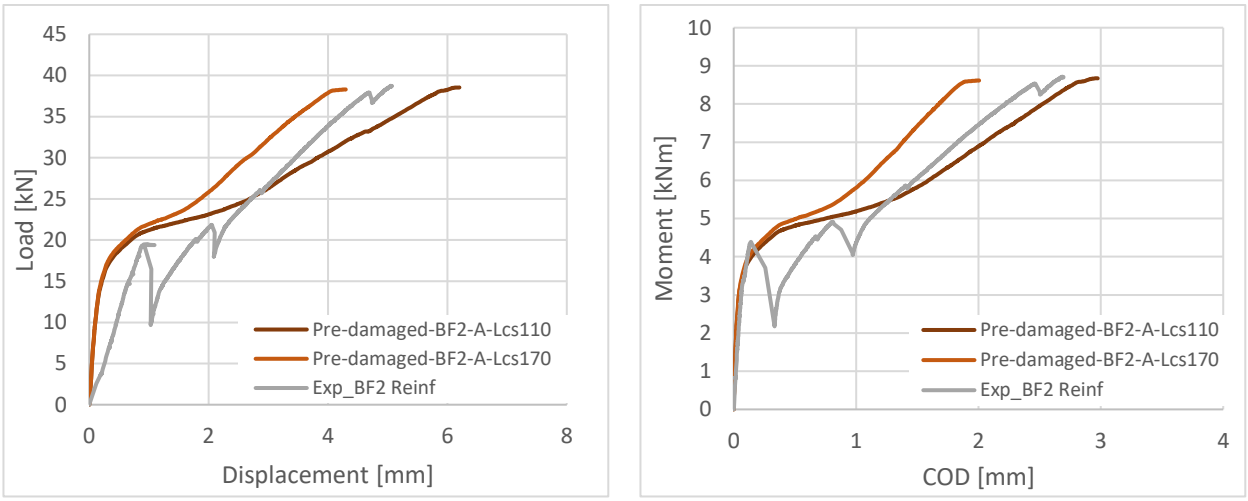

(a) (b)

Figure 6.39 Pre-Damaged SFRC beam, defined by the simple approach introduced with identified BF2 law and a reinforcement FRCM, F4 fabrics and M2 mortar, with lcs 110 and 170 mm stiffness modified model A, load vs. mid-span displacement (a); and moment vs. COD (b)

The plastic strain contour plots of the two models, Figure 6.40 and Figure 6.41, show a good representation. This proved that this approach could be used with more detailed definitions, for example, defining the damaged parts by referring to the localized plastic strains in the beam's zone, which was around the loading knives.

Finally, it may be concluded that this approach, with the given promising results, may be used and improved to further model a damaged beam, with some complex additions of defining a deflection of the beam or a method to include its effects in the response.

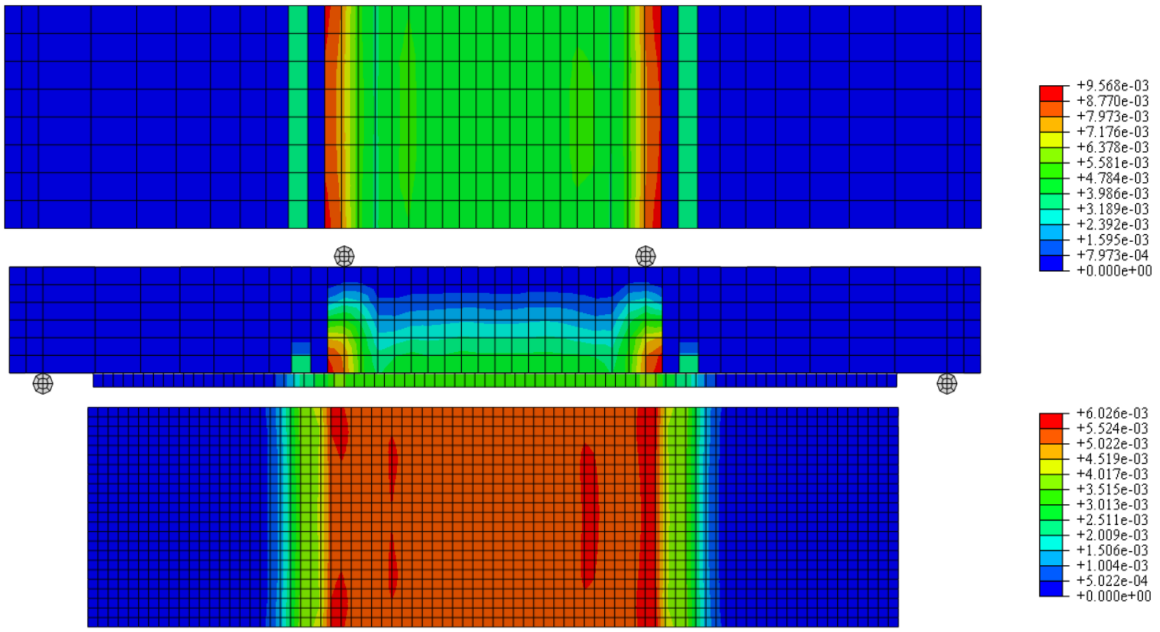

Figure 6.40 Plastic Strain, of max principal, of the Pre-Damaged SFRC beam, defined by the simple approach introduced with identified BF2 law and a reinforcement FRCM, F4 fabrics and M2 mortar, with lcs 110 mm stiffness modified model A

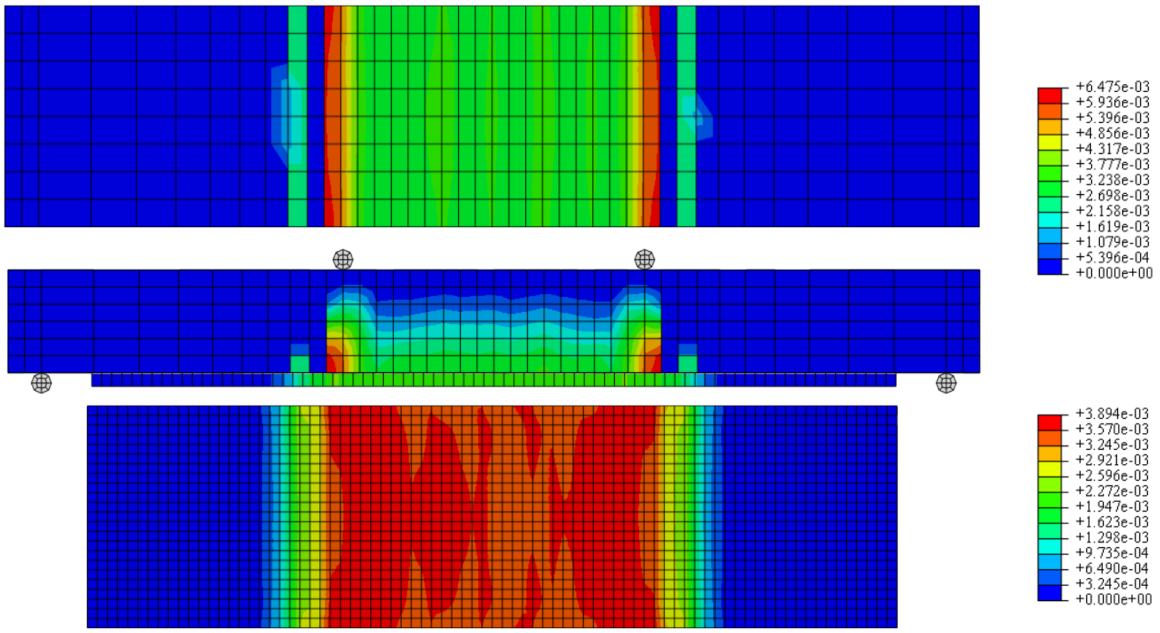

Figure 6.41 Plastic Strain, of max principal, of the Pre-Damaged SFRC beam, defined by the simple approach introduced with identified BF2 law and a reinforcement FRCM, F4 fabrics and M2 mortar, with lcs 170 mm stiffness modified model A

7 CONCLUSION

The ABAQUS software proved its capabilities to model such complex and non-linear behaviors, with high efforts of the material's defining and a substantial attention to the input methods used and its parameters, with their significant dependencies on the model's mesh.

The modeling of FRCM with the homogenous modeling provided acceptable results. While with the model "B", a perfect response was delivered compared with the experimental ones in both mortar cases. The calibration of the fracture energy with the used mesh was essential to obtain good results. Otherwise, the response will diverge from the desired one, proving that the MC2010 or MC1990 values were just a good first assumption and would require modifications according to the mesh element size, in addition to concluding that a more refined mesh may not deliver a better response and would require more attention on the GF parameter.

The regularization of the SFRC tensile behaviors was the primary key to obtain a good response, where the mesh size or the depth of the beam should be used to transform a general law into a specific beam model input. Otherwise, the model would highly localize the plastic strains, representing the crack, hence not allowing to provide a full post-cracking response. For this reason, it was found that the tensile behavior was best defined with a cracking displacement, converted from the law's strain, and regularized on the model mesh dimension.

The constitutive laws evaluated using the MC2010 could not simulate the full behavior of the SFRC beams; even with a good response until the first softening branch, they could not describe the hardening of the material, that is caused by to the micro-fibers. The simplified linear model with only two residual points taken from the experiments could not give good accuracy at different points. In contrast, the identified laws simulated a better behavior of the beam behavior, with some essential modifications to regularize the given law in the softening and hardening branches. It was found that ABAQUS, with a plain concrete first softening branch, was able to better catch the localization of the plastic strains.

The FRCM cracking pattern behaved differently when applied to an SFRC beam, from its tensile test one, as a stiffness variation of the fabrics was required to deliver a better response and allow crack localization along with the beam failure. Better results were obtained from the homogenous model "A", which was due to a better description of the behavior with the revised

ACK law than with the fracture energy of model “B” that proved its perfect results to describe the composite model unaccompanied with the beam. A final peak and softening branch were obtained with the simplified approach composite model, while a final response strictly related to the fabrics was given by the continuum shell model.

Future tasks to continue this research's aims may be done by improving the modeling methods to simulate an FRCM reinforced pre-damaged SFRC beam. Also, a parametric modeling study, with different fabrics or mortar materials of the reinforcement, in the uniaxial tensile test and the beam reinforcement one. It could be interesting to check diverse material behaviors requiring different calibrations of the same composite in the two different tests application. The bond between the FRCM and the beam is a critical task; hence, a study with a more detailed input of the constraint may better explain its effects on the final response and, finally, for a better simulation of the reinforced pre-damaged beam, step models could be done, with a first step of beam damaging, and a second step of the reinforcement addition.

8 BIBLIOGRAPHY

[1] M. C. Rampini, G. Zani, M. Colombo, and M. di Prisco, "Mechanical behaviour of TRC composites: Experimental and analytical approaches," *Appl. Sci.*, vol. 9, no. 7, 2019, doi: 10.3390/app9071492.

[2] M. C. Rampini, G. Zani, M. Colombo, and M. di Prisco, "The role of concrete substrate roughness on externally bonded Fabric-Reinforced Cementitious Matrix (FRCM) layers," *First Fib Italy YMG Symp. Concr. Concr. Struct.*, pp. 56–63, 2020.

[3] M. C. Rampini, G. Zani, M. Colombo, and M. Di Prisco, "Textile reinforced concrete composites for existing structures: Performance optimization via mechanical characterization," *Proc. 12th fib Int. PhD Symp. Civ. Eng.*, pp. 907–914, 2018.

[4] M. C. Rampini, G. Zani, M. Colombo, and M. Di Prisco, "Identification of FRCM mechanical parameters for the retrofitting design of existing structures," *High Tech Concr. Where Technol. Eng. Meet - Proc. 2017 fib Symp.*, no. April 2019, pp. 413–421, 2017, doi: 10.1007/978-3-319-59471-2-50.

[5] CNR, "CNR-DT 200/2004 Istruzioni per la Progettazione , l ' Esecuzione ed il Controllo di Interventi di Consolidamento Statico mediante l ' utilizzo di Compositi Fibrorinforzati," *CNR Cons. Naz. delle Ricecrche*, 2008.

[6] Y. Sümer and M. Aktaş, "Defining parameters for concrete damage plasticity model," *Chall. J. Struct. Mech.*, vol. 1, no. 3, pp. 149–155, 2015, doi: 10.20528/cjsmec.2015.07.023.

[7] Simulia, "ABAQUS / CAE User ' s Manual," *ABAQUS/CAE User's Man.*, pp. 1–847, 2001.

[8] M. C. Rampini, G. Zani, M. Colombo, and M. di Prisco, "Numerical modeling of FRCM composites for the seismic retrofitting of existing concrete structures," *ACI Fall Conv. 2019 Spec. Publ. (accepted Pap.*, 2020.

[9] J. Barros and J. Figueiras, "Flexural Behavior of SFRC: Testing and Modeling," *J. Mater. Civ. Eng. - J MATER Civ. ENG*, vol. 11, 1999, doi: 10.1061/(ASCE)0899-1561(1999)11:4(331).

[10] M. di Prisco, M. Colombo, and A. Pourzarabi, “Biaxial bending of SFRC slabs: Is conventional reinforcement necessary?,” *Mater. Struct. Constr.*, vol. 52, no. 1, pp. 1–15, 2019, doi: 10.1617/s11527-018-1302-0.

[11] FIB, *Model Code 2010*, no. September. 2011.

[12] M. C. Rampini, G. Zani, M. Colombo, and M. di Prisco, “Experimental study on SFRC beams and slabs strengthened with FRCM composite materials,” *V Work. New Boundaries Struct. Concr.*, 2019.

[13] A. Demir, H. Ozturk, K. Edip, M. Stojmanovska, and A. Bogdanovic, “Effect of Viscosity Parameter on the Numerical Simulation of Reinforced Concrete Deep Beam Behavior,” *Tojsat Online J. Sci. Technol.*, vol. 8, no. 3, pp. 50–56, 2018, [Online]. Available: www.tojsat.net.

[14] E. C. for Standardization, “EN 1992-1-1 Eurocode 2: Design of concrete structures - Part 1-1: General ruels and rules for buildings,” 2005.